Mohamed Khider University of Biskra
Faculty of exact sciences and natural and life sciences
Material sciences department

MASTER DISSERTATION

Material sciences
Physics
Energetic Physics and Renewable Energies

Ref. :

Presented by
ANGAR SALSABIL

On :10/06/2024

Study of instability issue in perovskite solar cell

Jury :

GUERGUEB Saida	MAA	University of Biskra	President
MEFTAH Afak	Prof	University of Biskra	Supervisor
LAZNEK Samira	MCB	University of Biskra	Examiner

Academic Year: 2024

Dedications

Praise be to God for the joy of achievement, and praise be to Him at the beginning and at the end. To my father, who illuminated my paths, guided my way, and served as my role model with every step I take. To the pure soul of my mother, may Allah have mercy on her. To the woman who raised me and never left me for a day. To the one who was eagerly awaiting my graduation, then passed away, my sister Zahra , may she rest in peace. To my brothers and sisters who have always stood by me and supported me throughout my journey. To my companion on the journey Malika , to my friend in the academic path sara, To my other half Lina, To the kind spirit Maroua, To my physics girlfriends Hadjer Sabrine Safa Hiba Amel Hadil.To all those whom my heart has expanded for, yet my paper could not encompass. I dedicate the fruit of my efforts to you

ACKNOWLEDGMENTS

Praise be to Allah, by whose grace righteous deeds are accomplished. From the standpoint of acknowledging kindness and recognizing reality, I extend my sincere thanks to the supervisor Pr, MEFTAH AFAK The one who did not hesitate to share her advice and guidance. I also express my gratitude to the committee chairman Pr GUERGUEB SAIDA, And to the examining Pr LAZNEK SAMIRA, For their discussion of my thesis. To all my dear teachers who taught me and guided me. Thank you all.

ABSTRACT

Our study investigates instability issues in $TiO_2 - MAPbI_3 - Spiro - OMeTED$ (n-i-p type) perovskite solar cells using SCAPS-1D numerical simulation software. The current-voltage density characteristics (J-V) and key photovoltaic output parameters, including short-circuit current density (J_{sc}), open-circuit voltage (V_{oc}), fill factor (FF), and power conversion efficiency (PCE) are calculated. The work focuses on the impact of defects induced by degradation factors such as prolonged illumination, UV radiation, corrosion, oxidation, and humidity. These defects, namelyN_R (recombination center),N_{DP} (deep donor), N_{DT} (shallow donor), and N_{AT} (shallow acceptor), are identified based on previous research. The possible defect locations, are at the interfaces; between the electron transport layer (ETL) and perovskite or the hole transport layer (HTL) and perovskite, as well as within the bulk perovskite layer. Initial electrical parameters are in agreement with wide range of experimental values, with J_{sc}=22.92mA/cm^2, V_{oc}=1.184V, FF=83.67%, and PCE=22.72%. However, high-density defects in the bulk layer (all $10^{16}cm^{-3}$) have the most significant impact, reducing PCE to 2.43%. Defects at the ETL/perovskite interface, with a surface density of $10^{14}cm^{-2}$, lower PCE to 16.61%, while defects at the perovskite/HTL interface result in a smaller decrease of PCE down to 21.73%. These defects were associated, respectively, to thermal stress, illumination and hysteresis effects. The introduction of a PbS buffer layer at HTL/bulk interface has improved considerably the electrical outputs degradation, mainly that related to bulk defects

Keywords: instability issues, perovskite solar cells, SCAPS-1D, interfaces, defects, cell efficiency

ملخص:

تبحث دراستنا في مشكلات عدم الاستقرار في خلايا البيروفسكايت الشمسية TiO_2-$MAPbI_3$-Spiro-OMeTED (نوع n-i-p) باستخدام برنامج المحاكاة العددية SCAPS-1D. يتم حساب خصائص كثافة الجهد الحالي (J-V) ووسائط الخروج الكهروضوئية الرئيسية، بما في ذلك كثافة تيار الدارة القصيرة (J_{sc})، وجهد الدارة المفتوحة (V_{oc})، ومعامل التعبئة (FF)، ومردود تحويل الطاقة (PCE). يركز العمل على تأثير العيوب الناجمة عن عوامل التحلل مثل الإضاءة الطويلة والأشعة فوق البنفسجية والتآكل والأكسدة والرطوبة وما إلى ذلك. تم تحديد هذه العيوب، وهي N_R (مركز إعادة التركيب)، وN_{Dp} (المانح العميق)، وN_{DT} (المانح غير العميق)، وN_{AT} (الاخذ غير العميق)، بناءً على اعمال بحثية سابقة. مواقع العيوب المحتملة موجودة في الواجهات؛ بين طبقة نقل الإلكترون (ETL) والبيروفسكايت أو طبقة نقل الثقب (HTL) والبيروفسكايت، وكذلك داخل طبقة البيروفسكايت . تتوافق وسائط الخروج الكهربائية الأولية مع نطاق واسع مع القيم التجريبية، مع J_{sc}=22.92 mA/cm^2، V_{oc} =1.184 V، FF=83.67%، وPCE=22.72%. وجدنا ان العيوب عالية الكثافة في طبقة البيروفسكيت (جميعها بكثافة 10^{16} cm^{-3}) لها التأثير الأكثر أهمية، مما يقلل من مردود التحويل للخلية إلى 2.43٪. يلي ذلك العيوب في واجهة ETL/perovskite، بكثافة سطحية تبلغ 10^{14} cm^{-2}،تؤدي إلى انخفاض PCE إلى 16.61%، بينما تؤدي العيوب في واجهة perovskite/HTL إلى انخفاض أصغر في PCE إلى 21.73%. أرجعت العيوب لتأثير الإجهاد الحراري ، الإضاءة و الهستيريزيس الناجم عن الإستقطاب الكهربائي. خفض تأثيرها بطبقة PbS عند السطح الفاصل HTL/bulk.

الكلمات المفتاحية: مشاكل اللااستقرار، الخلايا الشمسية البيروفسكية، SCAPS-1D ،الواجهات , العيوب ,مردود الخلية.

Contents

List of Figures

List of Tables

List of Abbreviations

PSCs	Perovskite solar cells.
DSSCs	Dye-Sensitized Solar Cells.
OMeTAD	Organic Metal Halide Absorber.
TiO_2	Titanium dioxide.
EDTA	Ethylenediaminetetraacetic Acid.
ETL	Electron Transport Layer.
HTL	Hole Transport Layer.
PCBM	Phenyl-C61-butyric acid methyl ester.
PEDOT:PSS	Poly(3,4-ethylenedioxythiophene):poly(styrenesulfonate).
HTM	Hole-Transporting Material.
P3HT	Poly(3-hexylthiophene).
PTAA	Poly(triarylamine).
SWCNT	Single-Walled Carbon Nanotube.
DMF	Dimethylformamide.
TEM	Transmission Electron Microscopy
XRD	X-ray Diffraction.
TSCs	Tandem Solar Cells.
FTO	Tin oxide doped with fluorine.
AFM	Atomic Force Microscopy.
SCAPS	Solar Cell Capacitance Simulator.
PCE	Power conversion efficiency
FF	Fill factor.
N_C	Effective density of conduction band (cm^{-3})
N_V	Effective density of valence band(cm^{-3})
E_g	Bandgap Energy (eV)
E_C	Conduction Band Edge (eV)
E_V	Valence Band Edge (eV)
J_{SC}	Short-circuit current density (mA/cm^2)
V_{OC}	Open circuit voltage (V).

Introduction

Perovskite solar cells, with their remarkable efficiency and affordability, present a ground-breaking alternative in the field of renewable energy. These cells exhibit great potential for general application, as evidenced by their power conversion efficiencies reaching 25% in laboratory circumstances [1,2]. Their configurable properties make them highly versatile, enabling incorporation into a wide range of applications, from large-scale installations to portable devices. Furthermore, they are a viable option for the development of photovoltaics in the future due to their compatibility with flexible substrates and scalable production processes [3,4]. Recent research has demonstrated that perovskite solar cells are a significant development in tackling the world's energy problems, providing a route towards ecologically friendly and sustainable power generation [5].

If perovskite solar cell materials are to be used in actual renewable energy systems, their stability in these applications must be guaranteed. The durability of the absorbing and charge transport layers poses a major obstacle in the commercialization of this photovoltaic (PV) technology. Halide perovskite materials, in particular, exhibit instability under real-world conditions, significantly shortening the lifespan of perovskite solar cells (PSCs) [6]. Environmental conditions like heat, humidity, light, and UV radiation can detrimentally affect the performance and longevity of perovskite-based devices [7–9]. This instability predominantly arises from ion migration within the perovskite material, resulting in defects and non-radiative recombination [7–9]. For instance, the PCE drops sharply from 14.62% to 2.36% after ninth thermal cycle for a perovskite structure with TiO_2 and spiro-MeOTAD as ETL and HTL, respectively [10]. Moreover, numerous factors have been suggested to contribute to the origin of hysteresis. Among them, variations in charge transport resulting from trapping and de-trapping at deep trap sites formed by defects, and ion migration and accumulation associated to changes in interfacial field and barriers [11,12].

To attain enduring stability and consistent high performance in PSCs, it is imperative to comprehensively investigate the degradation mechanisms of these layers under diverse conditions. Such understanding is vital for transitioning this technology from laboratory experimentation to industrial-scale production [13–15]. Several strategies were investigated to improve stability, including encapsulation techniques, compositional tuning, and interface engineering. The application of interface changes and passivation layers has proven successful in improving stability in operating setting [16,17]. Nevertheless,

these developments, problems still exist, highlighting the continuous research required to produce reliable and long-lasting perovskite solar cells fit for practical use [18,19].

The aim of this work is to study the instability issues prevalent in perovskite solar cells using numerical modeling, by simulation software SCAPS. The n-i-p structure of the solar cell included Titanium dioxide (TiO_2) as ETL, methyl-ammonium (MA) cations (CH_3NH_3+), lead (Pb_2+) cations, and iodide (I-) anions ($MAPbI_3$) as the active region for absorption and Spiro-OMeTAD ((N,N'-bis(2,2',7,7'-tetrakis(N,N-di-p-methoxyphenylamine)-9,9'-spiro-bi-fluorene))) as HTL. Various scenarios are analyzed to understand the impact of interface defects (ETL/perovskite, perovskite/HTL) as well as the bulk one.

The simulation enables the insertion of multiple defects at the interfaces, imitating as possible real-world conditions and providing insights into the mechanisms underlying perovskite instability. Through numerical modeling, researchers can investigate the complex interactions between materials and interfaces, optimize device design, and propose strategies to enhance stability and performance. This approach not only accelerates the development of stable perovskite solar cells but also contributes to advancing the understanding of fundamental processes governing their behavior.

This dissertation is organized as follows : Chapter 1 is about An Overview on perovskite solar cells . Chapter 2 explores Instability issue in perovskite solar cells mainly from recent literature. Chapter 3 study the possible defects monitoring instability issue in the solar cell by scaps.

References of Introduction

[1] Park, N. G., 2020, "High Efficiency Perovskite Solar Cells: Materials and Devices Engineering," Transactions on Electrical and Electronic Materials, 21(1).

[2] Roy, P., Ghosh, A., Barclay, F., Khare, A., and Cuce, E., 2022, "Perovskite Solar Cells: A Review of the Recent Advances," Coatings, 12(8).

[3] Li, X., Yu, H., Liu, Z., Huang, J., Ma, X., Liu, Y., Sun, Q., Dai, L., Ahmad, S., Shen, Y., and Wang, M., 2023, "Progress and Challenges Toward Effective Flexible Perovskite Solar Cells," Nanomicro Lett, 15(1).

[4] Liang, X., Ge, C., Fang, Q., Deng, W., Dey, S., Lin, H., Zhang, Y., Zhang, X., Zhu, Q., and Hu, H., 2021, "Flexible Perovskite Solar Cells: Progress and Prospects," Front Mater, 8.

[5] Zhang, P., Li, M., and Chen, W. C., 2022, "A Perspective on Perovskite Solar Cells: Emergence, Progress, and Commercialization," Front Chem, 10.

[6] Chowdhury, T. A., Bin Zafar, M. A., Sajjad-Ul Islam, M., Shahinuzzaman, M., Islam, M. A., and Khandaker, M. U., 2023, "Stability of Perovskite Solar Cells: Issues and Prospects," RSC Adv, 13(3), pp. 1787–1810.

[7] Kim, B., and Seok, S. Il, 2020, "Molecular Aspects of Organic Cations Affecting the Humidity Stability of Perovskites," Energy Environ Sci, 13(3), pp. 805–820.

[8] Zhao, P., Kim, B. J., and Jung, H. S., 2018, "Passivation in Perovskite Solar Cells: A Review," Mater Today Energy, 7, pp. 267–286.

[9] Boyd, C. C., Cheacharoen, R., Leijtens, T., and McGehee, M. D., 2019, "Understanding Degradation Mechanisms and Improving Stability of Perovskite Photovoltaics," Chem Rev, 119(5), pp. 3418–3451.

[10] Sharma, R., Sharma, A., Agarwal, S., and Dhaka, M. S., 2022, "Stability and Efficiency Issues, Solutions and Advancements in Perovskite Solar Cells: A Review," Solar Energy, 244, pp. 516–535.

[11] Miller, D. W., Eperon, G. E., Roe, E. T., Warren, C. W., Snaith, H. J., and Lonergan, M. C., 2016, "Defect States in Perovskite Solar Cells Associated with Hysteresis and Performance," Appl Phys Lett, 109(15).

[12] Son, D. Y., Kim, S. G., Seo, J. Y., Lee, S. H., Shin, H., Lee, D., and Park, N. G., 2018, "Universal Approach toward Hysteresis-Free Perovskite Solar Cell via Defect Engineering," J Am Chem Soc, 140(4), pp. 1358–1364.

[13] Zhao, P., Kim, B. J., and Jung, H. S., 2018, "Passivation in Perovskite Solar Cells: A Review," Mater Today Energy, 7, pp. 267–286.

[14] Wang, P., Wu, Y., Cai, B., Ma, Q., Zheng, X., and Zhang, W. H., 2019, "Solution-Processable Perovskite Solar Cells toward Commercialization: Progress and Challenges," Adv Funct Mater, 29(47).

[15] Kumar, A., Kumar, D., Jain, N., Kumar, M., Ghodake, G., Kumar, S., Sharma, R. K., Holovsky, J., Saji, V. S., and Sharma, S. K., 2023, "Enhanced Efficiency and Stability of Electron Transport Layer in Perovskite Tandem Solar Cells: Challenges and Future Perspectives," Solar Energy, 266.

[16] Li, T., Yuan, X. Z., Zhang, L., Song, D., Shi, K., and Bock, C., 2020, "Degradation Mechanisms and Mitigation Strategies of Nickel-Rich NMC-Based Lithium-Ion Batteries," Electrochemical Energy Reviews, 3(1), pp. 43–80.

[17] Cao, F., Zhang, P., Sun, H., Wang, M., and Li, L., 2022, "Degradation Mechanism and Stability Improvement of Formamidine-Based Perovskite Solar Cells under High Humidity Conditions," Nano Res.

[18] Luo, X., Lin, X., Gao, F., Zhao, Y., Li, X., Zhan, L., Qiu, Z., Wang, J., Chen, C., Meng, L., Gao, X., Zhang, Y., Huang, Z., Fan, R., Liu, H., Chen, Y., Ren, X., Tang, J., Chen, C. H., Yang, D., Tu, Y., Liu, X., Liu, D., Zhao, Q., You, J., Fang, J., Wu, Y., Han, H., Zhang, X., Zhao, D., Huang, F., Zhou, H., Yuan, Y., Chen, Q., Wang, Z., Liu, S. F., Zhu, R., Nakazaki, J., Li, Y., and Han, L., 2022, "Recent Progress in Perovskite Solar Cells: From Device to Commercialization," Sci China Chem, 65(12), pp. 2369–2416.

[19] Wu, T., Qin, Z., Wang, Y., Wu, Y., Chen, W., Zhang, S., Cai, M., Dai, S., Zhang, J., Liu, J., Zhou, Z., Liu, X., Segawa, H., Tan, H., Tang, Q., Fang, J., Li, Y., Ding, L., Ning, Z., Qi, Y., Zhang, Y., and Han, L., 2021, "The Main Progress of Perovskite Solar Cells in 2020–2021," Nanomicro Lett, 13(1).

Chapter 1

An Overview on perovskite solar cells

1.1 Introduction

Solar energy is a valuable renewable energy resource, as one hour of continuous sunlight can fulfill annual power requirements. The photovoltaic (PV) effect was discovered in 1839 by Edmund Becquerel , and Selenium photoconductivity was discovered in 1873. Albert Einstein introduced the photoelectric effect in 1905. Silicon-based solar cells were developed in 1918, with the first crystalline silicon-based cell reported in 1954 . Since the 1990s, developed countries have released grants for solar cell development, with second-generation and third-generation solar cells emerging. Three generations of solar cells have been developed to demonstrate cost-effective, stable, and efficient devices [1,2].

Researchers are exploring new PV technology that is cost-effective and provides higher photo-electrochemical efficiency (PCE) compared to first-generation Silicon solar cells . Thin film-based perovskite solar cells, categorized under the third generation, have gained popularity due to their desirable properties, improved stability, and PCE. Perovskites are essentially a family of compounds with an ABX_3 structure. These cells have been recognized as potential alternatives to Silicon solar cells due to their ease of fabrication, low cost, high absorption coefficient, controllable band gap, and high charge carrier mobility.

The PCE of perovskite solar cells has reached 3.1% to 25.7% for single junction and 31.3% for tandem architecture. However, factors such as high cost of gold electrodes, temperature, additives, degradation, toxicity of lead, thermal stress, and interfaces affect their performance. The maximum lifetime of perovskite solar cells is only a year, which poses a major obstacle to their commercialization [1,3–5].

In this chapter we present the performance of perovskite solar cells, focusing on historical background, properties, chemical nature, device architecture, development routes, and commercialization strategy, with recommendations for further improvement.

1.2 History of perovskite solar cells

1.2.1 Single junction perovskite solar cells

This section details the development history of perovskite material since 1839, including its demonstration in 2009 and subsequent power conversion efficiencies. The history is summarized in a pictorial representation in Figure 1.1 and tabulated in Table 1, providing a comprehensive overview of the progress made in this field [1].

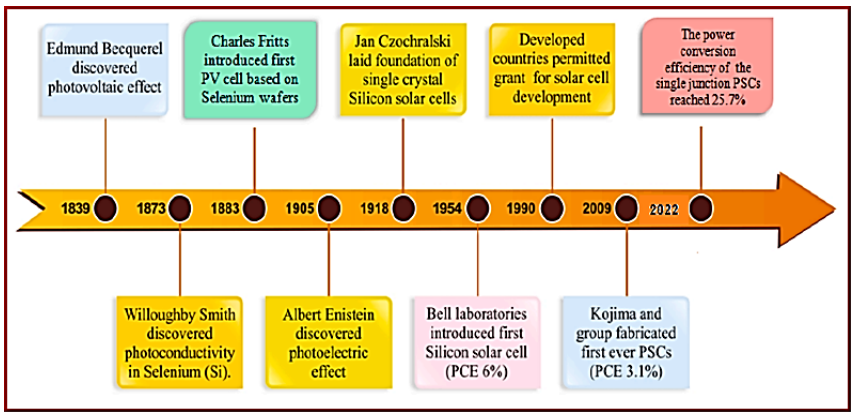

Figure 1.1: Schematic representation of development history to the solar cells [1].

In 1839, $CaTiO_3$ was discovered in Russia's Ural Mountains. Russian mineralogist Alexander Kammerer transported the sample to Berlin, where it was analyzed by Gustav Rose. The mineral was named perovskite after Russian mineralogist Count LevAleksevich Perovski. Its structure evolved to ABX_3 . In the 1990s, researchers studied the opto-electronic properties of organic and inorganic perovskites, finding their desirable features for solar cells . In 2009, Kojima and others used perovskite as a liquid sensitizer in dye-sensitized solar cells (DSSCs) , achieving efficiency of 3.8% and 3.1%, respectively. In 2011, $MAPbI_3$ quantum dots increased efficiency to 6.54%, but instability was caused by liquid electrolytes . In 2012, incorporating Spiro-OMeTAD as a hydrogen transfer layer (HTL) improved the device's performance, achieving a 9.7% PCE and a 500-hour lifetime [1,5,6].

In 2015, Li-doped mesoporous titania layer ($m - TiO_2$) was used to achieve a 19.3% photoelectric efficiency(PCE) . In 2016, a polymer named poly (methylmethacrylate) (PMMA) was used for fabrication, improving electronic and charge transport properties and nucleation processes . In 2017, multiple cations with FA and mixed halide anions were used as absorber layers, achieving 19.7% PCE for devices with 1 cm^2 area and 22.1% for small scale devices . In 2018, EDTA complexed $SnO_2/E - SnO_2$ was used as an ETL in planar perovskite solar cells, achieving 21.6% PCE. In 2019, phenethylammonium iodide (PEAI) was used for post-treatment of mixed perovskite ($FA_{1-x}MA_xPbI_3$) based solar cells, providing a higher PCE of 23.32% . The reported PCE for single junction perovskite solar cells is 25.7% [3,5–7].

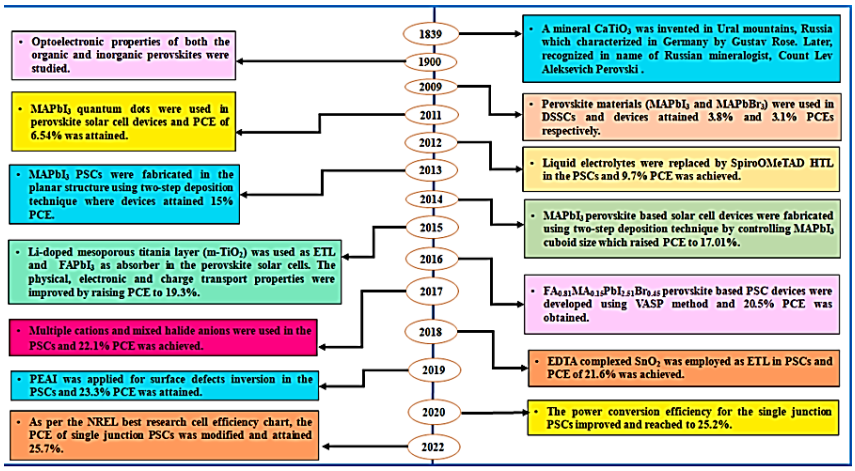

Figure 1.2: A schematic representation of development history to the PSCs [1].

1.2.2 Multi-junction/ tandem perovskite solar cells

The Shockley Queisser limit, based on detailed balance limits, suggests that single junction devices can be overcome by tandem architecture . The concept was initially introduced for III-V compound semiconductors, offering a wide range of optical energy band gap and lattice parameters. The ab-initio optical energy band-gap was calculated using detailed balance limits . Two junction $(Ga_{0.5}In_{0.5}P)/GaAs$ based tandem solar cells achieved a PCE of 27.3% using the metal organic chemical vapor deposition method . Recently, a methyl-substituted carbazole mono layer was applied to perovskite/Si tandem solar cells, providing a PCE $>$ 29% [1,2,8].

Tandem devices can be classified into three categories based on electrical connections: two-terminal (2T), three-terminal (3T), and four-terminal (4T) . These devices harvest more sunlight and have higher performance compared to single junction devices. The two-terminal (2T) tandem architecture requires a single transparent electrode, reducing fabrication costs and material usage. The four terminal (4T) tandem architecture stacks both bottom and top sub-cells independently, providing ease of processing and optimal fabrication conditions [1,9].

The 4T tandem devices operate via four electrical connections, with at least three showing high transparency in the wide spectral range and one in the infrared range. This makes the device less sensitive to spectral variations and reduces choice limitation to top sub-cell band gap. The phenomenon of luminescent coupling in 2T tandems is crucial, as it reduces current mis-matching and increases flexibility in sub-cell thickness. This technology has been shown to significantly decrease current mis-matching in 2T perovskite/silicon tandems [1,10].

The 2T tandems face drawbacks like current mismatching and 4T devices face higher fabrication costs and optical losses. 3T tandems can overcome these issues by employing three terminals for current extraction . These tandems consist of front and back contacts,

Table 1.1: Brief development history of perovskite material and single junction PSCs concerned [1,2,6].

Year	Development detail	PCE (%)
1839	- A mineral $CaTiO_3$ was discovered in Ural Mountains of Russia, Alexander Kämmerer transferred and handed- over to Gustav Rose. As per suggestion of Kämmerer, Rose named it in the name of mineralogist and politician, Count Lev Aleksevich Perovski.	-
1990	- Optoelectronic properties of organic and inorganic perovskites were reported.	-
2009	- Perovskite materials (MAPbI (I) and $MAPbBr_3$ (II)) were used in $DSSCs^2$ liquid sensitizers where the devices are named as perovskite solar cells.	3.8 (I) 3.1(II)
2011	- $MAPbI_3$ quantum dots (nanocrystalline material) were used in the perovskite solar cells.	6.54
2012	- Liquid electrolyte was replaced first time by SpiroOMeTAD (HTL) in the perovskite solar cells.	9.7
2013	- MAPbI $_3$PSCs$^{\text{were fabricated in the}}$ planar structure using two-step deposition technique.	15
2014	- MAPbI perovskite based solar cells were fabricated using two-step deposition technique. The size of $MAPbI_3$ cuboid was controlled which raised PCE.	17.01
2015	- Li-doped mesoporous titania layer (m- TiO_2) was used as ETL in perovskite solar cells. The electronic properties and charge transportation was improved.	19.3
2015	- $MAPbI_3$ was replaced by $FAPbI_3$ in the perovskite solar cells which improved physical properties and raised PCE.	20.1
2016	- $FA_{0.81}MA_{0.15}PbI_{2.51}Br_{0.45}$ perovskite devices were developed using VASP method.	20.5
2016	- PMMA polymer was used in the perovskite solar cells.	21.6
2017	- Multiple cations and mixed halide anions were applied in the perovskite solar cells.	22.1
2018	- EDTA complexed $SnO_2/E-SnO_2$ was employed as electron transport layer.	21.6
2019	- PEAI was applied for surface defects inversion which augmented the PCE.	23.32
2020	- The power conversion efficiency for the single junction improved, data taken from the solar cell PCE table.	25.2
2021	The PCE for the single junction was attained as revealed by PCE table.	25.5
2022	- PCE to PSCs is increased as per latest NREL, USA best research cell efficiency chart.	25.7

with the third terminal extraction either through an interdigitated back contact or middle contact. Under PV operation, maximum power can be extracted from the 3T device without current mismatching [1,11].

Perovskite-based tandems have shown promising results, with perovskite-based top sub-cells achieving PCEs of 17% and 18.6%, respectively. In 2016, monolithic two-terminal (2T) and mechanically stacked four terminal (4T) tandems combining low and high band gap perovskites achieved better PCEs. Recently, the recorded PCEs for perovskite/Si and perovskite/CIGS monolithic tandems reached 31.3% and 24.2%, respectively. The

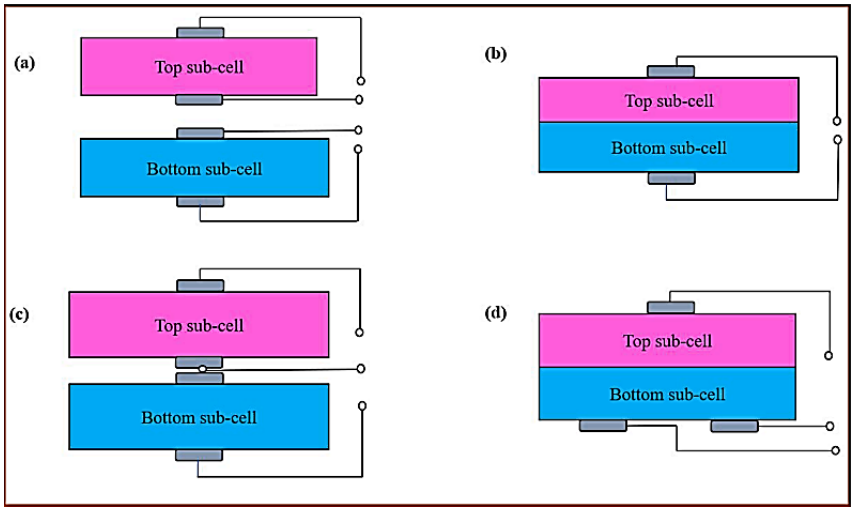

Figure 1.3: Typical illustration of electrical connections for (a) four-terminal (4T), (b) two-terminal (2T), (c) three-terminal (3T) middle and (d) three-terminal (3T) IBC tandem devices [1].

structure of perovskite materials and factors determining stability and PCE of PSCs are also discussed [1].

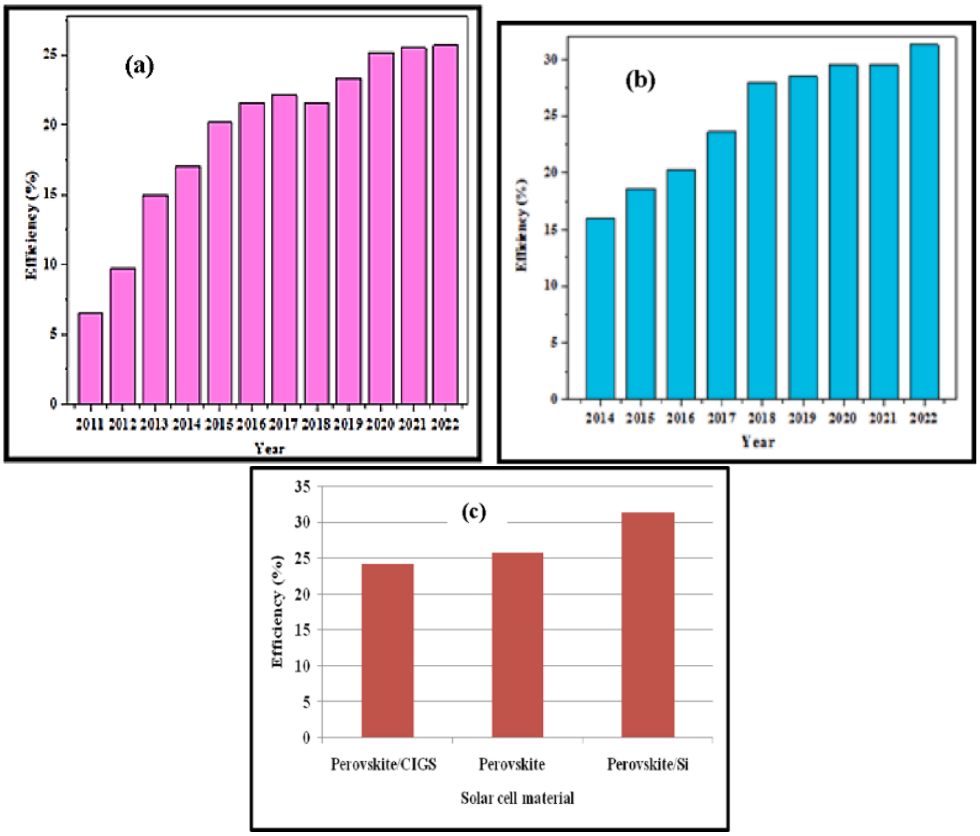

Figure 1.4: Bar diagram representing (a) PCE for the single junction PSCs during 2011–2022, (b) PCE for PSC based tandems during 2014–2022 and (c) an overview for the single junction PSC's PCE along with tandems concerned [1].

1.3 Structure of perovskite materials

Perovskites are compounds with a general crystal formula ABX_3 , with A and B being cations and X being an anion. They are commonly used in solar cell devices, with two types of halide perovskites: Alkali and Organic-inorganic based halide perovskites is represented in Figure 1.5. Alkali based halide perovskites have alkali monovalent cation (A), divalent cation (B), and halogen anion (X). Organic-inorganic based halide perovskites comprise organic monovalent cation (A) and halogen anion (X) . The structure and phase of perovskite materials are strongly affected by environmental conditions like temperature, moisture, and pressure. The most commonly used perovskite in solar cell devices is Methylammonium lead iodide ($CH_3NH_3PbI_3$) ,which has a volatile nature and can be replaced by Formamidinium [1,12].

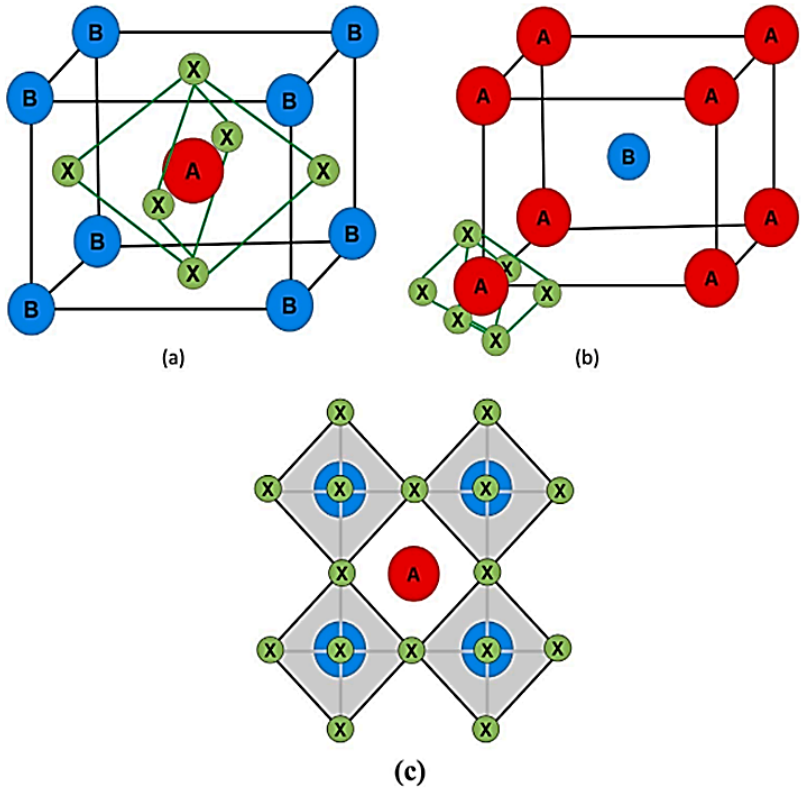

Figure 1.5: structure of unit cell to ABX_3 cubic perovskite wherein structures have (a) B at $< 0, 0, 0 >$ position, (b) A at position and (c) BX_6 octahedral structure [1].

Perovskite materials have a similar crystal structure to Calcium Titanate ($CaTiO_3$), with cations and anions forming cubic and octahedral geometries [1].

$$t = R_a + \frac{R_x}{\sqrt{2(R_b + R_x)}} \tag{1.1}$$

An ideal perovskite must be structurally stable, satisfies Goldschmidt tolerance and octahedral factors, which determine its stability.

The octahedral factor μ determines distortion and stability in perovskites, with a stable structure within the 0.45-0.89 range [1].

$$\mu = \frac{R_b}{R_x} \tag{1.2}$$

The next section discusses perovskite properties and chemical stability under various environmental conditions.

1.4 Properties and chemical nature

Halide-based perovskite materials are ideal for solar cell applications due to their high absorption coefficient, tunable band gap, electron and hole transportation, diffusion carrier length, electron mobility, and photoluminescence. These properties can be customized by controlling concentration, shape, and size, making them suitable for perovskite-based solar cell development [2,7]. The chemical stability of a perovskite structure under various environmental conditions is crucial for its durability and sustainability . Organo-metallic perovskites undergo a chain of chemical reactions under various conditions, degrading into components or other chemicals. The chemical reaction for methylammonium lead iodide (CH_3NH_3PbI) perovskite is as [13]:

$$CH_3NH_3I + PbI_2 \leftrightarrow CH_3NH_3PbI_3 \tag{1.3}$$

and in the presence of water and oxygen, it decomposes [14]:

$$CH_3NH_3PbI_3 \leftrightarrow CH_3NH_3I_{(ac)} + PbI_{2(s)} \tag{1.4}$$

$$CH_3NH_3I_{(ac)} \leftrightarrow CH_3NH_{2(ac)} + HI_{(ac)} \tag{1.5}$$

$$4HI_{(ac)} + O_{2(g)} \leftrightarrow 2I_{(s)} + 2H_2O_{(1)} \tag{1.6}$$

$$2HI_{(ac)} \leftrightarrow H_{2(g)} + I_{2(s)} \tag{1.7}$$

At second stage to the reaction represented by Eq.(1.5), CH_3NH_3I degrades into CH_3NH_2 and HI and in third stage by Eq.(1.6), HI further degrades in presence of Oxygen or may degrade into H_2 and I_2 as given by Eq.(1.7) . $CH_3NH_3PbBr_3$ and $CH_3NH_3PbI_2Cl$ perovskites also undergo similar degradation mechanisms. The device architecture is essential for achieving desired PCE in solar cells while maintaining stability [1,14].

1.5 Mechanistic processes in perovskite solar cell

The basic energy diagram and elements of the mechanistic process of perovskite solar cells are represented in Figure.1.6. The key idea behind efficient solar energy conversion is the combination of 'carrier generation' by light absorption and 'charge separation'. In the absorber perovskite (see Figure.1.6(a)), electrons undergo excitation. Figure.1.6(b) shows the electron transport layer (ETL) and hole transport layer (HTL), both in contact with the perovskite. These electrons and holes are separated by an ETL that is conductive to electrons and rejects holes, and by an HTL that allows transport of the holes with no impedance, while blocking electrons, respectively. Such arrangements permit the Fermi level in the metal contacts to equilibrate with the separate Fermi levels of the electrons and holes, generating an external voltage, and to extract the carriers, giving a photocurrent in the external circuit [15].

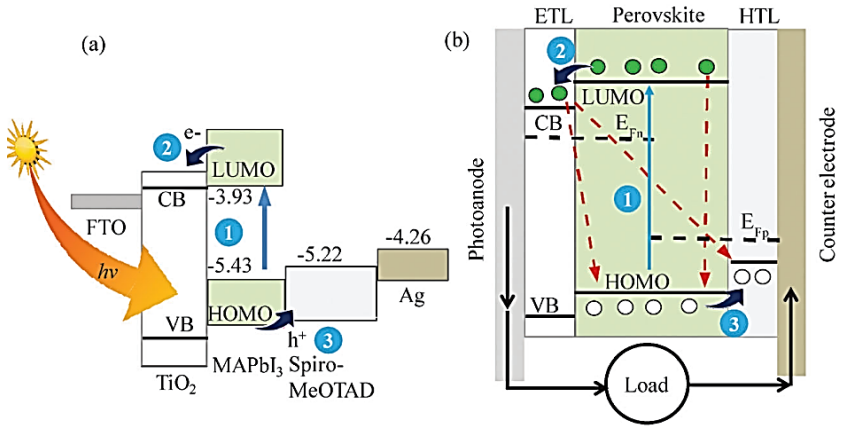

Figure 1.6: (a) Schematic representation of the energy diagram in an PSCs (1) generating electrons and hole carriers that rapidly relax (2) to the conduction band E_C of the ETL TiO_2 and (3) to the HOMO of the HTL, respectively. (b) The scheme of the main process in PSCs, formed by the perovskite absorber material, supplemented by two selective contacts, the ETL and HTL [15].

The present mechanistic representation is explained as follows: the perovskite absorbs light and an excited state (electron–hole pair) is produced. Charge separation can take place at the interface through two processes: injection of a photogenerated electron into a TiO_2 or hole injection into a HTL. Charge separation reactions are in kinetic competition with other reactions, such as exciton annihilation, and lead to photoluminescence, recombination in the perovskite, as well as recombination of the charge carriers at the different interfaces [15].

1.6 Device architecture of single junction perovskite solar cells

Solar cell devices are typically a p-n junction with substrate, electrodes, optical window, and absorber layers. To enhance power conversion efficiency, different architectures have been employed in substrate and superstrate structures. The PCE to PSCs depends on device architecture (mesoporous and planar), growth recipes, and pre- and post-treatments to the constituent layers . Two types of device architectures are reported for PSCs: planar structure (n-i-p) and inverted structure (p-i-n) as depicted in Figure 1.7. In a planar superstrate structure, ETL is coated onto transparent conducting oxide (TCO) coated glass substrates, followed by the perovskite absorber layer and HTL. Various materials are optimized for the constituent layers and electrodes, with materials like Titanium Oxide, Tin Oxide, Zinc Oxide, PCBM, and Aluminum, Silver, Gold, Molybdenum, or Carbon being applied based on their advantages [16].

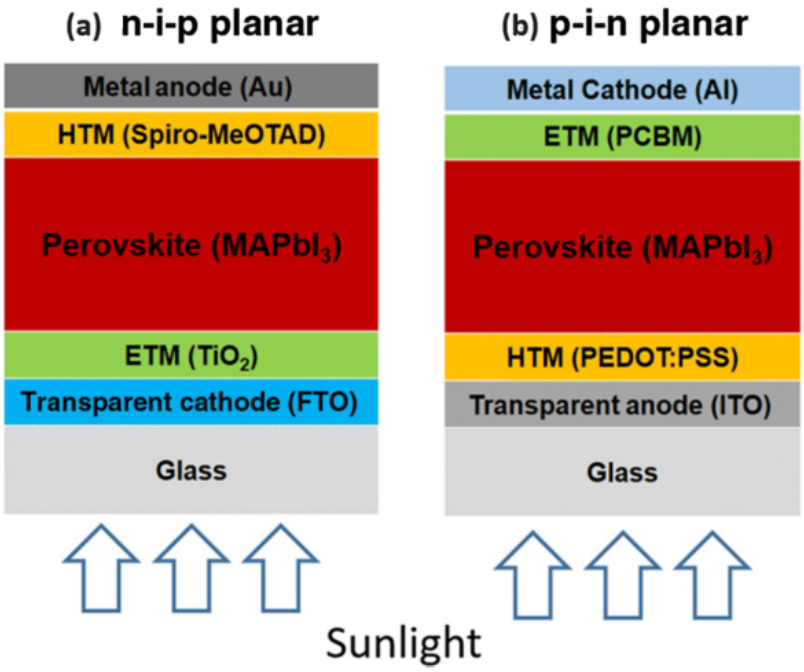

Figure 1.7: Typical device architectures for the PSCs in (a) n-i-p and (b) p-i-n configurations [1].

In an inverted structure, HTL is coated onto TCO substrate, followed by perovskite absorber and ETL, and electrode/metal contact deposition. Common materials for ETL and HTL are PCBM and PEDOT:PSS . Pre- and post-treatments are undertaken to develop better devices. Proper selection of constituent layers is crucial for performance and stability. Superstrate architecture uses solar irradiance from the glass side, while substrate structure uses an opaque base. Top layer must be transparent, cover perovskite layer, and be treated at low temperatures [17].

1.6.1 Electron transport layer (ETL)

The electron transport layer (ETL) plays a crucial role in perovskite solar cell devices. Initially, mesoporous TiO2 was used due to its lower cost, easy processing, and large electron lifetime. Later, organic and inorganic ETLs like PCBM, $TIO_2, ZnO, Al_2O_3, ZrO_3, SnO_2$, SiO_2 were used . Inorganic ETLs are preferred due to their higher stability and lower cost [1,5].

1.6.1.1 Inorganic ETLs

The first reported PSC was made of an inorganic ETL, TiO_2, which achieved PCE 3.81% and 3.1% for $MAPbI_3$ and $MAPbBr_3$. Materials evolution led to improved stability and stability under UV illumination . In 2015, compact $TiO_2/(c-TiO)_2$ was used in PSC devices, achieving higher PCE of 12.2%. In 2018, TiO_2 was enhanced to 16.75% using compact $TiO_2/(c-TiO)_2$. However, TiO_2 is commonly used due to degraded electron transport materials under UV illumination. ZnO became widely used due to its higher stability and electron mobility. ZnO nanoparticles and nanorods are increasingly used as ETLs as an alternative to $meso-TiO_2$, as they can be processed at low temperatures. They have achieved a PCE of 18.9% with better stability compared to TiO_2 ETL-based devices. Doping with n-type NPs has also improved performance. Al-doped ZnO nanorods have shown PCEs of 8.5% without and 10.7% with doping . However, chemical instability in ZnO at low temperatures and instability in the UV region have led to potential replacements like SnO_2 [1,5,12,18].

1.6.1.2 Organic ETLs

Fullerene C_{60} and its derivatives are commonly used in inverted structures due to their tunable band gap and high electron mobility. $PC_{61}BM$ and $PC_{71}BM$ have been used as ETLs in $CH_3NH_3PbI_3$ based PSCs, achieving 9.92% and 16.32% PCEs, respectively. A new organic ETL TDTP was introduced , achieving 18.2% PCE. Wang and coworkers spin coated fullerene bilayers on perovskite layers, achieving 12.2% PCE. The use of combination of bilayers (2ETLs) like SnO_2/TiO_2 , SnO_2/ZnO, and TiO_2/ZnO has been applied to improve stability in perovskite solar cells (PSCs). TiO_2/ZnO bilayers have shown enhanced PCE of 17.2%, while SnO_2/TiO_2 bilayers have achieved greater PCE of 15.2%. SnO_2 is the most popular inorganic ETLs due to improved stability and PCE, while PCBM is widely used but degrades easily [16,17].

1.6.2 Hole transport layer (HTL)

The hole transport layer (HTL) significantly influences the stability and photocatalytic efficiency (PCE) of perovskite solar cells. The choice of an appropriate HTM depends

on factors like thermal stability, hole mobility, light-to-power conversion efficiency, cost effectiveness, ease of fabrication, and less sensitivity to humidity and air. hole transport layers are classified in three types namely: inorganic, organic and polymeric HTLs [19,20].

1.6.2.1 Inorganic HTLs

CZTS, an inorganic HTL, gained popularity as a material in PSC devices, achieving a PCE of 12.75% Nickel oxide (NiOx) is another popular inorganic HTM with desirable properties like better chemical stability, lower cost, and desired optical energy band gap . Tang et al used NiO nanocrystals (NCs) of varying thicknesses in inverted planar device architecture to PSCs, achieving better PCE of 15.47% compared to other NCs . In order to present topography and morphology, TEM and SEM images are depicted in Figure 1.8 for pristine and annealed NiO samples [21,22].

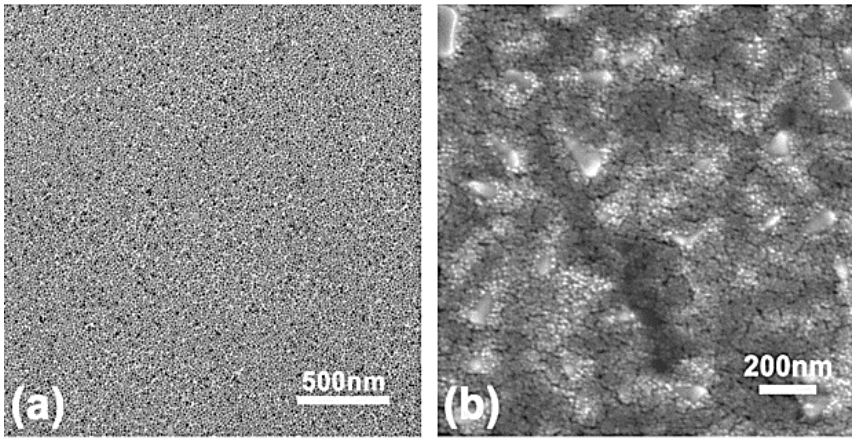

Figure 1.8: (a) TEM image of pristine NiO and (b) SEM image of $500°C$ annealed NiO samples [1].

1.6.2.2 Organic HTLs

Spiro-OMeTAD, an organic HTL with suitable ionization potential and wide absorption spectrum, has been used to enhance PCE and stability in PSC devices. However, its hygroscopic nature reduces device stability . Spiro-OMeTAD's fabrication requires large-scale synthesis, making it costly. In 2018, it resulted in a 22% higher PCE, but stability and cost remain drawbacks . A novel HTM, Nickel phthalocyanine (NiPc), was used, achieving 12.2% PCE and boosted stability where the normalized efficiency decay curves to both the primary and novel HTM as discussed are shown in Figure 1.9 . This has led to the development of polymeric materials as hole transport materials, potentially improving cost effectiveness and power conversion efficiency [19,20,23,24].

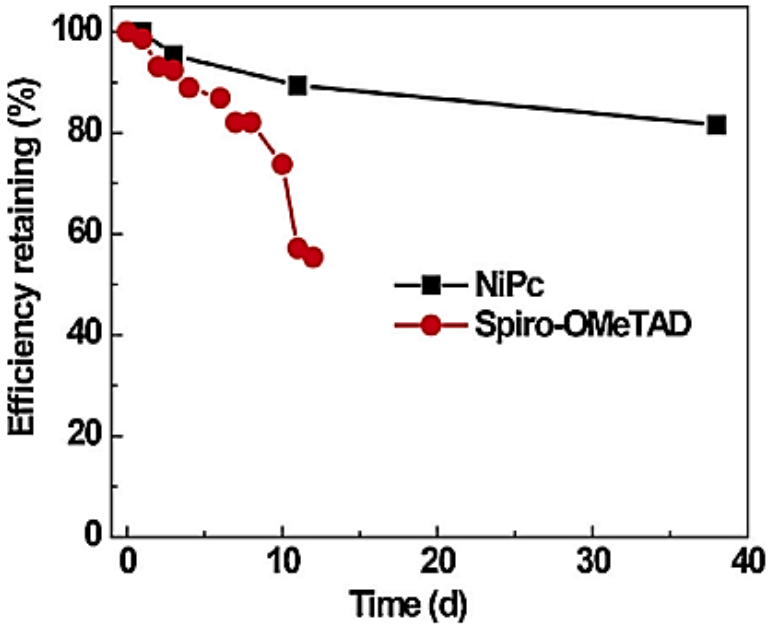

Figure 1.9: Normalized efficiency decay curves for PSCs embracing NiPc and SpiroOMeTAD as HTL [24].

1.6.2.3 Polymeric HTLs

Polymeric HTLs like P3HT and PTAA are commonly used, but P3HT has lower PCE compared to PTAA. To improve carrier density and mobility, P3HT has been combined with Li-TFSI and tBP. Efforts to improve charge carrier transport include removing HTL, introducing buffer layers, and achieving PCEs like 19.4% and 20.2% in molecularly doped F4TCNQ .Inorganic HTLs have good opto-electronic properties and stability, but not outdated organic HTLs. Organic HTLs have good stability but are not cost-effective. Polymeric HTLs only improve device performance, while HTL-free devices face issues with charge transport. The main focus is on combining two different HTMs for improved PCE and stability. Carbon-based HTMs like SWCNT and graphene have achieved a 15.5% PCE .An overview on types, merits and demerits to various ETLs and HTLs is provided in Table 1.2 for better understanding. Perovskite absorbers are currently used in solar cell devices[20,25,2].

1.6.3 Perovskite thin film absorber layers

Perovskite solar cells use a perovskite-based absorber sandwiched between hole and electron transport layers. The optoelectronic properties of perovskite thin films are influenced by factors like morphology, crystallinity, and stoichiometry . Physical and chemical routes are used, including vapor deposition and one- and two-step solution-based methods. Methods include vapor, solution, hybrid, and diffusion. Samples are kept in a graphite block at elevated temperatures to diffuse the compound [2,26].

Table 1.2: Types, merits and demerits to Electron Transport Layers (ETLs) and Hole Transport Layers (HTLs) which are employed so far in perovskite solar cells [20,25].

Types	Merits	Demerits
Organic ETLs (PCBM, ICBA, ThCBM etc.).	- Can be used at low temperatures, and having suitable band gap and good electron mobility.	Stability issues.
Inorganic ETLs (TiO_2, ZnO, Al_2O_3,ZrO_2 SnO_2,SiO_2 etc.)	- Simple fabrication and cost effective, having suitable band gap with longer lifetime and their bilayers are applied to attain higher PCE.	Requires high temperatures and these are having low electron mobility.
Organic HTLs (Spiro-OMeTAD).	- Suitable ionization potential and , wide absorption spectrum.	Hygroscopic nature and stability issues with higher cost.
Inorganic HTLs (CZTS, NiOx etc.).	- Chemically stable, economically , viable and ecofriendly and provides higher performance.	PCE and stability are still lower vis-a-vis to organic HTLs.
Polymeric HTLs (P3HT, PTAA etc.).	- Good environmental stability	Higher cost and lower PCE.

1.6.3.1 Vapor deposition method

The thermal evaporation method, also known as co-evaporation technique, is used to create perovskite absorber layers. This technique was initially used for mixed/hybrid $CH_3NH_3PbI_{3X}Cl_X$ perovskite, achieving a 15.4% PCE. However, it requires high vacuum, increasing operational costs. Solution process methods are widely used for perovskite device development [28].

1.6.3.2 One-step and two-step solution based methods

Chemical-based routes in perovskite solar cell development involve liquid and gas phases, spin coating or dip coating, and varying absorber and transport layers for desired PCE, stability, and cost-effectiveness.

In the one-step solution-based method which is pictorially represented in Figure 1.10 The one-step solution-based method involves selecting desired materials for CH_3NH_3I and PbI_2 , preparing a solution using appropriate solvents, coating it on the substrate, and heat treating the deposited perovskite layer [29].

Others prepared a perovskite absorber layer by dissolving $CH_3NH_3I_3$ and PbI_3 compounds in γ-butylrolacetone (GBL), stirring for 12 hours, and filtering. They found annealed samples showed better PCE compared to pristine samples. Perovskite films did not change color at annealing temperatures between $60 - 200°C$, but at temperatures above $200°C$, they decomposed into $CH_3NH_3I_3$ and PbI_3. A technique was used to prepare a perovskite absorber layer, dissolved in Dimethylformamide and diethyl ether

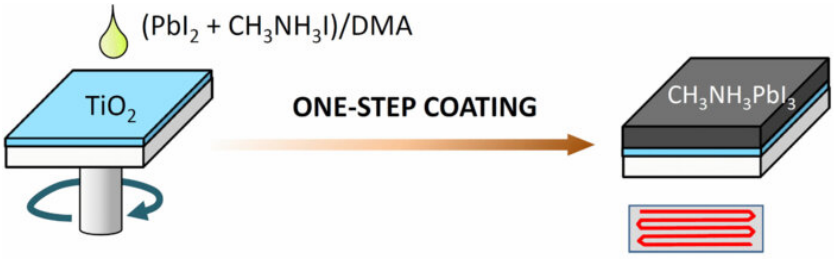

Figure 1.10: Representation of one step solution-based method for developing $CH_3NH_3PbI_3$ perovskite absorbers [28].

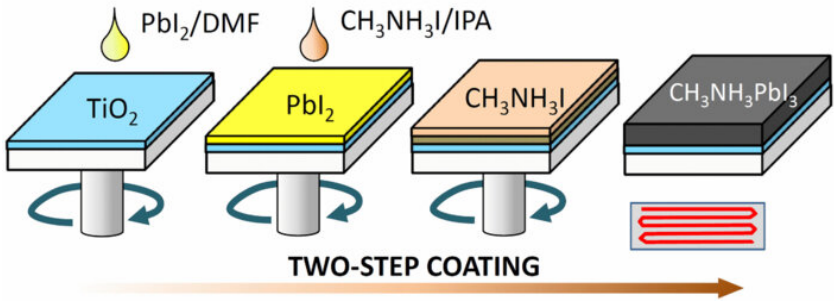

Figure 1.11: Graphical view of two-step solution-based method for developing $CH_3NH_3PbI_3$ absorber layers [28].

solvents. The devices achieved a PCE of 19.7%. The impact of solvents on surface morphology was investigated using one-step approaches.Three solvents (DMF, GBL, and DMF:GBL) were used to achieve compact perovskite layers in PSCs, resulting in PCE of over 6%. Excess PbI_2 may affect device performance, achieving 19% PCE [30]. The two-step solution-based method involves preparing and depositing CH_3NH_3I and PbI_2 solutions sequentially using spin coating, followed by thermal annealing for conversion into $CH_3NH_3PbI_3$ perovskite absorber. However, this method has limitations such as lack of reproducibility and uniformity, making one-step solution-based methods preferred for fabrication of perovskite layers in solar cell devices . A graphical view of two-step solution method is depicted in Figure 1.11. The compositional engineering of perovskite solar cells (PSCs) significantly impacts the performance and stability of the absorber layer due to variations in constituent elements [28].

1.7 Compositional engineering to perovskite solar cells

As stated, the stability and PCE of perovskite solar cells are also affected by varying typical composition AXB_3 of perovskite structure. An impact of compositional variation on stability and PCE have been reported so far where three kinds of variations could be made in monovalent cation (A), divalent cation (B) and halide or anion (X) and details on

the variations along with impact on properties and performance is provided in following sub-sections.

1.7.1 Monovalent cation replacement

Perovskite absorbers replace Methylammonium MA^+ monovalent cation with Formamidinium (FA^+), Cesium (Cs^+), Ethylammonium (EA^+), and Butylammonium (BA^+), with FA^+ and Cs^+ primarily used. The substitution of MA^+ by FA^+ enhances the electrical properties, symmetry, and PCE of perovskite absorbers, but also decreases the band gap . study found that replacing MA^+ with FA^+ resulted in a higher PCE of 12.81% for $FAPbI_3$ compared to 7.39% for $MAPbI_3$ under similar conditions. A study by found that replacing MA^+ with Cs^+ improves thermal stability but lowers PCE compared to MA devices due to orthorhombic phase change. The substitution of MA^+ cations with larger cations like EA^+ or BA^+ resulted in the formation of an orthorhombic phased structure, increasing the band gap of perovskite layers. Perovskite devices with hybrid cation $MA_XFA_{1-X}PbI_3$ absorbers achieved a 14.9% higher PCE by adjusting MA and FA compositions, resulting in a tailored energy band gap. Consequently, hybrid cation $MA_XFA_{1-X}PbI_3$ absorbers were applied by changing MA and FA compositions, and as a result, energy band gap to perovskite absorbers was tailored by achieving higher PCE of 14.9% for composition $MA_{0.6}FA_{0.4}PbI_3$. Higher PCE and stability are two other goals for which hybrid or mixed cation perovskite devices are developed. According to, perovskite devices with hybrid cations have been reported to reach 16.84% PCE and improved stability for over 180 days . Perovskite devices with variable Cs^+ cation composition ($Cs_x(MA_{0.17}FA_{0.83})_{100-x}Pb(I_{0.83}Br_{0.17})_3$) showed improved stability with the intended PCE of 21.1% [31–33].

1.7.2 Divalent cation replacement

Due to its high stability and PCE, lead Pb^{+2} is a divalent cation that is commonly utilized in perovskite absorbers. However, because lead is fatal, non-toxic and environmentally acceptable alternatives are needed; as a result, either tin Sn^{+2} or germanium Ge^{+2} is employed in place of Pb^{+2} in perovskite absorbers .The GW calculation method and ab-initio density functional theory (DFT) were used to study the $MASnI_3$ and $MAPbI_3$ perovskites . The results showed that $MASnI_3$ perovskites may have superior charge carrier transportation and optical properties compared to $MAPbI_3$, making it a potential candidate for lead-free solar cell devices. While Sn and Ge are both environmentally friendly, they have drawbacks under ambient circumstances since Sn^{+2} is rapidly converted to Sn^{+4} and Ge is rarely used due to its unpredictable behavior in the + 2-oxidation state. The use of hybrid or mixed divalent cations in perovskite devices allowed for higher PCE. As a result, devices embracing mixed divalent cations, such as $FAPb_{0.5}Sn_{0.5}I_3$, achieved

higher PCE of 14.09% as opposed to 12.81% for $FAPbI_3$ devices. In a different study, devices comprising hybrid $CH_3NH_3Pb_{0.5}Sn_{0.5}ICl_2$ and $CH_3NH_3Pb_{0.5}Sn_{0.5}I_3$ perovskite absorbers showed greater PCEs of 10.20% and 10.61%, respectively, while devices devoid of Sn showed lower PCEs of 7.39% [25,28,32].

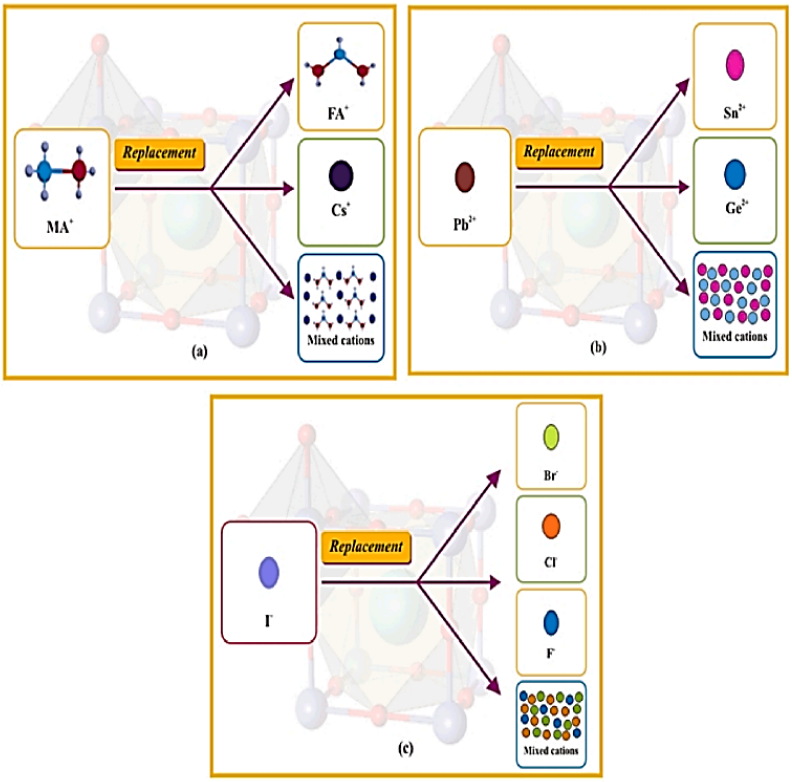

Figure 1.12: Pictorial representation of compositional replacement for (a) monovalent cation (A), (b) divalent cation (B) and (c) anion (X) in perovskite solar cells [1].

1.7.3 Anion/halide replacement

In perovskite absorbers, iodine I^- is typically favored since it has a stronger electro negativity than lead (Pb). Nevertheless, I- can be substituted with bromine Br^-, chlorine Cl^-, or fluorine F^-. Figure 1.12 shows a graphic representation of compositional replacements.

Both the Br^- and the Cl^- have a cubic structure in the ambient, suggesting strong stability; however, the larger crystals in the Br^- cause lattice distortion, which results in a lower PCE. The diffusion length and charge carrier lifespan might also be increased by employing Cl^-; however, Clprecursor has reduced miscibility. As a result of these shortcomings with bromine (Br^-) and chlorine (Cl^-) , mixed halide perovskite absorbers are used in the device in question [34–36].

The varying Br composition $CH_3NH_3Pb(I_{1-X}Br_X)_3$ absorber based devices demonstrated higher PCE of 12.3% for x = 0.2 with stability too. Devices based on the mixed

halide $CH_3NH_3PbI_2Cl$ achieved a PCE of 10.9% with improved stability. However, recent research trends point to the necessity of correctly optimizing modifications to the composition and compositional engineering of perovskite absorbers in order to attain higher PCE with stability. Figure 1.13 is a schematic representation that summarizes the compositional variance in PSCs. The following part effectively outlines these factors along with the potential solutions. Environmental circumstances that deal with device degradation often affect the PCE and stability in PSCs [35,36].

References of Chapter 1

[1] Sharma, R., Sharma, A., Agarwal, S., and Dhaka, M. S., 2022, "Stability and Efficiency Issues, Solutions and Advancements in Perovskite Solar Cells: A Review," Solar Energy, 244, pp. 516–535.

[2] Roy, P., Kumar Sinha, N., Tiwari, S., and Khare, A., 2020, "A Review on Perovskite Solar Cells: Evolution of Architecture, Fabrication Techniques, Commercialization Issues and Status."

[3] "Best Research-Cell Efficiency Chart — Photovoltaic Research — NREL" [Online]. Available: https://www.nrel.gov/pv/cell-efficiency.html. [Accessed: 17-May-2024].

[4] Nelson, J., 2003, "The Physics of Solar Cells," The Physics of Solar Cells.

[5] Kojima, A., Teshima, K., Shirai, Y., and Miyasaka, T., 2009, "Organometal Halide Perovskites as Visible-Light Sensitizers for Photovoltaic Cells," J Am Chem Soc, 131(17), pp. 6050–6051.

[6] Green, M. A., Dunlop, E. D., Hohl-Ebinger, J., Yoshita, M., Kopidakis, N., and Hao, X., 2020, "Solar Cell Efficiency Tables (Version 56)," Progress in Photovoltaics: Research and Applications, 28(7), pp. 629–638.

[7] Yang, D., Yang, R., Priya, S., and Liu, S. (Frank), 2019, "Flexible Perowskit-Solarzellen: Herstellung Und Anwendungen," Angewandte Chemie, 131(14), pp. 4512–4530.

[8] Yamaguchi, M., Dimroth, F., Geisz, J. F., and Ekins-Daukes, N. J., 2021, "Multi-Junction Solar Cells Paving the Way for Super High-Efficiency," J Appl Phys, 129(24).

[9] Khan, M. A. K., Urmi, S. S., Ferdous, T. T., Azam, S., and Alim, M. A., 2021, "Highly Efficient Cesium Titanium (IV) Bromide Perovskite Solar Cell and Its Point Defect Investigation: A Computational Study," Superlattices Microstruct, 156, p. 106946.

[10] Werner, J., Niesen, B., and Ballif, C., 2018, "Perovskite/Silicon Tandem Solar Cells: Marriage of Convenience or True Love Story? – An Overview," Adv Mater Interfaces, 5(1).

[11] Jäger, K., Tillmann, P., Katz, E. A., and Becker, C., 2021, "Perovskite/Silicon Tandem Solar Cells: Effect of Luminescent Coupling and Bifaciality," Solar RRL, 5(3).

[12] Lin, L., Jones, T. W., Yang, T. C. J., Duffy, N. W., Li, J., Zhao, L., Chi, B., Wang, X., and Wilson, G. J., 2021, "Inorganic Electron Transport Materials in Perovskite Solar Cells," Adv Funct Mater, 31(5).

[13] Kundu, S., and Kelly, T. L., 2017, "Improving the Moisture Stability of Perovskite Solar Cells by Using PMMA/P3HT Based Hole-Transport Layers," Mater Chem Front, 2(1), pp. 81–89.

[14] Gujar, T. P., Unger, T., Schönleber, A., Fried, M., Panzer, F., Van Smaalen, S., Köhler, A., and Thelakkat, M., 2017, "The Role of PbI2 in CH3NH3PbI3 Perovskite Stability, Solar Cell Parameters and Device Degradation," Physical Chemistry Chemical Physics, 20(1), pp. 605–614.

[15] Berhe, T. A., Su, W. N., Chen, C. H., Pan, C. J., Cheng, J. H., Chen, H. M., Tsai, M. C., Chen, L. Y., Dubale, A. A., and Hwang, B. J., 2016, "Organometal Halide Perovskite Solar Cells: Degradation and Stability," Energy Environ Sci, 9(2), pp. 323–356.

[16] Kumari, N., Patel, S. R., and Gohel, J. V., 2018, "Current Progressand Future Prospectiveof Perovskite Solar Cells: Acomprehensive Review," Reviews on Advanced Materials Science, 53(2), pp. 161–186.

[17] Ciro, J., Betancur, R., Mesa, S., and Jaramillo, F., 2017, "High Performance Perovskite Solar Cells Fabricated under High Relative Humidity Conditions," Solar Energy Materials and Solar Cells, 163, pp. 38–42.

[18] Rombach, F. M., Haque, S. A., and Macdonald, T. J., 2021, "Lessons Learned from Spiro-OMeTAD and PTAA in Perovskite Solar Cells," Energy Environ Sci, 14(10), pp. 5161–5190.

[19] Rombach, F. M., Haque, S. A., and Macdonald, T. J., 2021, "Lessons Learned from Spiro-OMeTAD and PTAA in Perovskite Solar Cells," Energy Environ Sci, 14(10), pp. 5161–5190.

[20] Wang, H., Yu, Z., Jiang, X., Li, J., Cai, B., Yang, X., and Sun, L., 2017, "Efficient and Stable Inverted Planar Perovskite Solar Cells Employing CuI as Hole-Transporting Layer Prepared by Solid–Gas Transformation," Energy Technology, 5(10), pp. 1836–1843.

[21] Patel, S. B., Patel, A. H., and Gohel, J. V., 2018, "A Novel and Cost Effective CZTS Hole Transport Material Applied in Perovskite Solar Cells," CrystEngComm, 20(47), pp. 7677–7687.

[22] Tang, J., Jiao, D., Zhang, L., Zhang, X., Xu, X., Yao, C., Wu, J., and Lan, Z., 2018, "High-Performance Inverted Planar Perovskite Solar Cells Based on Efficient Hole-Transporting Layers from Well-Crystalline NiO Nanocrystals," Solar Energy, 161, pp. 100–108.

[23] Maniarasu, S., Korukonda, T. B., Manjunath, V., Ramasamy, E., Ramesh, M., and Veerappan, G., 2018, "Recent Advancement in Metal Cathode and Hole-Conductor-Free Perovskite Solar Cells for Low-Cost and High Stability: A Route towards Commercialization," Renewable and Sustainable Energy Reviews, 82, pp. 845–857.

[24] Haider, M., Zhen, C., Wu, T., Liu, G., and Cheng, H. M., 2018, "Boosting Efficiency and Stability of Perovskite Solar Cells with Nickel Phthalocyanine as a Low-Cost Hole Transporting Layer Material," J Mater Sci Technol, 34(9), pp. 1474–1480.

[25] Nia, N. Y., Matteocci, F., Cina, L., and Di Carlo, A., 2017, "High-Efficiency Perovskite Solar Cell Based on Poly(3-Hexylthiophene): Influence of Molecular Weight and Mesoscopic Scaffold Layer," ChemSusChem, 10(19), pp. 3854–3860.

[26] Sharma, R., Sharma, A., Agarwal, S., and Dhaka, M. S., 2022, "Stability and Efficiency Issues, Solutions and Advancements in Perovskite Solar Cells: A Review," Solar Energy, 244, pp. 516–535.

[27] Cho, A. N., and Park, N. G., 2017, "Impact of Interfacial Layers in Perovskite Solar Cells," ChemSusChem, 10(19), pp. 3687–3704.

[28] Liu, M., Johnston, M. B., and Snaith, H. J., 2013, "Efficient Planar Heterojunction Perovskite Solar Cells by Vapour Deposition," Nature, 501(7467), pp. 395–398.

[29] Xu, X., Zhang, H., Shi, J., Dong, J., Luo, Y., Li, D., and Meng, Q., 2015, "Highly Efficient Planar Perovskite Solar Cells with a TiO2/ZnO Electron Transport Bilayer," J Mater Chem A Mater, 3(38), pp. 19288–19293.

[30] Kim, H. B., Choi, H., Jeong, J., Kim, S., Walker, B., Song, S., and Kim, J. Y., 2014, "Mixed Solvents for the Optimization of Morphology in Solution-Processed, Inverted-Type Perovskite/Fullerene Hybrid Solar Cells," Nanoscale, 6(12), pp. 6679–6683.

[31] Zhang, R., Liu, D., Wang, Y., Zhang, T., Gu, X., Zhang, P., Wu, J., Chen, Z. D., Zhao, Y., and Li, S., 2018, "Theoretical Lifetime Extraction and Experimental Demonstration of Stable Cesium-Containing Tri-Cation Perovskite Solar Cells with High Efficiency," Electrochim Acta, 265, pp. 98–106.

[32] Kumari, N., Patel, S. R., and Gohel, J. V., 2019, "Superior Efficiency Achievement for FAPbI3-Perovskite Thin Film Solar Cell by Optimization with Response Surface Methodology Technique and Partial Replacement of Pb by Sn," Optik (Stuttg), 176, pp. 262–277.

[33] Pellet, N., Gao, P., Gregori, G., Yang, T. Y., Nazeeruddin, M. K., Maier, J., and Grätzel, M., 2014, "Mixed-Organic-Cation Perovskite Photovoltaics for Enhanced Solar-Light Harvesting," Angewandte Chemie - International Edition, 53(12), pp. 3151–3157.

[34] Ansari, M. I. H., Qurashi, A., and Nazeeruddin, M. K., 2018, "Frontiers, Opportunities, and Challenges in Perovskite Solar Cells: A Critical Review," Journal of Photochemistry and Photobiology C: Photochemistry Reviews, 35, pp. 1–24.

[35] Noh, J. H., Im, S. H., Heo, J. H., Mandal, T. N., and Seok, S. Il, 2013, "Chemical Management for Colorful, Efficient, and Stable Inorganic-Organic Hybrid Nanostructured Solar Cells," Nano Lett, 13(4), pp. 1764–1769.

[36] Lee, M. M., Teuscher, J., Miyasaka, T., Murakami, T. N., and Snaith, H. J., 2012, "Efficient Hybrid Solar Cells Based on Meso-Superstructured Organometal Halide Perovskites," Science (1979), 338(6107), pp. 643–647.

Chapter 2

Instability issue in perovskite solar cells

2.1 Introduction

Perovskite solar cells have emerged as a promising technology for next-generation photovoltaics due to their high efficiency and low-cost fabrication. However, despite their remarkable performance, stability remains a significant challenge hindering their commercial viability. The susceptibility of perovskite materials to moisture, light, heat, and other environmental factors poses a considerable obstacle to their long-term reliability and widespread adoption. This chapter explores the various degradation mechanisms affecting perovskite solar cell stability, along with strategies to mitigate these issues and enhance device durability. Understanding and addressing stability concerns are crucial steps toward realizing the full potential of perovskite solar cells for sustainable energy generation. As given in chapter 1, the structure of PSCs includes a heterojunction device comprising a perovskite active layer, a charge transport layer (CTL), and an electrode [1], [2]. The first PSCs were studied using MAPbI3, a perovskite, which is a light-absorbing material for dyesensitized solar cells, instead of organic dyes. PSCs can be divided into three structures based on the direction of electron movement with respect to the transparent electrode: mesoporous n-i-p, planar n-i-p, and planar p-i-n. In general, various compounds, such as SnO_2 [3], TiO_2 [4], ZnO [5] , and phenyl-C61-butyric acid methyl ester (PCBM) [6], are used as the electron transport layer (ETL) [7]. Moreover, 2,20,7,70-tetrakis[N,N-di(4-methoxyphenyl) amino]-9,90-spiro-bifluorene (spiro-OMeTAD) [8], poly(3,4- ethylenedioxythiophene):poly(styrenesulfonic acid) (PEDOT:PSS) [9], NiOx [10], and copper(I) thiocyanate (CuSCN) [11] have been used as the hole transport layer (HTL).

The perovskite that is used as the active layer in PSCs has anABX_3 structure, and there are primarily single cations (CH_3NH_3 p(MA_p), HC(NH_2)2 p (FA_p), Cs_p, Rb_p) at

the A-site, and metallic cations (Pb_{2p}, Sn_{2p}, Bi_{2p}, Ge_{2p}) at the B-site. In addition, the Xd site is composed of halide anions I, Br, and Cl [12], [13]. Thus, the $MAPbI_3$ perovskite is used in PSCs because it has a structure that satisfies the Goldschmidt tolerance factor (t)[14].

Despite the excellent efficiency of PSCs, perovskite has disadvantages in that it can be easily decomposed by moisture, heat, ultraviolet rays, oxygen, and electric fields [15]. This makes it difficult to satisfy the solar cell conditions that must operate stably for more than 25 years. In addition, it is difficult to produce a uniform large-area perovskite film without pinhole [16]. These instabilities and difficulties in upscaling make the commercialization of PSCs difficult. Essentially, it is essential to increase the stability and efficiency of PSCs to achieve commercialization. Therefore, numerous studies in various fields, such as structural engineering, additive engineering, fabrication deformation, and interface engineering, are currently ongoing to increase the stability and efficiency of PSCs [17], [18]. Currently, the highest PSC efficiency achieved is 25.7% [19].

2.2 Research progress in the stability of PSCs

The long-term stability of the absorbing layer/charge transport layer (ETL/HTL) is a significant challenge for commercializing PV technology. Halide perovskite materials are unstable, limiting the lifetime of PSCs. Understanding degradation in different conditions is crucial for achieving long-term stability and high PCE in PSCs (Figure 2.1). Intrinsic problems, such as chemical instability, originate from the perovskite material. The structure of perovskite material influences its optoelectronic characteristics, including bandgap, absorption cross-section, and charge carrier motilities Crystal distortion caused by phase changes can reduce photovoltaic efficiency.

Perovskites undergo state transitions, including cubic, tetragonal, and orthorhombic structures. Phase transitions from temperature and external pressure must be considered when fabricating and operating PSCs. A-site mixing can create larger phase stability, and issues can be resolved using additivities, mixed halide perovskite, or microstructural phase control engineering[20], [21]. Extrinsic environmental factors like water, oxygen, UV light, and heat cause perovskite layer degradation, impacting PSC stability [22], [23]. Strategies include additivities, barrier layers, and surface modifications. Recent progress in ETL stability includes 2D/3D hetero-structured[24], [25].

2.2.1 Stability against moisture-induced degradation

Moisture-induced stability is the primary factor for the degradation of perovskite materials, with the decomposition mechanism involving water-induced hydrolysis of the perovskite layer. This process involves the formation of PbI_2 and loss of CH_3NH_2 and HI

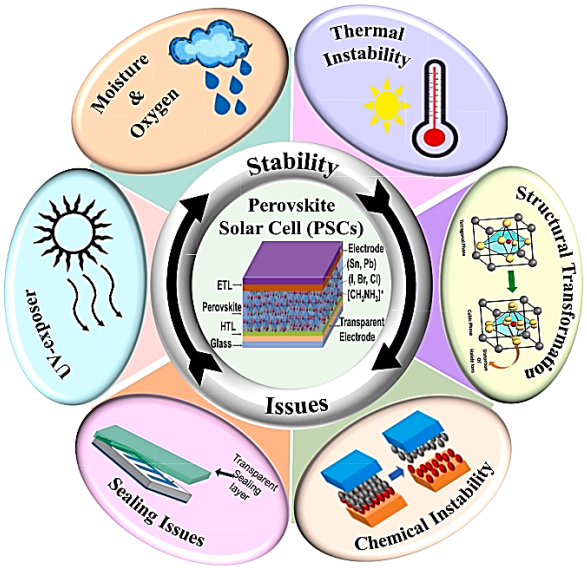

Figure 2.1: Intrinsic and extrinsic issues in the stability of the PSCs [21].

(Eq.2. 1,2)[21],[26].

$$CH_3NH_3PbI_3 \leftrightarrow PbI_2 + CH_3NH_3I \tag{2.1}$$

$$CH_3NH_3I \leftrightarrow HI + CH_3NH_2 \tag{2.2}$$

The stability of photovoltaic solar cells (PSCs) is impacted by the perovskite layer's degradation, which can alter the device color from dark brown to yellow. To prevent this, researchers have used a barrier layer and an ultra-thin Al_2O_3 layer at the interface. This improved stability is demonstrated in TEM images (Figures 2.2(a-b)). The efficiency of an ultra-thin Al_2O_3 layer on $CH_3NH_3PbI_{3-\delta}/Cl_\delta$/ETL of PSCs was 18%, with an estimated 3% increase in efficiency compared to the pristine device (Figure 2.2(c)). XRD patterns of $CH_3NH_3PbI_{3-\delta}/Cl_\delta$/ETL under 40% and 60% humidity conditions are presented in Figures 2.2(d-e). The perovskite film degrades after 10 days in moisture, while an Al_2O_3 layer-coated device enhances stability [27], [28], [29].

Hangoma et al. studied moisture-induced degradation of PSCs and improved device stability using a PCBM layer (Figure 2.2(f)) [30]. Optical micro-scopic images revealed that device electrodes rapidly degraded with exposure to moisture, as depicted in Figure 2.2 (g). Moisture enters PCBM-ETL layer, diffuses into perovskite layer, and decomposes to MAI/HI or I, negatively impacting device PV performance due to PCBM/Al interface degradation (Figure 2.2(h)). A device was fabricated using stearic acid as a barrier between the electrode and ETL to enhance stability against moisture in the perovskite layer (Figure 2.2(i)). Figure 2.2(j) displays the XRD pattern of the untreated and stearic acid-treated device submerged in water [21], [27],[31].

The stearic acid-treated device retained 80% of its original efficiency for 2 hours in water, while the pristine device only retained 10% (Figure 2.2(k)). The stearic acid-treated

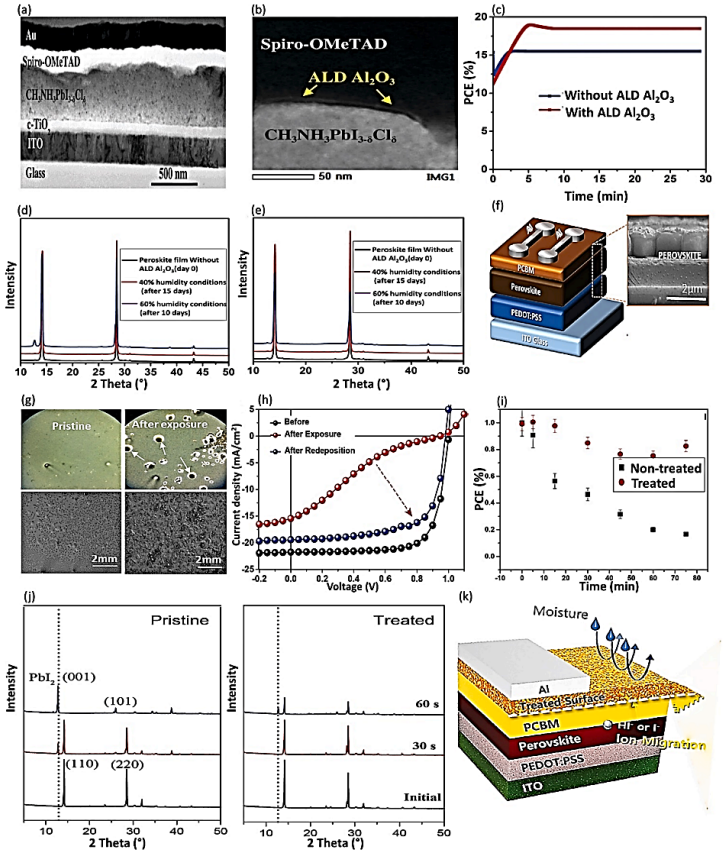

Figure 2.2: (a) Bright field cross-sectional TEM image of glass/ITO-/c-$TiO_2/CH_3NH_3PbI_{(3-\delta)}Cl_\delta$/ALD Al_2O_3/Spiro-OMeTAD device, (b) dark field TEM image of the magnified perovskite/ALD Al_2O_3/Spiro-OMeTAD interface, (c) PCE of the device tracking for 30 min with and without ALD Al_2O_3 barrier layer at the interface of perovskite/ETL. XRD pattern of the perovskite films before and after exposure to moisture (d) without ALD Al_2O_3, (e) with ALD Al_2O_3 barrier layer at the interface of perovskite/ETL. (f) Schematic device structure, glass/ITO/PEDOT: PSS/perovskite/PCBM/Al, and inset the cross sectional SEM image before prolonged exposure to air, (g) Optical microscopic and top-down SEM images of the device before and after exposure to the moisture, (h) J-V characteristics of glass/ITO/PEDOT:PSS/ perovskite/PCBM/Al device before and after exposure to the humidity,(i) Schematic illustration of the PSCs with a surface-treated PCBM using stearic acid monolayers,(j) XRD pattern of the pristine and stearic acid treated devices after exposure to the moisture, (k) Normalised PCEs of the treated and non-treated devices when exposure to water [31].

PCBM layer effectively masks the moisture sensitivity of the perovskite film stability. Huang et al. developed inverted solar cells using a blend of $MAPbI_3$ solution and exfoliated montmorillonite [21], [32], [33].

ExMMT protects perovskite film from moisture for 195 days, improving photovoltaic stability. Exfoliated montmorillonite incorporated perovskite forms a protective shell, enhancing solar cell stability. Wang et al. fabricated $CsPbIBr_2$-based PSCs using a modified Cs-NiOx/N749 HTL layer, improving device performance and humidity stability [34]. Hu et al. developed an inverted planar heterojunction PSC based on a tri-cation

Cs-FA-MA perovskite, introducing a narrow bandgap NFA interface layer, Y6, which effectively suppressed phase separation and moisture-induced degradation (Figure 2.3(a)) [35]. The PCE of PSCs with Y6 and PCBM interface layers showed initial efficiency of 95% for 1400 minutes, while PCBM-based PSCs degraded 95% in 60 minutes (Figure 2.3(b)). Y6 ETL devices showed long-term stability and retained 72% efficiency (Figure 2.3(c)). The NFA interface layer of Y6 was utilized as a near-infrared absorbing moisture barrier in PSCs, enhancing device efficiency from 19% to 21% and enhancing stability to humidity [21], [27].

Encapsulation offers protection against moisture-induced degradation of PSCs by requiring a material with good process ability, low water absorbency, and good permeability. Encapsulation materials should exhibit excellent chemical inertness, mechanical strength, and adhesion. Studies have shown that encapsulated devices retain 70% of their initial efficiency in excess humidity, and provide perovskite stability when exposed to moisture and light [36].

The fabricated device with an n-i-p structure (Glass/FTO/SnO_2/ Perovskite/Spiro-OMeTAD/Au) is designed to protect PSCs from moisture-induced degradation (Figure 2.3(e)).

The device is exposed to flowing N2 containing 85% RH at $25°C$ in a controlled environment box, and the LBIC measurements show the effectiveness of the encapsulated SnO_2 layer (Figure 2.3(d)). The study found that devices without a SnO_2 protection layer rapidly degraded to 50% within 160 minutes and completely degraded in 560 minutes, while those with a SnO_2-protected layer functioned without significant degradation within 1800 minutes (Figure 2.3(f)). Encapsulation with a SnO_2 layer improved device stability and efficiency under extreme humidity conditions, with a significant improvement in thickness (Figure 2.3(g)) [27].

Li et al used 4-[(trifluoromethyl) sulphanyl]-aniline (4TA) to create a polycrystalline perovskite film for improving the stability of PSCs against humidity, demonstrating hydrophobicity after water application (Figs2.3(h-i)). The hydrophilic film, $MAPbI_3 - 4TA$, demonstrated resistance to moisture intrusion, with $MAPbI_3 - 4TA$-based devices maintaining 93% of their initial efficiency, while $MAPbI_3$-based devices lost 77% over 30 days at 55% relative humidity and $25°C$ temperature (Figure 2.3(j)). The efficiency of $MAPbI_3$ decreased due to PbI_2 formation, while the $MAPbI_3 - 4TA$-based device remained unaffected in humidity conditions (Figures 2.3(k-l)) [27]. The $MAPbI_3 - 4TA$ film exhibits minimal lead concentration compared to $MAPbI_3$ at 70% humidity, demonstrating its long-term stability against moisture-induced degradation, demonstrating an effective method for improving the stability of PSCs (Figures 2.3(m-n)) [21], [24], [27].

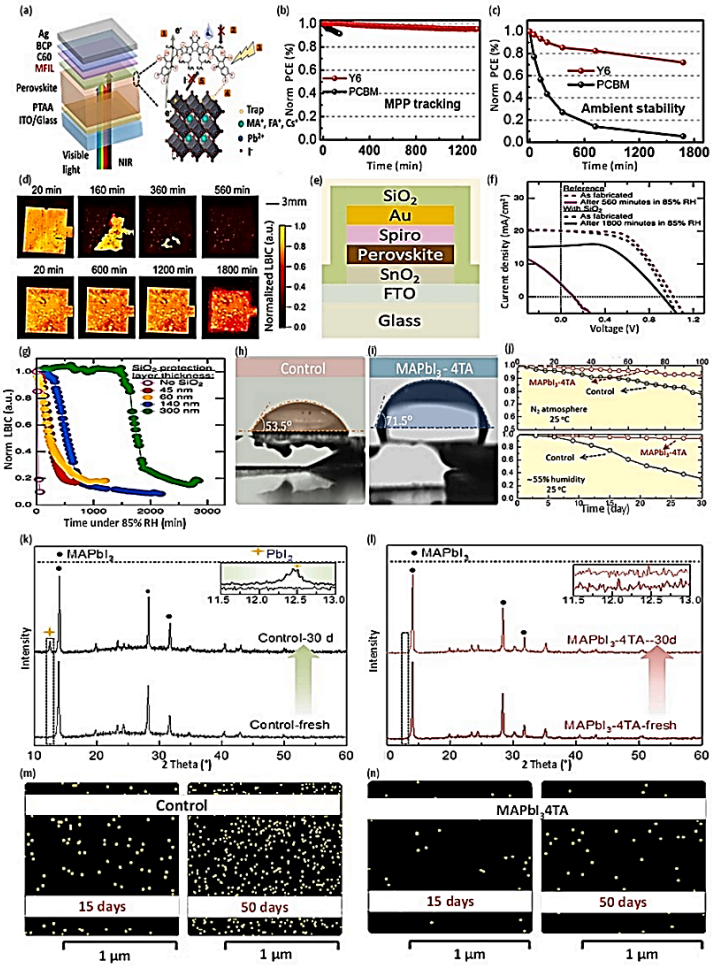

Figure 2.3: (a) Schematic illustration of ITO/PTAA/perovskite/ETL/C60/BCP/Ag fabricated with and without multi-functional interface layer of Y6, (b) PCE of the PSCs with Y6 and PCBM ETL under AM 1.5G 1 sun illumination with the relative humid environment of 60 65%, (c) PCE of PSCs with Y6 and PCBM ETL in a RH of 65% at room temperature under dark [35], (d) Laser Beam Induced Current (LBIC) measurement with the image of devices with and without encapsulation under flowing N_2 containing 85% RH at 25 $°C$, (e) schematic cross-section of encapsulated PSCs device with SiO_2,(f) J-V characteristics of encapsulated and unencapsulated PSCs, and (g) normalized LBIC signal as a function of exposure time [36]. (h-i) water contact angles of $MAPbI_3$ and $MAPbI_3$-4TA films after applying the drops of water, (j) PCE of $MAPbI_3$ and$MAPbI_3$-4TA at 55% RH, (k) and (l) XRD pattern of $MAPbI_3$ and $MAPbI_3$-4TA devices after 30 days exposed at 55% RH and 25 $°C$, (m) and (n) SEM-EDS measurement for the detection of Pb concentration under 70% of RH of $MAPbI_3$ and $MAPbI_3$-4TA for 15 and 50 days, respectively[21],[24].

2.2.2 Stability against thermal-induced degradation

Thermal stability of PSCs is crucial due to their thermal sensitivity, causing decomposition of perovskite materials to PbI_2, with volatile organic cations easily lost at high temperatures,likely due to an inert atmosphere. proceeding with the following equation [37].

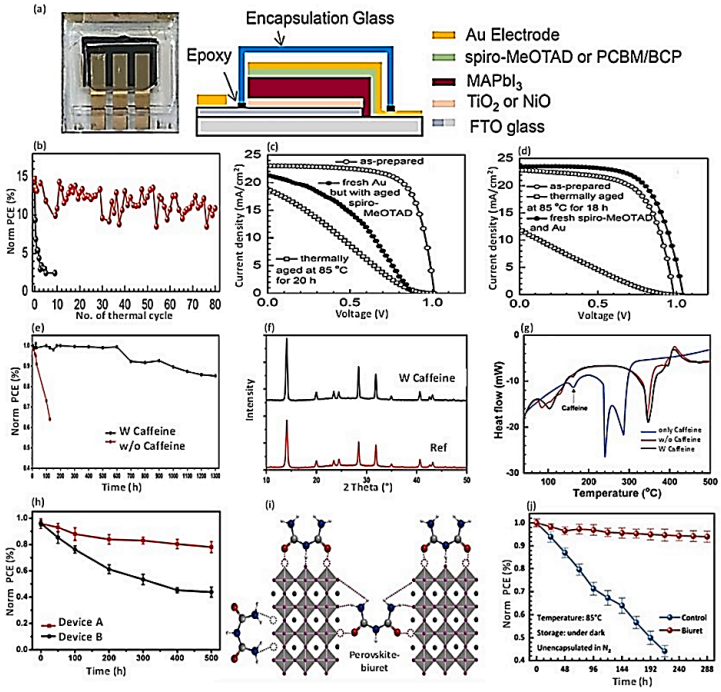

Figure 2.4: (a) Photograph of the encapsulated device along with a cross-section of schematic structure for both types of normal n-i-p and inverted p-i-n structure, (b) PCE of both standard FTO/bl-TiO_2/mp-TiO_2/$MAPbI_3$/spiro-MeOTAD/Au (black) and inverted structure FTO/NiO/$MAPbI_3$/PCBM/BCP/Au (Red) at 85°C in dark environment. The J-V characteristics of the as-prepared and thermally aged device at 85 °C when (c) removed only the aged Au electrode and re-deposited a new Au electrode and (d) removed both Au and spiro-MeOTAD and re-deposited new spiro-MeOTAD layer and an Au electrode [39]. (e) Normalized PCE of PSCs with and without caffeine additivity at 85°C in nitrogen box, (f) XRD pattern of PSCs with and without caffeine additivity at 85°C, (g) thermogravimetric analysis of heat flow as a function of the temperature of caffeine, $MAPbI_3$ and $MAPbI_3$ with caffeine [38]. (h) PCE of device A: FTO/NiOx/perovskite/20PCPB/BCP/Au and device B: FTO/NiOx/perovskite/ PCBM/BCP/Au at 85°C [24]. (i) Schematic design for the biuret-containing MAPbI3 structure, (j) PCE of MAPbI3 and biuret-containing $MAPbI_3$ based solar cell at 85°C in nitrogen box. (k) Photographs of ZnO (ETL) and ZnO-MACl (ETL) based PSCs heated at 85°C thermal stress. XRD pattern of (l) ZnO (ETL), and (m) ZnO-MACl (ETL) based PSCs (n) $MAPbI_3$ perovskite film, $MAPbI_3$ with surface-coated SAN copolymer film, SAN copolymer incorporated $MAPbI_3$ film evaluated at 100 °C for 24 h, (o) Schematic illustration of the device structure of thermal test of devices at 100 °C, PCE of $MAPbI_3$ and with SAN surface coated and incorporated $MAPbI_3$ of two SAN concentrations (p) 0.5 and (q) 1 mg/mL[37].

$$CH_3NH_3PbI_3 \leftrightarrow CH_3NH_2(g) + HI(g) + PbI_{2s} \tag{2.3}$$

Zhao et al. studied the thermal stability of $MAPbI_3$-based inverted and non inverted PSCs at elevated temperatures (Figure 2.4(a)). They found that the standard n-i-p structure showed rapid degradation, while the inverted p-i-n structure showed little degradation when exposed to 85°C and room temperature for 2 hours (Figure 2.4(b)) [27]. The study

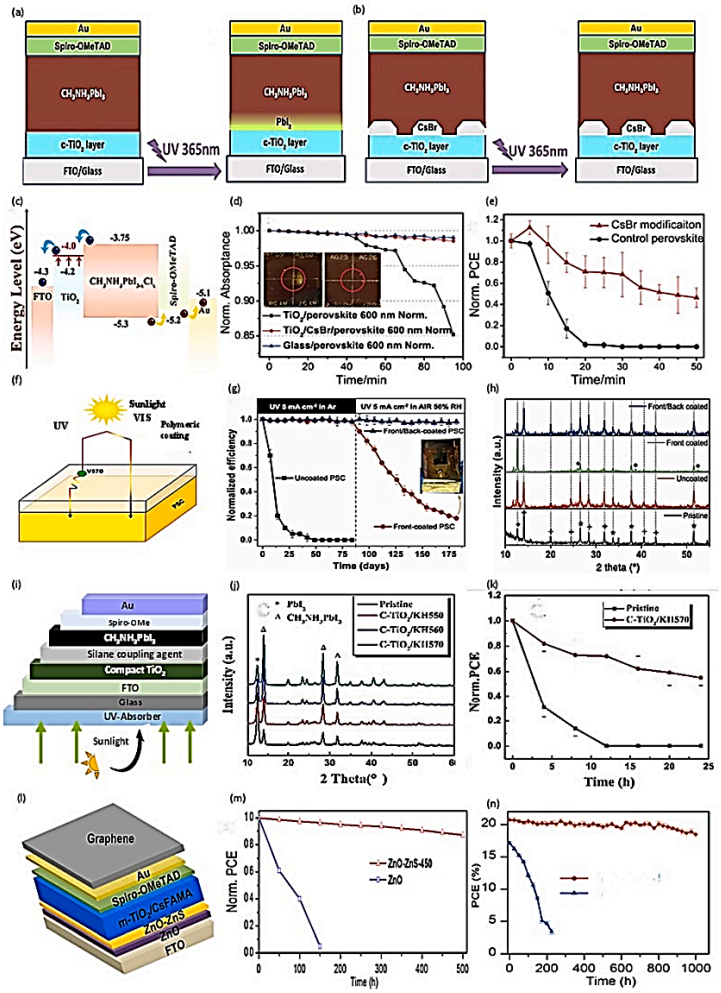

Figure 2.5: (a-b) Schematic illustration of the PSCs under UV irradiation (a)TiO_2/perovskite (b) $TiO_2(CsBr)$/perovskite, (c) Energy level diagram with the structure of FTO/$c-TiO_2(CsBr)$/ perovskite/spiro-OMeTAD/Au device, (d) Normalized absorbance of TiO_2/perovskite films with and without modification under UV Irradiation (where the inset showed the corresponding photographs), (e) Normalized PCE of PSCs with and without modification under UV Irradiation. (f) Schematic illustration of the operation of PSCs coated with a luminescent polymeric layer, (g) The normalised efficiency of uncoated, front coated and the front/back coated PSCs under UV irradiation, and their (h) corresponding XRD pattern after 6 months of UV exposure, (i) The schematic structure of the planar PSCs with UV-absorber, (j) XRD pattern of the perovskite film with and without UV absorber layer, and (k) The normalized PEC of the pristine device and modified PSCs with KH 570 interface layer and UV absorbance upon UV irradiation environments at room temperature without encapsulation. (l) Schematic of PSCs based on ZnO-ZnS ETL encapsulated with graphene, and (m) Normalized PCE of ZnO and ZnO-ZnS ETL-based PSCs encapsulated with graphene under UV irradiation with 70% RH at 25 $°C$, (n) Under UV illumination, the ageing test with normalized PCE of the corresponding PSCs and KH 570 [21], [41].

found that the photovoltaic efficiency (PCE) of a standard structure with TiO_2 and spiro-MeOTAD decreased significantly after the 9th thermal cycle due to charge accumulation and interfacial resistance, indicating the thermal stability of perovskite materials (Figures

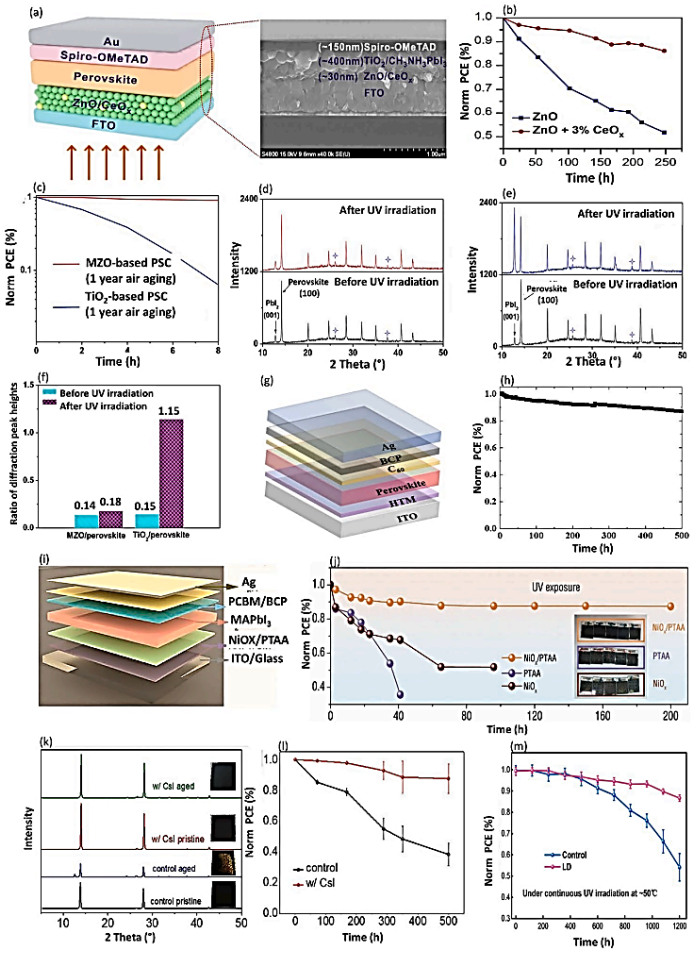

Figure 2.6: (a) The schematic structure of PSCs with cross-sectional SEM image, and (b) Normalized PCE of ZnO and CeO_X-doped ZnO-based PSCs under continuous UV irradiation. (c) Normalized current density (J_{sc}) of TiO_2 and MZO-based PSCs under UV irradiation. XRD pattern of (d) MZO-based PSCs, (e) TiO_2-based perovskite and (f) The ratio of diffraction peak heights of PbI_2 with TiO_2- and MZO-based perovskite films before and after UV exposer. (g) The schematic structure and (h) Normalized PEC of PSCs based on hydrogen-bonded dopant-free hole transport material. (i) The schematic structure of complete NiO_X/PTAA bilayer HTL of PSCs, (j) Normalized PCE of PSCs with NiO_X, PTAA, and NiO_X/PTAA bilayer HTL under UV exposure with 43% RH [44]. (k) XRD pattern of pristine and UV aged perovskite films, the SnO_2 and $CsI - SnO_2$-based ETL and the corresponding photos as inset, (l) Normalized PCE of PSCs based on SnO_2 and $CsI - SnO_2$ ETL under UV irradiation. (m) Normalized PCE of TiO_2 and LD-TiO_2-based PSCs under UV irradiation[45].

2.4 (c-d)). Wang et al. improved PSCs' photovoltaic methyl ester and PCPB by adding caffeine, retaining 80% of initial PCE and 50% of PCE after 500 hours of exposure (Figure 2.4(h)). Shi et al. used a bifunctional additive (biuret) to enhance the thermal stability of PSCs in high-temperature working environments. The biuret acted with Pb^{2+} and iodide, forming an iodoplumbate complex and enhancing the thermal durability of $MAPbI_3$ film (Figure 2.4(i)). The biuret containing $MAPbI_3$-based PSCs retained 94% of its initial efficiency after 288 hours, while without biuret, it only retained 50% of its original efficiency

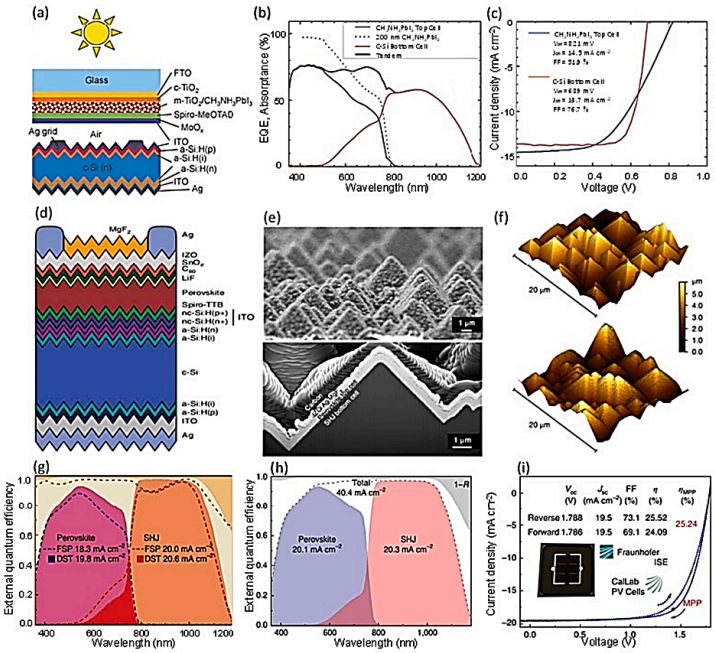

Figure 2.7: (a) Schematic structure of mechanically stacked four-terminal tandem. The system comprises a high-efficiency a-Si:H/c-Si HJ solar cell and a high-efficiency $CH_3NH_3PbI_3$ top cell with a metal-free MoO_X/ITO transparent electrode. (b) External quantum efficiency (EQE) and (c) current density–voltage curves of two individually connected subcells in a four-terminal perovskite/Si TSC [51]. (d) Schematic view of a fully textured monolithic perovskite/SHJ tandem, (e) Secondary electron SEM image of the perovskite layer and cross-section view of the full perovskite top cell deposited on the SHJ bottom cell, (f) AFM surface morphology 3D views of bare c-Si pyramids and c-Si pyramids covered with the perovskite layer. (g) EQE of perovskite/SHJ monolithic tandem cells with double-side-textured (DST) or front-side-polished (FSP) bottom cells, (h) EQE spectra of a current-matched fully textured monolithic perovskite/SHJ tandem cell, (i) corresponding certified J-V data [42], [53], [55].

(Figure 2.4(j)) [27], [37-38].

Liu et al. found that ZnO-based PSCs improved thermal stability by modifying the $ZnO - MAPbI_3$ interface with methylammonium chloride. This enhanced crystallinity and reduced degradation, while Zhou et al used a polystyrene-co-polyacrylonitrile-based additive technique. The XRD pattern of MAPI perovskite films with and without SAN polymer showed PbI_2 crystal formation after 6 hours of thermal exposure, while films with SAN showed no crystal formation. The schematic diagram for a PSC device's thermal stability test at 100 $°C$. The study examines the photovoltaic efficiency (PCE) of thermally aged PSCs of SAN-applied MAPI perovskites. The results show that PSCs without SAN polymer decreased to 70% after 6 hours and below 60% after 24% thermal stress exposure. The addition of SAN polymer significantly improved thermal stability of MAPI-based PSCs [21], [24], [27].

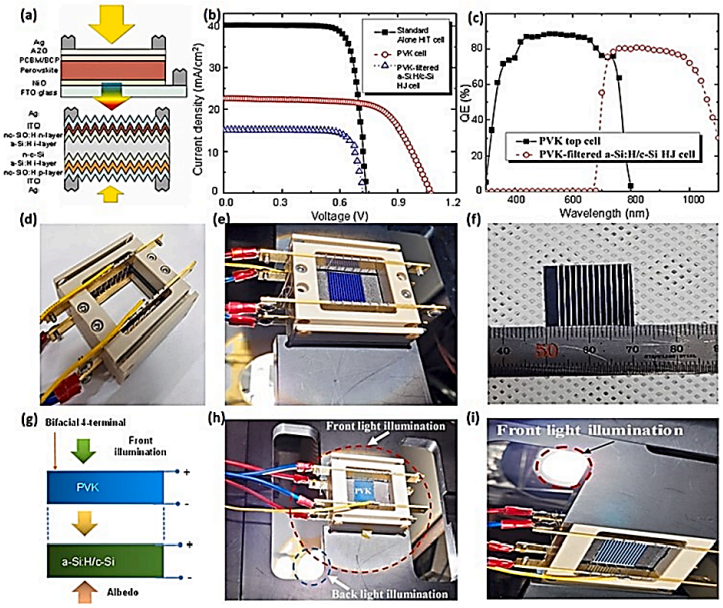

Figure 2.8: (a) Schematic cell structure of the bifacial 4-terminal PVK/c-Si HJ TSC with albedo reflection, (b) current–voltage curves under 1 Sun irradiation standard alone c-Si HJ solar cell (black color), PVK filtered c-Si HJ solar cell (blue color) and the PVK solar cell (red color), (c) Quantum efficiency of the PVK top sub-cell and PVK-filtered c-Si HJ solar cell, (d) A photo image of a solar cell Zig for bifacial 4-terminal TSC measurement. (e) The solar cell Zig with an a-Si:H/c-Si HJ solar cell, (f) An actual image of the semi-transparent PVK solar cell, (g) A configuration of the front and albedo light source; the distance between the cell holder and the albedo light source can be adjusted. (h) The solar cell Zig with PVK/c-Si HJ TSC and bi-directional light irradiation turned on. (i) The actual image from the back-side view of the bifacial 4-terminal PVK/c-Si HJ TSC with a light source turned on [54], [56].

2.2.3 Stability against UV light-induced degradation

UV light significantly influences the stability of perovskite solar cells (PSCs), leading to degradation and the production of methylamine, PbI_2, and I_2 reaction products. Studies by Abdelmageed et al. suggest a chemical reaction mechanism for this degradation [21].

$$CH_3NH_3PbI_3 \Leftrightarrow CH_3NH_3I + PbI_2 \tag{2.4}$$

$$2CH_3NH_3I + \frac{1}{2}O_2(h\nu) \leftrightarrow 2CH_3NH_2 + I_2 + H_2O \tag{2.5}$$

$$CH_3NH_3I + CO_2(h\nu) \leftrightarrow CH_3NH_2 + \frac{1}{2}I_2 + HCO_2 \tag{2.6}$$

Researchers have developed a method to improve the stability of perovskite solar cells (PSCs) under UV light exposure. They coated a cesium bromide layer between the electron collection and perovskite absorber layers to enhance the stability of PSCs (Figure 2.5(d)). The normalized absorbance of TiO_2/perovskite and $TiO_2(CsBr)$/perovskite films showed

little decay in the first 20 minutes, but after 95 minutes of UV exposure, the absorbance increased to over 98%. The structure also showed no signs of degradation (Figure 2.5(e)). The normalized PCE of a planar heterojunction device (PSC) was found to be over 70% higher than its initial value even after 20 minutes of UV exposure (Figures 2.5(a-b)), indicating that the CsBr interface modification significantly enhanced the device's stability and performance under UV light soaking conditions [40-41].

Bella et al. improved PSCs' stability against UV irradiation by coating them with photocurable fluoropolymers (Figure 2.5(f)). The efficiency of uncoated, front-coated, and front/back-coated devices was compared for six months (Figure 2.5(g)). Uncoated devices lost 70% efficiency after three months, while front-coated devices retained 98% [27]. The study demonstrates excellent stability of front/back coated perovskite films under UV irradiation with a 50% RH environment (Figure 2.5(h)). The luminescent photopolymers improve the efficiency and stability of PSCs. A coupling agent KH570 was introduced to improve stability, along with a UV absorber layer (Figure 2.5(i)). The XRD pattern showed no degradation of perovskite under UV irradiation (Figure 2.5(j)) while the color of PSCs with UV-absorber modification remained unchanged. The PCE of PSC devices without modification rapidly reduced to nearly zero Figure 2.5(k)) [27] .

Chen et al. found that the ZnS interlayer with the cascade ETL and surface passivation layer at the ZnO/perovskite interface improves the stability of PSCs encapsulated with graphene (Figure 2.5(l)). Graphene-encapsulated PSCs retained over 87% of their initial efficiency under UV irradiation, while ZnO ETL-based PSCs dropped rapidly (Figures 2.5(m-n)) [27], [42]. Meng et al. introduced CeOx-doped ZnO ETL to improve PSCs' UV and thermal stability (Figure 2.6(a)). ZnO/CeOx-based PSCs maintained 86% of their initial efficiency under UV illumination, while ZnO-based PSCs lost 51% (Figure 2.6(b)). Han et al. used MZO nanocrystals as ETL to fabricate UV-stable PSCs, retaining 76% of initial Jsc after 1 year of air ageing and 8 hours of UV irradiation (Figure 2.6(c)). The diffraction peak intensity increased under UV-light irradiation (Figures 2.6(d-e-f)) [27], [43].

TiO_2 can accelerate perovskite degradation under UV irradiation by producing O^{2-}. MZO can suppress this by protecting the perovskite layer. Li et al. reported efficient PSCs-based dopant-free hydrogen-bonded hole transport material (Fig.2.6(g)) retaining 87% efficiency after 500 hours of illumination (Figure 2.6(h)) [27] . The study demonstrates that NiOx/PTAA bilayer HTL-based PSCs maintain 87% of their original efficiency under UV irradiation, despite rapid degradation of NiOx and PTAA-based devices (Figure 2.6(i-j)). The redox reaction at the NiOx/perovskite interface passively reduces degradation, enhancing PSC stability. $CsI - SnO_2$-based PSCs are also reported as efficient and UV-stable materials (Figure.2.6(k)) [40], [42].

UV irradiation caused a change in the color of SnO_2-based devices, indicating perovskite degradation. $CsI - SnO_2$-based PSCs retained 88% of their initial PCE after 500 hours of

UV illumination, while SnO_2-based PSCs had only 38% (Figure 2.6(l)). CsI modification of SnO_2 reduced defects at the perovskite bulk and interface. Huang et al. demonstrated a ligand-engineered partition (LD) for efficient and stable PSCs, with $LD-TiO_2$ retaining 87% of their original PEC after 1200 hours of continuous UV exposure (Figure 2.6(m)) [45-47].

2.3 Tandem junction solar cells

Solar cells were initially single-junction cells with one p-n junction. Multijunction solar cells, also known as TSCs, use multiple p-n junctions of different materials to improve efficiency [48]. TSCs are currently dominant in solar technology. Perovskite-based TSCs have shown significant performance in harvesting solar energy, with PCEs exceeding 30%. The latest work in PV magazine reported a maximum efficiency of 31.25%, surpassing conventional Si TSCs [49]. The previous world record was 29.8% achieved by HZB scientists in 2021 [50]. Loper et al. reported the perovskite/silicon TSC structure, which achieved a maximum efficiency of 13.4% (Figure 2.7(a)) [51]. They fabricated two different PSCs with MoO_X/Ag and MoO_X/ITO structures, with conversion efficiency of 11.6% and 6.2%, respectively. The combined perovskite/silicon TSC showed broad absorption in the 400-1000 nm range, achieving a maximum efficiency of 7.2% (Figure 2.7(b)).

The study demonstrates the efficiency of perovskite/Si TSC solar cells, with a total transmittance ratio of 26.7%. The efficiency was achieved with a total transmittance ratio of 550/1000 nm [52]. The fully textured perovskite/Si TSC demonstrated maximum efficiency at 25.2% [53]. The device structure and microscopic SEM images are shown in Figure 2.7(c-d-e). The study analyzed the microstructure of bare c-Si pyramids covered with a perovskite layer and evaluated their optical performance using EQE spectra (Figure 2.7(f-g)). The results showed a current loss of 3.14 $mAcm^{-2}$ in the wavelength range of 360–1200 nm (Figure 2.7(h)) and a maximum efficiency of 25.4% (Figure 2.7(i)). The perovskite/Si TSC achieved broader wavelength absorption and improved IR light trapping [27].

The perovskite/TSC has a maximum efficiency of over 30% using a bifacial 4-terminal heterojunction structure (Figure 2.8(a)) [54]. A perovskite/Si TSC was designed on FTO glass, while a Si solar cell was prepared on n-cSi wafer. The PVK-filtered a-Si:H/c-Si HJ solar cell showed a performance reduction due to a conversion efficiency of 8.68% (Figure 2.8(b)). The conversion efficiency of the four-terminal perovskite-HIT structure was 25.78% (Figure 2.8 (c). The bifacial solar cell was developed to evaluate the current density-voltage characteristics of the four-terminal TSC (Figure 2.8(d)). Images of a bifacial solar cell Zig and a semi-transparent PVK solar cell are shown in Figure 2.8(e) [27], [42].

The superficial microstructure of bare c-Si pyramids covered with the perovskite layer

was determined from AFM topography (Figure 2.8(f)). The optical performance of the device was evaluated by measuring the EQE from the polished front side to the double-side textured architecture (Figure 2.8.(g)). The current loss was reported to be 3.14 $mAcm^{-2}$ in the wavelength range of 360–1200 nm (Figure 2.8(h)). The EQE spectra for both perovskite (top cell) and silicon (bottom cell) exhibited the maximum absorption at their respective wavelength and achieved the broader wavelength for the perovskite/Si TSC [27], [56][57].

Figure 2.8(i) shows the conversion efficiency of the bifacial four-terminal arrangement was calculated by combining the conversion efficiencies of the PVK cell and PVK-filtered a-Si:H/c-Si HJ bottom sub-cell. Perovskite/Si TSCs have achieved over 30% efficiency compared to traditional Si-based TSCs, but stability remains a primary concern. Researchers are working to increase PSCs' stability using various approaches, including introducing inorganic and stable materials, teaching materials in perovskite structure, and encapsulating perovskite with materials like epoxy. Inorganic perovskites exhibit lower PCE but better stability in ambient conditions. Inorganic materials for ETL and HTL layers also enhance device performance [57-60].

2.4 Factors affecting the performance of perovskite solar cells and possible solutions

Unlike silicon solar cells, PSCs can only last up to a year. Factors affecting PSC stability include thermal instability, moisture, oxygen, toxicity, electrical biasing, additives, interfaces, and illumination. A two dimensional bar diagram comprising the lifetime of Silicon and perovskite solar cells is shown in Figure 2.9.

2.4.1 Thermal instability in the perovskite solar cells

Thermal treatment is essential for thin film devices and PSCs to improve physical properties but may cause instability by degrading the perovskite absorber. Studies show that $MAPbI_3$ perovskite devices exhibit stability at room temperature, but decomposition occurs at elevated temperatures. The replacement of MA cation with FA provides thermal stability, as demonstrated in a study where $MAPbI_3$ and $FAPbI_3$ perovskite absorbers were thermally annealed at 150°C [62-64].

2.4.2 Moisture and Oxygen driven degradation

Perovskite absorbers in PSC devices often degrade due to moisture and oxygen exposure [65]. Hydrophobic passivation, a process where a hydrophobic material is used, can help address moisture degradation problems. Spin coating a PTFE layer on the device can

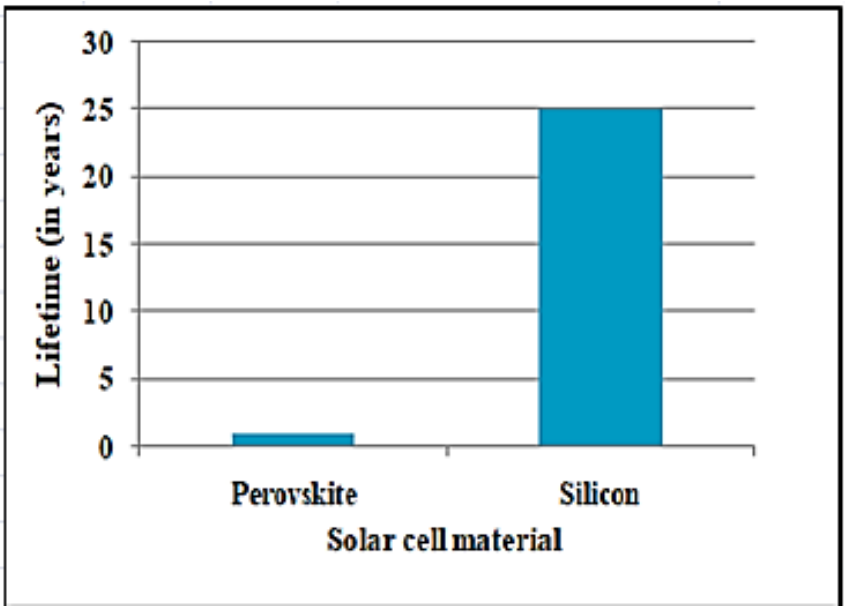

Figure 2.9: 2D bar diagram comparing the lifetime of perovskite and Silicon solar cells [61].

prevent negligible decomposition for up to 30 days. An additional Al_2O_3 layer can also prevent degradation. Oxygen ions from the ETL, like TiO_2, can also contribute to device degradation. Compositional engineering can minimize oxidation effects [66-68].

2.4.3 Toxicity of Lead-based perovskite solar cells

Lead (Pb) is a major concern in perovskite solar cell devices, but reducing its content or replacing it can help avoid its fatal nature. Sn-based mixed/hybrid inverted planar devices show better stability and charge collection with lower recombination rate. Inorganic $KBaTeBiO_6$ perovskite absorbers predicted better charge transport and optical properties, but experimental validation was limited. Lead-free, inorganic Cs_2TiBr_6 perovskite-based planar devices predicted a PCE of 18.15% but, simulation codes do not consider grain boundaries, making validation challenging [69-71].

2.4.4 Bias-dependent degradation of perovskite solar cells

Solar cell devices have a build-in-potential, causing ions to migrate towards the interface between perovskite layers and electrodes, affecting device performance [72-74]. Degradation is faster under open circuit conditions, while short circuit and maximum power point conditions lead to slower degradation. Day-night cycling affects biasing and degradation mechanisms, with fatigue behavior observed in $CH_3NH_3PbI_3$ devices. Degradation experiments on Glass/ITO/TiO_2/$CH_3NH_3PbI_3$ / SpiroOMeTAD/Au and Glass/ITO/SnO_2/$Cs_{0.05}$ $(CH_3NH_3)_{0.15}$ $((CH(NH_2)_2)_{0.85})_{0.95}$ $PbI_{2.55}$ $Br_{0.45}$/SpiroOMeTAD)/Au devices showed irreversible and reversible processes under electrical biasing conditions [75-77].

2.4.5 Role of additives in the perovskite solar cells

Additives like polymers, ZnPc, bidentate, Tpy, fullerene, and Li-TFSI significantly impact PCE and stability of PSC devices. Polymers, like PEG, are known for their solubility in solvents, making them moisture-resistant and achieving better PCE. Guo et al. incorporated PVP in precursor solutions for hybrid $CH_3NH_3PbI_{(3-X)}Cl_X$ based devices, achieving 7.34% PCE and thermal stability [78-80].

2.4.6 Role of interfaces/contacts in the perovskite solar cells

The interfaces between the absorber layer and charge transport layers (ETLs and HTLs) are crucial for proper charge collection and performance in perovskite solar cell devices. Defects at these interfaces can trap charge carriers, requiring the introduction of a buffer layer like Al_2O_3 [81].

2.4.7 Degradation of perovskite solar cells under illumination

Perovskite devices undergo photo-induced degradation when exposed to UV light. TiO_2 is commonly used as the ETL in PSC devices, which can be degraded under UV illumination. The degradation mechanism under UV illumination can be explained by Eqs. (1.7)-(1.9). This degradation occurs when electrons are extracted from the TiO2 layer, breaking the perovskite structure and forming I^- ions [82-83].

$$2I^- \leftrightarrow I_2 + 2e \tag{2.7}$$

$$3CH_3NH_3^+ \leftrightarrow 3CH_3NH_2 \uparrow +3H^+ \tag{2.8}$$

$$I^- + I_2 + 3H^+ + 2e \leftrightarrow 3HI \tag{2.9}$$

The titania ETL layer can be protected from degradation by removing it from fabricated PSCs and preventing UV irradiance exposure through encapsulation [84-85]. Factors affecting PSC performance are depicted in Figure 2.10, with solutions to mitigate them in Table 2.1.

Table 2.1: Factors affecting PSC device performance along with their solutions [75], [77], [86].

Factors	Solutions
Thermal instability Moisture and Oxygen Toxicity Electrical Biasing Additives Interfaces Illumination	By replacing cation MA by By using hydrophobic HTLs By applying additional layer between absorber and HTL. By replacing Pb by Sn or Ge. By reducing Lead content or Lead free structure. Proper optimization of charge extraction and diurnal cycles. By using polymers with good solubility in precursors. By inserting buffer layer between perovskite and charge transport layers. Proper encapsulation of titania ETL.

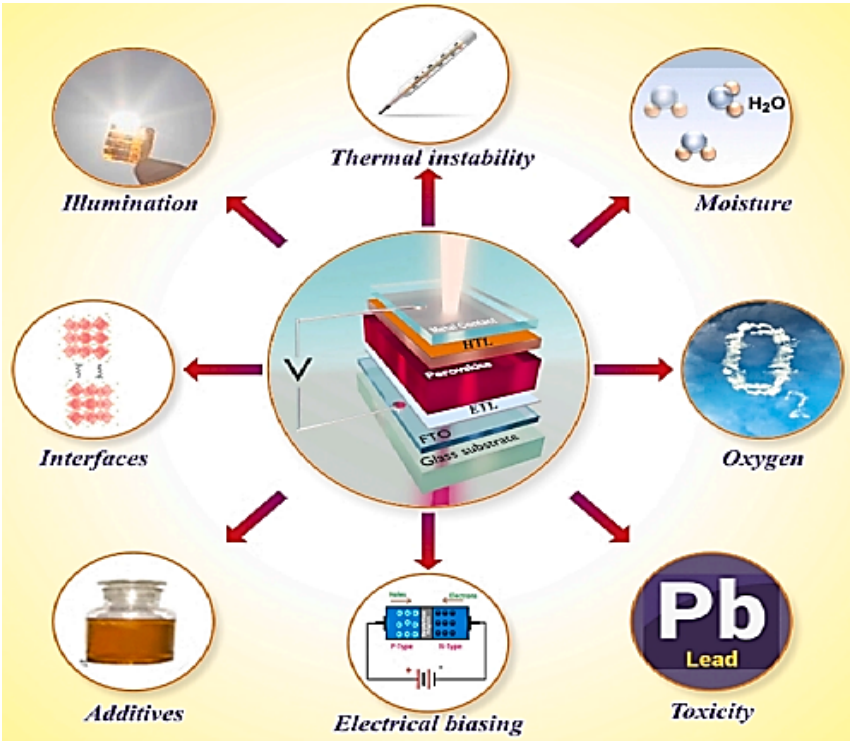

Figure 2.10: Schematic illustration of the factors which affect PSC device performance [21].

References of Chapter 2

[1] N. G. Park, "Perovskite solar cells: an emerging photovoltaic technology," Materials Today, vol. 18, no. 2, pp. 65–72, Mar. 2015.

[2] M. A. Green, A. Ho-Baillie, and H. J. Snaith, "The emergence of perovskite solar cells," Nature Photonics 2014 8:7, vol. 8, no. 7, pp. 506–514, Jun. 2014.

[3] Q. Jiang et al., "Enhanced electron extraction using SnO2 for high-efficiency planar-structure HC(NH2)2PbI3-based perovskite solar cells," Nature Energy 2016 2:1, vol. 2, no. 1, pp. 1–7, Nov. 2016.

[4] Z. Li et al., "Single-Layered MXene Nanosheets Doping TiO2for Efficient and Stable Double Perovskite Solar Cells," J Am Chem Soc, vol. 143, no. 6, pp. 2593–2600, Feb. 2021.

[5] M. K. A. Mohammed and M. Shekargoftar, "Surface treatment of ZnO films with carbon nanotubes for efficient and stable perovskite solar cells," Sustain Energy Fuels, vol. 5, no. 2, pp. 540–548, Jan. 2021.

[6] L. Zhou et al., "Enhanced planar perovskite solar cell efficiency and stability using a perovskite/PCBM heterojunction formed in one step," Nanoscale, vol. 10, no. 6, pp. 3053–3059, Feb. 2018.

[7] R. Azmi et al., "Damp heat-stable perovskite solar cells with tailored-dimensionality 2D/3D heterojunctions," Science (1979), vol. 376, no. 6588, pp. 73–77, Apr. 2022.

[8] Y. Liu et al., "Inhibited aggregation of lithium salt in spiro-OMeTAD toward highly efficient perovskite solar cells," Nano Energy, vol. 70, p. 104483, Apr. 2020.

[9] Y. Xia and S. Dai, "Review on applications of PEDOTs and PEDOT:PSS in perovskite solar cells," Journal of Materials Science: Materials in Electronics, vol. 32, no. 10, pp. 12746–12757, May 2021.

[10] W. Chen, F. Z. Liu, X. Y. Feng, A. B. Djurišić, W. K. Chan, and Z. B. He, "Cesium Doped NiOx as an Efficient Hole Extraction Layer for Inverted Planar Perovskite Solar Cells," Adv Energy Mater, vol. 7, no. 19, p. 1700722, Oct. 2017.

[11] N. Arora et al., "Perovskite solar cells with CuSCN hole extraction layers yield stabilized efficiencies greater than 20%," Science (1979), vol. 358, no. 6364, pp. 768–771, Nov. 2017.

[12] D. E. Lee, S. Y. Kim, and H. W. Jang, "Lead-free all-inorganic halide perovskite quantum dots: review and outlook," Journal of the Korean Ceramic Society, vol. 57, no. 5, pp. 455–479, Sep. 2020.

[13] M. J. Seol, J. W. Han, S. H. Hwang, and S. Y. Kim, "Recent Research Trends for Improving the Stability of Organo/Inorgano Halide Perovskites," Journal of Korean Institute of Metals and Materials, vol. 60, no. 1, pp. 1–13, Jan. 2022.

[14] A. K. Cheetham, C. N. R. Rao, and R. K. Feller, "Structural diversity and chemical trends in hybrid inorganic–organic framework materials," Chemical Communications, no. 46, pp. 4780–4795, Nov. 2006.

[15] C. C. Boyd, R. Cheacharoen, T. Leijtens, and M. D. McGehee, "Understanding Degradation Mechanisms and Improving Stability of Perovskite Photovoltaics," Chem Rev, vol. 119, no. 5, pp. 3418–3451, Mar. 2019.

[16] Z. Li et al., "Scalable fabrication of perovskite solar cells," Nature Reviews Materials 2018 3:4, vol. 3, no. 4, pp. 1–20, Mar. 2018.

[17] Y. Li, H. Xie, E. L. Lim, A. Hagfeldt, and D. Bi, "Recent Progress of Critical Interface Engineering for Highly Efficient and Stable Perovskite Solar Cells," Adv Energy Mater, vol. 12, no. 5, p. 2102730, Feb. 2022.

[18] T. Matsui et al., "Compositional Engineering for Thermally Stable, Highly Efficient Perovskite Solar Cells Exceeding 20% Power Conversion Efficiency with 85 C/85% 1000 h Stability," Advanced Materials, vol. 31, no. 10, p. 1806823, Mar. 2019.

[19] M. Kim et al., "Conformal quantum dot-SnO2 layers as electron transporters for efficient perovskite solar cells," Science (1979), vol. 375, no. 6578, pp. 302–306, Jan. 2022.

[20] P. Zhao, B. J. Kim, and H. S. Jung, "Passivation in perovskite solar cells: A review," Materials Today Energy, vol. 7. Elsevier Ltd, pp. 267–286, Mar. 01, 2018.

[21] A. Kumar et al., "Enhanced efficiency and stability of electron transport layer in perovskite tandem solar cells: Challenges and future perspectives," Solar Energy, vol. 266. Elsevier Ltd, Dec. 01, 2023.

[22] A. Abate, J. Correa-Baena, M. Saliba, M. S. Su'ait, and F. Bella, "Frontispiece: Perovskite Solar Cells: From the Laboratory to the Assembly Line," Chemistry – A European Journal, vol. 24, no. 13, 2018.

[23] F. Arabpour Roghabadi, N. Mansour Rezaei Fumani, M. Alidaei, V. Ahmadi, and S. M. Sadrameli, "High Power UV-Light Irradiation as a New Method for Defect Passivation in Degraded Perovskite Solar Cells to Recover and Enhance the Performance," Sci Rep, vol. 9, no. 1, 2019.

[24] X. Li et al., "Moisture-preventing MAPbI3 solar cells with high photovoltaic performance via multiple ligand engineering," Nano Res, vol. 15, no. 2, pp. 1375–1382, Feb. 2022.

[25] H. S. Kim et al., "Reduced Graphene Oxide Improves Moisture and Thermal Stability of Perovskite Solar Cells," Cell Rep Phys Sci, vol. 1, no. 5, May 2020.

[26] Q. Hu et al., "Improving Efficiency and Stability of Perovskite Solar Cells Enabled by A Near-Infrared-Absorbing Moisture Barrier," Joule, vol. 4, no. 7, pp. 1575–1593, Jul. 2020.

[27] D. Y. Heo, W. J. Jang, and S. Y. Kim, "Recent review of interfacial engineering for perovskite solar cells: effect of functional groups on the stability and efficiency," Mater Today Chem, vol. 26, p. 101224, Dec. 2022.

[28] J. H. Noh, S. H. Im, J. H. Heo, T. N. Mandal, and S. Il Seok, "Chemical management for colorful, efficient, and stable inorganic-organic hybrid nanostructured solar cells," Nano Lett, vol. 13, no. 4, pp. 1764–1769, Apr. 2013.

[29] H. X. Dang et al., "Multi-cation Synergy Suppresses Phase Segregation in Mixed-Halide Perovskites," Joule, vol. 3, no. 7, pp. 1746–1764, Jul. 2019.

[30] P. Hangoma and M. Chewe, "Should We Worry About Spillover Effects of Sugar Sweetened Beverage Taxation Policies? Comment on 'Understanding Marketing Responses to a Tax on Sugary Drinks: A Qualitative Interview Study in the United Kingdom, 2019,'"

Int J Health Policy Manag, vol. 12, 2023.

[31] P. M. Hangoma et al., "Improved Moisture Stability of Perovskite Solar Cells with a Surface-Treated PCBM Layer," Solar RRL, vol. 3, no. 2, Feb. 2019.

[32] L. Le Bras, K. Chaitou, S. Aloïse, C. Adamo, and A. Perrier, "Aggregation-caused quenching: Versus crystallization induced emission in thiazolo[5,4-b] thieno[3,2-e] pyridine (TTP) derivatives: Theoretical insights," Physical Chemistry Chemical Physics, vol. 21, no. 1, 2019.

[33] H. H. Huang, Y. C. Shih, L. Wang, and K. F. Lin, "Boosting the ultra-stable unencapsulated perovskite solar cells by using montmorillonite/CH3NH3PbI3 nanocomposite as photoactive layer," Energy Environ Sci, vol. 12, no. 4, pp. 1265–1273, Apr. 2019.

[34] M. Ablikim et al., "Model-independent determination of the relative strong-phase difference between And its impact on the measurement of the CKM angle MODEL-INDEPENDENT DETERMINATION of the RELATIVE ABLIKIM M. et al.," Physical Review D, vol. 101, no. 11, 2020.

[35] R. Fitzpatrick and A. O. Nelson, "An improved theory of the response of DIII-D H-mode discharges to static resonant magnetic perturbations and its implications for the suppression of edge localized modes," Phys Plasmas, vol. 27, no. 7, 2020.

[36] R. Hosseinian Ahangharnejhad et al., "Protecting Perovskite Solar Cells against Moisture-Induced Degradation with Sputtered Inorganic Barrier Layers," ACS Appl Energy Mater, vol. 4, no. 8, 2021.

[37] X. Zhao, H. S. Kim, J. Y. Seo, and N. G. Park, "Effect of Selective Contacts on the Thermal Stability of Perovskite Solar Cells," ACS Appl Mater Interfaces, vol. 9, no. 8, pp. 7148–7153, Mar. 2017.

[38] R. Wang et al., "Caffeine Improves the Performance and Thermal Stability of Perovskite Solar Cells," Joule, vol. 3, no. 6, pp. 1464–1477, Jun. 2019.

[39] Y. Zhou et al., "Improving Thermal Stability of Perovskite Solar Cells by Suppressing Ion Migration Using Copolymer Grain Encapsulation," Chemistry of Materials, vol. 33, no. 15, pp. 6120–6135, Aug. 2021.

[40] Y. Sun et al., "Enhanced UV-light stability of organometal halide perovskite solar cells with interface modification and a UV absorption layer," J Mater Chem C Mater, vol. 5, no. 34, pp. 8682–8687, 2017.

[41] W. Li et al., "Enhanced UV-light stability of planar heterojunction perovskite solar cells with caesium bromide interface modification," Energy Environ Sci, vol. 9, no. 2, pp. 490–498, Feb. 2016.

[42] F. Bella et al., "Improving efficiency and stability of perovskite solar cells with photocurable fluoropolymers," Science (1979), vol. 354, no. 6309, pp. 203–206, Oct. 2016.

[43] Y. Chen et al., "Properties of two-variety natural luffa sponge columns as potential mattress filling materials," Materials, vol. 11, no. 4, Mar. 2018.

[44] N. Rengaswamy, R. Calderbank, and H. D. Pfister, "Unifying the Clifford hierarchy

via symmetric matrices over rings," Phys Rev A (Coll Park), vol. 100, no. 2, 2019.

[45] F. Han, Z. Wan, J. Luo, J. Xia, H. Shu, and C. Jia, "Planar MgxZn1-xO-based perovskite solar cell with superior ultraviolet light stability," Solar Energy Materials and Solar Cells, vol. 208, May 2020.

[46] H. Xu et al., "CsI Enhanced Buried Interface for Efficient and UV-Robust Perovskite Solar Cells," Adv Energy Mater, vol. 12, no. 2, Jan. 2022.

[47] H. Huang et al., "24.8%-efficient planar perovskite solar cells via ligand-engineered TiO2 deposition," Joule, 2022.

[48] M. Grätzel, "Photovoltaic performance and long-term stability of dye-sensitized meosocopic solar cells," Comptes Rendus Chimie, vol. 9, no. 5–6, 2006.

[49] A. Ahmadi et al., "Recent residential applications of low-temperature solar collector," Journal of Cleaner Production, vol. 279. 2021.

[50] N. H. Nickel, F. Lang, V. V. Brus, O. Shargaieva, and J. Rappich, "Unraveling the Light-Induced Degradation Mechanisms of CH3NH3PbI3 Perovskite Films," Adv Electron Mater, vol. 3, no. 12, Dec. 2017.

[51] K. Suzuki, K. Hasegawa, and M. Ihara, " Effects of Reaction Conditions with Methylammonium Iodide on the Grain of CH 3 NH 3 PbI 3 Perovskite for Thin Top Cell of Tandem Solar Cells ," ECS Meeting Abstracts, vol. MA2017-02, no. 15, 2017.

[52] W. Pan, H. Wei, and B. Yang, "Development of Halide Perovskite Single Crystal for Radiation Detection Applications," Frontiers in Chemistry, vol. 8. 2020.

[53] F. Li, T. Yang, and R. Zheng, "Radiation Detection Technologies Enabled by Halide Perovskite Single Crystals," in Advanced Materials for Radiation Detection, 2021.

[54] T. N. Ng, J. A. Marohn, and M. L. Chabinyc, "Comparing the kinetics of bias stress in organic field-effect transistors with different dielectric interfaces," J Appl Phys, vol. 100, no. 8, 2006.

[55] H. Huang et al., "24.8%-efficient planar perovskite solar cells via ligand-engineered TiO2 deposition," Joule, 2022.

[56] F. Han, Z. Wan, J. Luo, J. Xia, H. Shu, and C. Jia, "Planar MgxZn1-xO-based perovskite solar cell with superior ultraviolet light stability," Solar Energy Materials and Solar Cells, vol. 208, May 2020.

[57] T. Leijtens, K. A. Bush, R. Prasanna, and M. D. McGehee, "Opportunities and challenges for tandem solar cells using metal halide perovskite semiconductors," Nat Energy, vol. 3, no. 10, pp. 828–838, Oct. 2018.

[58] F. Sahli et al., "Fully textured monolithic perovskite/silicon tandem solar cells with 25.2% power conversion efficiency," Nat Mater, vol. 17, no. 9, pp. 820–826, Sep. 2018.

[59] P. Löper et al., "Organic-inorganic halide perovskite/crystalline silicon four-terminal tandem solar cells," Physical Chemistry Chemical Physics, vol. 17, no. 3, pp. 1619–1629, Jan. 2015.

[60] X. X. Gao et al., "Stable and High-Efficiency Methylammonium-Free Perovskite Solar Cells," Advanced Materials, vol. 32, no. 9, Mar. 2020.

[61] Y. Y. Kim et al., "Roll-to-roll gravure-printed flexible perovskite solar cells using eco-friendly antisolvent bathing with wide processing window," Nat Commun, vol. 11, no. 1, 2020.

[62] R. K. Misra et al., "Temperature- and component-dependent degradation of perovskite photovoltaic materials under concentrated sunlight," Journal of Physical Chemistry Letters, vol. 6, no. 3, pp. 326–330, Feb. 2015.

[63] B. Conings et al., "Intrinsic Thermal Instability of Methylammonium Lead Trihalide Perovskite," Adv Energy Mater, vol. 5, no. 15, Aug. 2015.

[64] G. E. Eperon, S. D. Stranks, C. Menelaou, M. B. Johnston, L. M. Herz, and H. J. Snaith, "Formamidinium lead trihalide: A broadly tunable perovskite for efficient planar heterojunction solar cells," Energy Environ Sci, vol. 7, no. 3, pp. 982–988, Mar. 2014.

[65] B. Esmaeilnejad et al., "PCR-based detection of Babesia ovis in Rhipicephalus bursa and small ruminants," J Parasitol Res, vol. 2014, 2014.

[66] I. Hwang, I. Jeong, J. Lee, M. J. Ko, and K. Yong, "Enhancing Stability of Perovskite Solar Cells to Moisture by the Facile Hydrophobic Passivation," ACS Appl Mater Interfaces, vol. 7, no. 31, pp. 17330–17336, Aug. 2015.

[67] Q. Qiu, H. Liu, Y. Qin, C. Ren, and J. Song, "Efficiency enhancement of perovskite solar cells based on Al2O3-passivated nano-nickel oxide film," J Mater Sci, vol. 55, no. 28, pp. 13881–13891, Oct. 2020.

[68] W. Chen, L. Xu, X. Feng, J. Jie, and Z. He, "Metal Acetylacetonate Series in Interface Engineering for Full Low-Temperature-Processed, High-Performance, and Stable Planar Perovskite Solar Cells with Conversion Efficiency over 16% on 1 cm2 Scale," Advanced Materials, vol. 29, no. 16, Apr. 2017.

[69] S. Shao et al., "Highly Reproducible Sn-Based Hybrid Perovskite Solar Cells with 9% Efficiency," Adv Energy Mater, vol. 8, no. 4, Feb. 2018.

[70] A. S. Thind et al., "KBaTeBiO6: A Lead-Free, Inorganic Double-Perovskite Semiconductor for Photovoltaic Applications," Chemistry of Materials, vol. 31, no. 13, pp. 4769–4778, Jul. 2019.

[71] M. A. K. Khan, S. S. Urmi, T. T. Ferdous, S. Azam, and M. A. Alim, "Highly efficient Cesium Titanium (IV) Bromide perovskite solar cell and its point defect investigation: A computational study," Superlattices Microstruct, vol. 156, Aug. 2021.

[72] C. J. Patrick et al., "Latent variable modeling of item-based factor scales: Comment on Triarchic or septarchic?—Uncovering the Triarchic Psychopathy Measure's (TriPM) Structure, by Roy et al.," Personality Disorders: Theory, Research, and Treatment, vol. 12, no. 1. 2021.

[73] P. Roy, N. Kumar Sinha, S. Tiwari, and A. Khare, "A review on perovskite solar cells: Evolution of architecture, fabrication techniques, commercialization issues and

status," Solar Energy, vol. 198. Elsevier Ltd, pp. 665–688, Mar. 01, 2020.

[74] W. Tress, N. Marinova, T. Moehl, S. M. Zakeeruddin, M. K. Nazeeruddin, and M. Grätzel, "Understanding the rate-dependent J-V hysteresis, slow time component, and aging in CH3NH3PbI3 perovskite solar cells: The role of a compensated electric field, Energy Environ Sci, vol. 8, no. 3, pp. 995–1004, Mar. 2015.

[75] M. V. Khenkin, K. M. Anoop, E. A. Katz, and I. Visoly-Fisher, "Bias-dependent degradation of various solar cells: Lessons for stability of perovskite photovoltaics," Energy Environ Sci, vol. 12, no. 2, pp. 550–558, Feb. 2019.

[76] K. Domanski et al., "Migration of cations induces reversible performance losses over day/night cycling in perovskite solar cells," Energy Environ Sci, vol. 10, no. 2, pp. 604–613, Feb. 2017.

[77] F. Huang et al., "Fatigue behavior of planar CH3NH3PbI3 perovskite solar cells revealed by light on/off diurnal cycling," Nano Energy, vol. 27, pp. 509–514, Sep. 2016.

[78] Y. Guo, K. Shoyama, W. Sato, and E. Nakamura, "Polymer Stabilization of Lead(II) Perovskite Cubic Nanocrystals for Semitransparent Solar Cells," Adv Energy Mater, vol. 6, no. 6, Mar. 2016.

[79] T. Li, Y. Pan, Z. Wang, Y. Xia, Y. Chen, and W. Huang, "Additive engineering for highly efficient organic-inorganic halide perovskite solar cells: Recent advances and perspectives," J Mater Chem A Mater, vol. 5, no. 25, pp. 12602–12652, 2017.

[80] M. Prete et al., "Bias-Dependent Dynamics of Degradation and Recovery in Perovskite Solar Cells," ACS Appl Energy Mater, vol. 4, no. 7, pp. 6562–6573, Jul. 2021.

[81] Q. Qiu, H. Liu, Y. Qin, C. Ren, and J. Song, "Efficiency enhancement of perovskite solar cells based on Al2O3-passivated nano-nickel oxide film," J Mater Sci, vol. 55, no. 28, pp. 13881–13891, Oct. 2020.

[82] G. Niu, X. Guo, and L. Wang, "Review of recent progress in chemical stability of perovskite solar cells," J Mater Chem A Mater, vol. 3, no. 17, pp. 8970–8980, May 2015.

[83] P. H. Joshi et al., "The physics of photon induced degradation of perovskite solar cells," AIP Adv, vol. 6, no. 11, Nov. 2016.

[84] B. S. Babu et al., "Initial default among diagnosed sputum smear-positive pulmonary tuberculosis patients in Andhra Pradesh, India," International Journal of Tuberculosis and Lung Disease, vol. 12, no. 9, 2008.

[85] N. Chander et al., "Reduced ultraviolet light induced degradation and enhanced light harvesting using YVO4:Eu3+ down-shifting nano-phosphor layer in organometal halide perovskite solar cells," Appl Phys Lett, vol. 105, no. 3, Jul. 2014.

[86] M. A. K. Khan, S. S. Urmi, T. T. Ferdous, S. Azam, and M. A. Alim, "Highly efficient Cesium Titanium (IV) Bromide perovskite solar cell and its point defect investigation: A computational study," Superlattices Microstruct, vol. 156, Aug. 2021.

Chapter 3

Study of instability issue by SCAPS

3.1 Introduction

Perovskite solar cells have emerged as a promising technology in the field of photovoltaics due to their high power conversion efficiencies and low-cost fabrication processes. However, one of the major challenges hindering their commercialization is their inherent instability, particularly when exposed to moisture, heat, or light over extended periods. Understanding and mitigating these instability issues are crucial for the widespread adoption of perovskite solar cells [1].

SCAPS (Solar Cell Capacitance Simulator) is a powerful simulation tool widely used for studying the performance and characteristics of various types of solar cells, including perovskite solar cells. By employing SCAPS, researchers can simulate the behavior of perovskite solar cells under different operating conditions and investigate the underlying mechanisms contributing to their instability [2].

This study aims to explore the instability problems associated with perovskite solar cells using SCAPS simulation. By simulating the degradation processes triggered by environmental factors such as moisture ingress, thermal stress, and light exposure, researchers can gain valuable insights into the degradation mechanisms. Understanding the impact of these degradation-induced defects on device performance is crucial for devising strategies to enhance stability and prolong device lifetime. In this study, we employ SCAPS (Solar Cell Capacitance Simulator) to investigate the stability issues in perovskite solar cells, with a focus on elucidating the influence of different types of defects created by degradation processes. Through comprehensive analysis, we aim to gain insights into the intricate interplay between defect formation and device performance degradation, ultimately paving the way for the development of more stable and reliable perovskite solar cell technologies.

3.2 SCAPS

SCAPS-1D has been developed to simulate the operation of thin-film solar cells. SCAPS is originally developed for cell structures of the CuInSe2 and the CdTe family. Several extensions however have improved its capabilities so that it is also applicable to crystalline solar cells (Si and GaAs family) and amorphous cells (a-Si and micromorphous Si) [3]. SCAPS is a Windows-oriented program, which is opened with the 'Action Panel' (Figure 3.1).

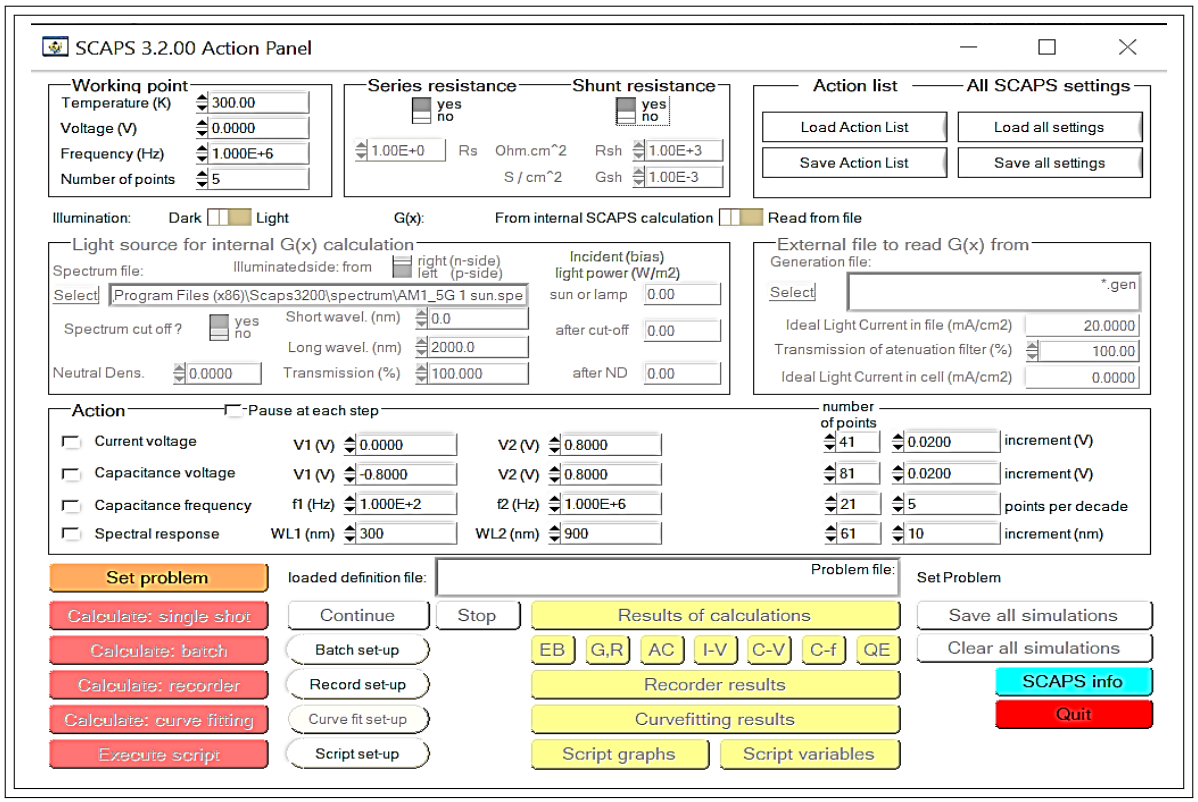

Figure 3.1: The SCAPS start-up panel: the Action panel or main panel.

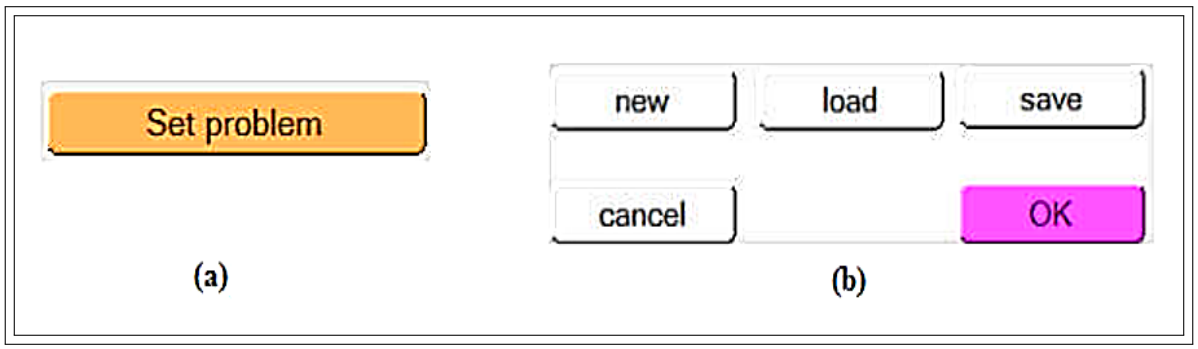

Figure 3.2: (a) Defining problem panel and (b) selecting an example.

3.2.1 Definition of the problem

By clicking the button set problem (Figure 3.2(a)) in the action panel, we can chose load in the lower right corner of the new opened panel (Figure 3.2(b)) to select an example to study which can be modified in the cell properties [3].

3.2.2 Define the working point

The working point specifies the parameters which are not varied in a measurement simulation, and which are relevant to that measurement (Figure 3.3). Thus:

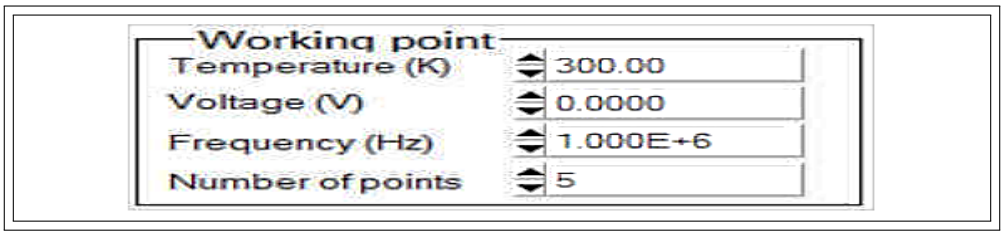

Figure 3.3: Define the working point.

- Temperature (T): Necessary for all measurements. $N_c(T)$, $N_v(T)$, the thermal velocities, the thermal voltage K_BT and all their derivaties are the only variables which have anexplicit temperature dependence. These parameters must be inserted manually for each temperature[3].
- The voltage V: is unnecessary in I-V and C-V simulation, but it is taken as the dc-bias voltage in C-f simulation and in $QE(\lambda)$ simulation. SCAPS always starts at 0V, and proceeds at the working point voltage in a number of steps that also should be specified [3].
- The frequency f: is neglected in I-V, $QE(\lambda)$ and C-f simulation. But C-V measurement is taken into account[3].
- The illumination: is used for all measurements. For the QE(λ) measurement, it determines the bias light conditions. The basis settings are: dark or light, choice of the illuminated side, choice of the spectrum. The default is one sun(=1000 W/m^2) illumination with the 'air mass 1.5, global' spectrum, but there is a large choice of monochromatic light and spectra for specialized simulations[3].

3.2.3 Selection of the measurement(s) to simulate

In the action-part of the Action Panel, the following measurements: I-V, C-V, C-f and $QE(\lambda)$ can be simulated [3]. Adjust if necessary the start and end values of the argument, and the number of steps (Figure 3.4).

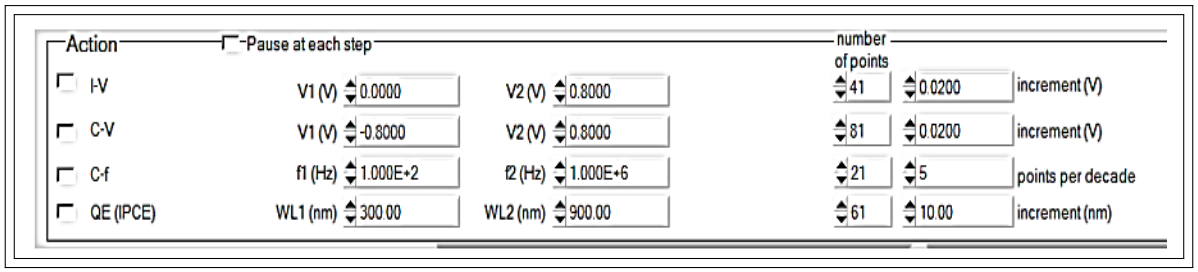

Figure 3.4: Define the working point.

3.2.4 Starting the calculation(s)

By clicking the button calculate: single shot in the action panel. The Energy Bands Panel opens, and the calculations start. Meanwhile, SCAPS offers a free movie how the conduction and valence bands, the Fermi levels and the whole caboodle are evolving [3].

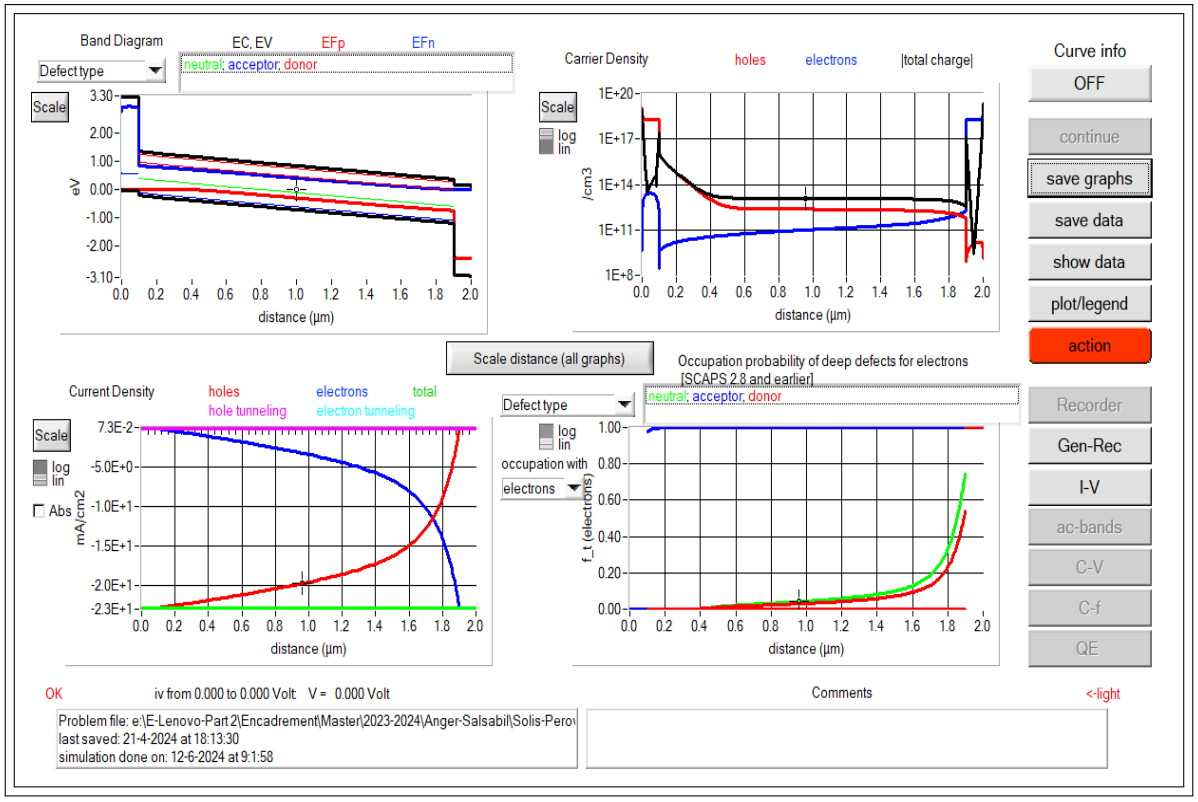

Figure 3.5: Results panels.

3.2.5 Displaying the simulated curves

After the calculation(s), SCAPS switches to the Energy band panel (or the AC-band panel) in which the band diagrams, carrier densities, current densities are shown. The results (buttons save graphs, show data (the numbers are shown on screen) or save data

(the numbers are saved to a file). One of specialized output panels can be switched (Figure 3.5) [3]. Simulation procedure using SCAPS software can be summarized by the scheme presented in Figure 3.6.

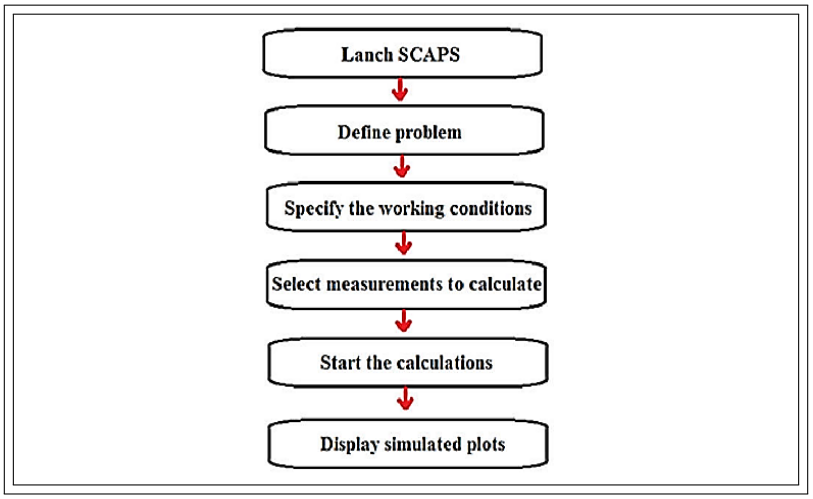

Figure 3.6: Simulation procedure using SCAPS software.

3.3 Defects in perovskite-halide materials

3.3.1 Compositional engineering

The instability of the perovskite material $MAPbI_3$ is due to the smaller size of the MA-ion, which makes it adopt the less symmetrical tetragonal phase [4]. Replacement of the MA-ions either partially or fully with a suitable ion size at the A site will change it toward a symmetrical lattice structure, which will improve the stability [4,5]. The mixture strategy and the change of component at the A site, such as using a mixture of MA and formamidinium (FA) as well as the cations with acetamidinium (Ace) and MA, can deliver a high PCE of 19.5% and a promoted device stability. The substitution of larger Ace cations induced distortion of the lattice cubic structure with a changed tolerance factor [6]. The compositional engineering of PSCs via substituting MA with Ace has not yet been investigated to enhance the stability of devices. The mixture strategy of FA and MA increases the lattice expansion and strengthens the interaction with I- ions as well as increases the tolerance factor. The PSC efficiency of 21.24% was realized by mixing MA with FA with low stability under illumination because of the unstable yellow phase in the perovskite material due to the incorporation of the FA cation [7].

The enhancement of light stability via the full replacement of MA cations at the A site with cesium (Cs) can be realized due to the intrinsic nature of Cs [4]. The enhancement of light stability with $CsPbI_3$-based PSCs with an efficiency of over 16% has already been realized after 3000 h of light soaking [8,9].

The main issue of $CsPbI_3$-based PSCs is their low efficiency. More investigations are necessary on the site-based substitution method to enhance the efficiency and stability of PSCs by tuning the tolerance factor in the range of 0.9–1. A mixed Cs/MA/FA-based PSC efficiency of around 21% was realized under illumination with enhanced stability. The Cs/MA/FA mixture-based PSCs need further investigation for achieving stable and high-efficiency devices. The efficiency of Rb/Cs/FA-based PSCs was realized at over 20%under illumination with good stability due to the better crystallinity and the suppressed yellow phase of $FAPbI_3$ [10,11]. The cation-mixing strategy facilitates the growth of the desired crystal structure with the required orientation, mitigates trap states through the formation of a smooth perovskite film, reduces charge recombination, enhances electron extraction and transport and improves the thermal stability [12].

Iodine (I) is the most used anion at the X site in perovskite materials. Under illumination, perovskites with $I-$ anions suffer from oxidation. Oxidation under light soaking can be reduced by mixing the halides. The band gap of perovskite materials can be tuned by mixing halides, improving their stability, and accelerating charge transport [4]. The crystallization of $MAPbI_3$ can be enhanced by $Cl-$ at the X site. It can accelerate charge transfer, and the carrier diffusion length increases the carrier collection, thus enhancing the PSC device efficiency and stability [13]. The bonding strength of MA–Pb is increased via the combination of Br and I, which compresses the lattice as well as enlarges the crystal grain size, improving both the thermal stability and efficiency. With the formation of a high-quality $MAPbI_{3-x}Br_x$ absorber layer, the PSC efficiency is increased up to 19.2% [14]. The concentration of Br in $MAPbI_{3-x}Br_x$ needs to be optimized to achieve high-efficiency and stable PSCs. An excess of Br at the X site creates recombination centers due to the generation of I-rich inclusions. Special attention should be paid to X-site compositional engineering for the better performance and stability of PSCs. Anion substitution at the X site is playing a critical role in the improvement of thermal and light stability [4].

The simultaneous substitution of both A and X sites can be more effective for the improvement of PSC efficiency and stability [15–17]. For example, the substitution of I by Br at the X site leads to a reduction of octahedral tilting and lattice distortion, and simultaneously adding Cs at the A site helps with formation of the cubic phase with tolerance factor modulation for a high-quality perovskite film. The perovskite $CsPbBr_3$ material shows excellent stability under illumination [4].

However, these material-based PSCs have a low efficiency because of their large bandgap of 2.3 eV and their narrow-spectra absorption of less than 550 nm [18]. Mixing Br with I at the X site in $CsPbBr_3$, such as in $CsPbI_{3-x}Br_x$, can increase the PSC efficiency up to 18.5% due to the reduction of bandgap energy and crystallinity as well as non-radiative recombination suppression [19]. Cl-doping in the $CsPbI_3$ material contributed to enhancing the PSC efficiency (up to 19%) and stability under illumination [20]. The mixing of Cs and

FA at the A site with the Br/I mixture at the X site, such as in $FA_{0.83}Cs_{0.17}PbI_{2.7}Br_{0.3}$-based PSCs, has achieved an efficiency of 20.32% due to perovskite phase crystallization and halide segregation reduction [21]. On the basis of a $Cs/FA/MA$ mixture at the A site and a Br/I mixture at the X site, a PSC efficiency of 21.5% was realized due to the formation of a high-quality perovskite film with a larger grain size and a reduction of defect states [22].

Mixing and selecting appropriate ions with an optimal concentration at both the A and X sites, we can simultaneously achieve light-stable and high-efficiency PSCs. Both high-efficiency and light-stable PSCs can be realized using the compositional engineering strategy with a preferred perovskite crystal orientation, a uniformity of film morphology with a large grain size, and a reduced trap density [4].

The device stability is also related to the lead (Pb) element at the B site in PSCs because of the soft nature of Pb–I bonding and Pb^{2+} ions [23]. Under illumination and/or at a higher temperature, the Pb^{2+} ions tend to form into Pb atoms and generate deep defect states, which leads to severe degradation [24,25].

Replacement Pb^{2+} ions at the B site with tin (Sn) either fully or partially is one of the options for promoting the stability of PSC devices [24,26]. The oxidation of Sn^{2+} ions creates fewer grain boundary defects, improves the crystal quality, and generates a higher Voc, which enhances both the efficiency and stability of PSCs [27]. The replacement of Pb with Ca at the B site has also promoted the efficiency to 19.3% and enhanced the stability under illumination [28]. CaI_2 enhances both the efficiency and light stability of PSCs due to the passivation of defects, and the formation of a smooth, uniform, and dense film with large crystal grains. The partial substitution of Pb by strontium (Sr) has also suppressed the heat degradation of PSCs due to mitigation of the defect density, preventing perovskite decomposition, and generating compact perovskite films [29].

The substitution of Pb^{2+} ions with cadmium ions (Cd^{2+}) can also improve the stability of PSCs due to the stronger Cd–I ionic bonds, which have a higher binding energy. An impressive PSC efficiency of 21.9% and sustainable stability under light illumination are achieved via the replacement of Pb with Cd at the B site [30]. Optimization of ion substitution at A, B, and X sites for the development of compositional engineering along with alternative materials will improve both the stability and the efficiency of PSCs for commercial applications. Moreover, some studies have demonstrated that external additives such as PCBM and NH_4Cl in the perovskite structure can also have an effect on reducing defects and improving the stability of perovskites [31–33].

3.3.2 Defects in perovskite

There are 12 possible native point defects in the $MAPbI_3$ structure, such as vacancies VMA, VPb, and VI; interstitials MA_i, Pb_i, and I_i; and anti-site occupations MA_{Pb}, MA_I,

Pb_{MA}, Pb_I, I_{MA}, and I_{Pb}, which have been widely studied [4] [34–41]. The common message about point defects in $MAPbI_3$ are that these defects with a high energy can contribute to the formation of deep levels in the bandgap, and low-energy defects can contribute to the formation of shallow defect states [4].

Deep-level point defects may not contribute a high density of non-radiative recombination centers. However, there is some variation in opinion about which point defects can contribute to deep levels including I_{Pb}, I_{MA}, Pb_i, Pb_I, V_I, and Pb_{MA} [34,40,41]. The defect formation energies of I_{MA}, Pb_I, and V_I are low enough to contribute a significant density of recombination centers [34,36].

The formation energy of the Pb_I anti-site defect is low under iodine-rich conditions. The stable charge state of the Pb_I defect can make a transition at the Fermi level. Acceptors of shallow point defects are V_{Pb}, V_{MA}, MA_{Pb}, and I_i under some growth conditions with low formation energies, and MA_i, V_I, andMA_I are donors of shallow point defects [36,41]. The donors and acceptors of shallow point defects can convert the $MAPbI_3$ material from p-type to n-type by intrinsic doping. Under stoichiometric growth conditions, the cation and anion vacancies may also dominate the defect formation [39]. If the defect formation energies are low, unintentional doping can be minimized by compensating the vacancy with opposite charge carriers [4].

The four native defects, V_x, $_{V_A}$, V_{Pb}, and Pb_i, in the perovskite crystal and the probable migration path for these four point defects were identified from the theoretical calculations, as shown in Figure 3.7(b) [43]. The proposed migration pathways are designed based on comparable migration energies to different defects with the displacement of the same chemical species [4].

For example, MA-related defects (e.g., MA_{Pb} or MA_i) should display a similar activation energy as that calculated for V_{MA}. In fact, the activation energies of V_I and I_i are essentially the same. The migration process of V_{Pb} in $MAPbI_3$ is quite slow (1.2 s^{-1}) due to its high activation energy, E_a, of 0.80 eV. The activation energy of 0.46 eV for V^{MA} has been measured experimentally [44]. The migration rate of $6.5\times10^5 s^{-1}$ at room temperature for V_{MA} is estimated from the activation energy value [4].

The calculated activation energies of V_I and I_i are predicted to be 0.08 eV, which is sufficient for a full hop to take place in each crystallographic direction. In the absence of an external field, the charged defect can indistinctly migrate forward or backward in any crystallographic direction. Under illumination within the operating conditions of PSCs, the charged defect (positive/negative) favors migration towards the side of the perovskite film that contacts the hole/electron transporting layer. The interstitial defects V_I and I_i can migrate towards the hole/electron contacts that are stabilized due to electrostatic interaction with the electrode. The defects can reach the electrode within tens of nanoseconds, which is much faster than the scanning rate in photovoltaic current–voltage (I–V) measurements [4].

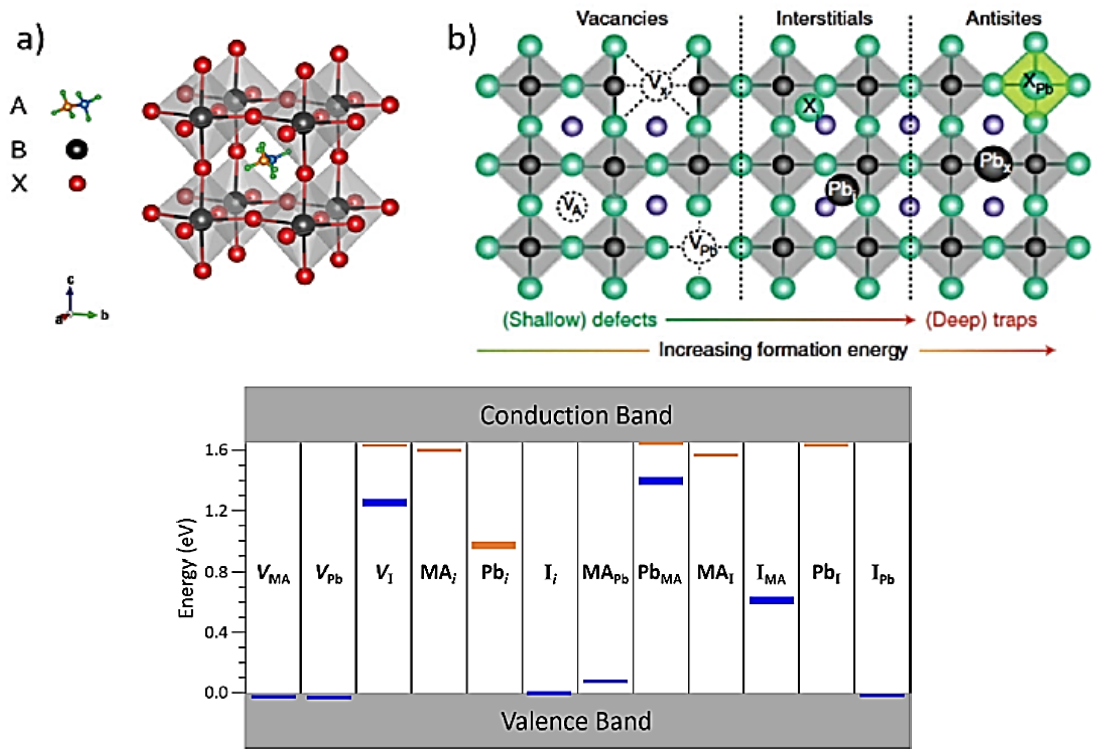

Figure 3.7: .(a) Crystal structure of organic–inorganic metal halide perovskite, where the A position contains an organic cation (CH_3NH_{3+}), B is a metal cation (Pb), and X is a halide anion (I) [42]. (b) Schematic diagram of the $MAPbI_3$ perovskite structure and diffusion paths of the point defects; V_A (cation vacancy), V_I (iodide ion vacancy), V_{Pb} (lead ion vacancy), and Pb_i (lead interstitial) defects [43]. (c) Calculated charge-state transition levels within the band gap for 12 intrinsic defects in $CH_3NH_3PbI_3$ [4].

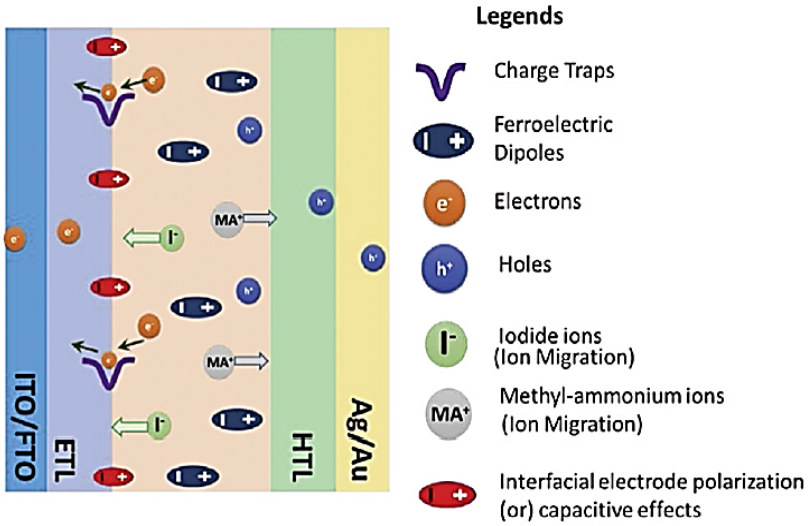

Figure 3.8: Schematic diagram showing the various defects and ions that are generated under illumination in the perovskite solar cell device structure, which leads to degradation of the device and the hysteresis phenomenon during I–V measurements from [44].

Figure 3.8 summarizes the generated probable defects, dipoles, and ions in perovskite solar cells under illumination, which can lead to device degradation and the hysteresis

phenomenon during I–V measurements. During I–V measurements, concerning the scan rate/direction, various processes with respect to ion migration, ferroelectricity, charge trapping, and associated capacitive effects can occur simultaneously, which lead to the resultant hysteresis [44]. To overcome the hysteresis problem, as well as enhancing the PSC efficiency and device stability, it is very important to control and minimize the various defects and ions in the device structure under illumination [4].

The investigation of degradation will focus on defects, selecting four types from the 12 listed below. These include the Recombination center situated at $E_v + 0.6$ eV , which is electrically neutral, the shallow donor trap situated at $E_c - 0.1$ eV (known for trapping electrons), the deep donor trap situated at $E_c - 0.38$ eV, and the shallow Acceptor trap situated at $E_v + 0.1$ eV (which serves as hole traps). This analysis will consider various probable locations of these defects, as outlined in Table 3.1.

Table 3.1: Probable locations of the considered defects.

	ETL/perovskite interface	Bulk-perovskite	HTL/perovskite interface
Recombination center	Probability 1	Probability 2	Probability 3
Shallow donor	Probability 4	Probability 5	Probability 6
Deep Donor	Probability 7	Probability 8	Probability 9
Shallow Acceptor	Probability 10	Probability 11	Probability 12

Table 3.2: Material's inputs used in the simulation [45,46].

	$TiO_2(ETL)$	$MAPbI_3$	$SpiroOMeTAD$	PbS
$d(\mu m)$	0.1	1.8	0.1	0.006
E_g (eV)	3.2	1.55	3.3	1.44
N_c (cm^{-3})	110^{21}	210^{18}	110^{19}	7.3110^{17}
N_v (cm^{-3})	210^{20}	210^{19}	110^{19}	7.3110^{17}
$q\chi$ (eV)	4.1	3.9	2	3.87
μ_n (cm/Vs)	20	40	210^{-3}	50
μ_p (cm/Vs)	10	10	210^{-4}	20
N_D (cm^{-3})	210^{18}	/	/	/
N_A (cm^{-3})	/	/	210^{18}	/

3.4 Results and discussion

3.4.1 Initial case with low defect density

Figure 3.9 presents the electrical outputs generated by the investigated perovskite solar cell, which were calculated utilizing SCAPS simulation. Notably, the design under study mirrors the prevalent design favored by numerous other works, for instance [46–48].

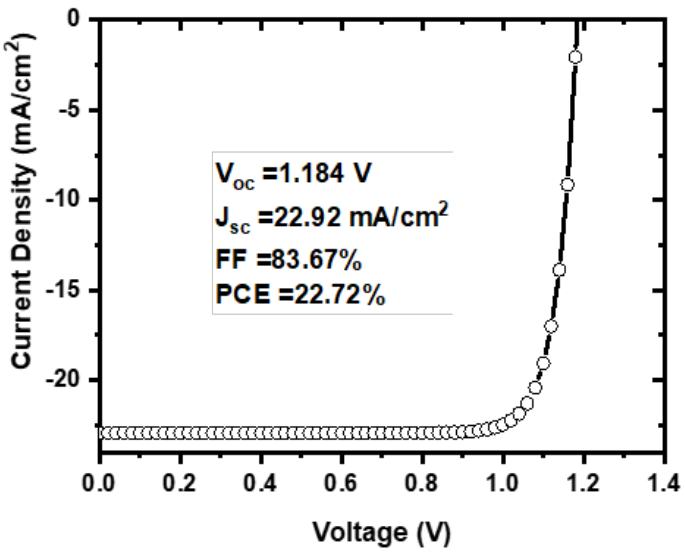

Figure 3.9: J-V characteristic calculated by SCAPS for initial case, i.e. low defect densities.

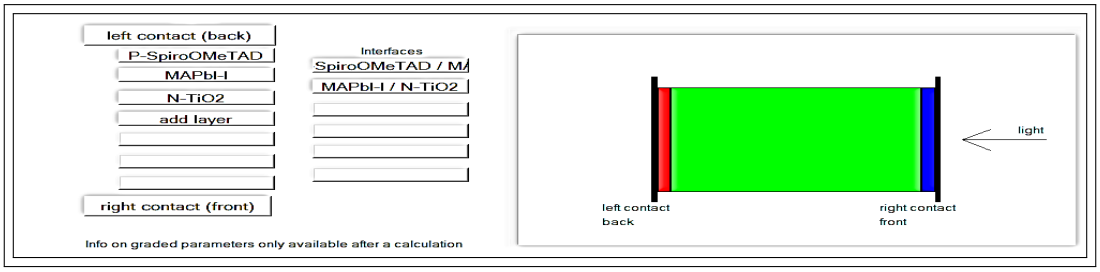

Figure 3.10: The structure of the perovskite solar cell simulated by SCAPS.

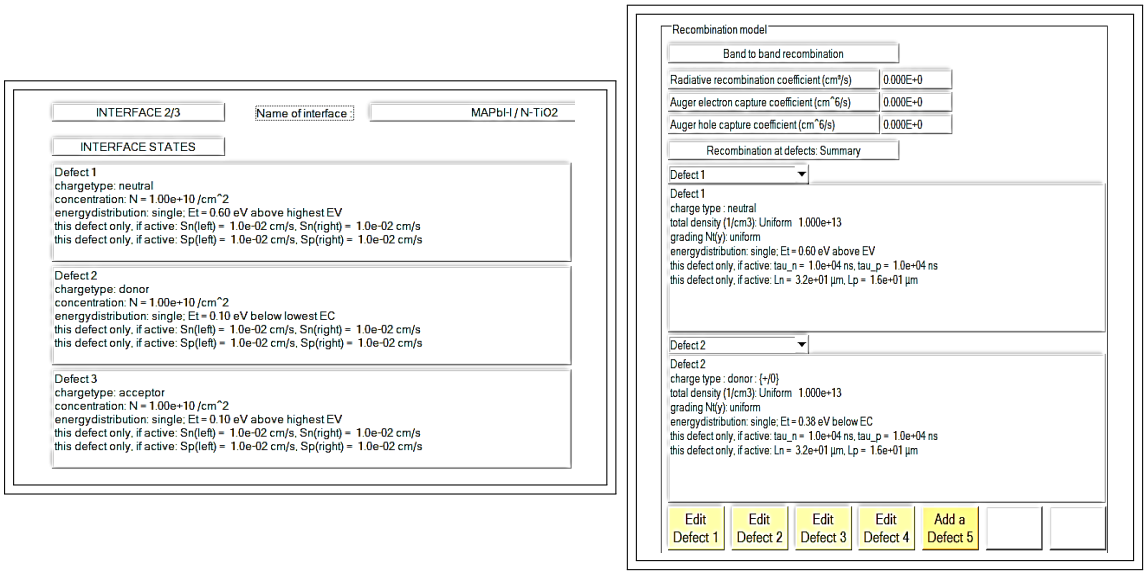

Figure 3.11: Defects definition in SCAPS at interface and bulk.

Illustrated in Figure 3.10, this structure comprises Titanium Dioxide (TiO_2) serving as the Electron Transport Layer (ETL), Methylammonium Lead Iodide ($MAPbI_3$) as the

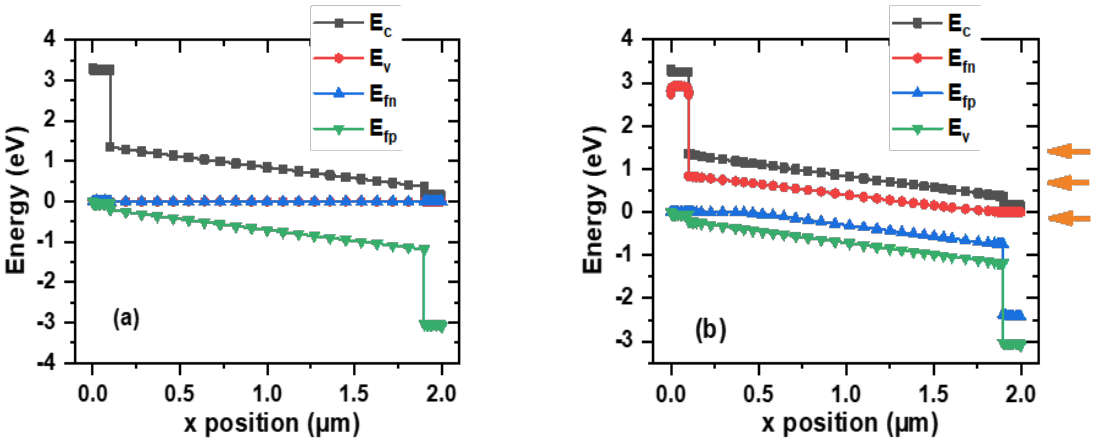

Figure 3.12: Band gap energy in dark (a) and under illumination (b).

fundamental perovskite material for light absorption and carrier generation, and Spiro-OMeTAD, an organic semiconductor, functioning as the Hole Transport Layer (HTL). In the initial scenario, we are referring to the state before any degradation or instability occurs, which is characterized by low defect densities. Defects are defined in SCAPS as shown in Figure 3.11. The first case is for the interface defects while the second is for the bulk one. A defect is defined by indicating its nature (neutral, acceptor or donor), capture cross section, energy position and density (see Figure 3.11). The band gap energy diagram in dark (equilibrium) and under illumination (short circuit condition) is presented in Figure 3.12. The electrical outputs obtained are consistent enough with other previous measured results as shown in Table 3.3.

Table 3.3: Electrical outputs obtained in this study compared to other works.

$J_{sc}(mA/cm^2)$	$V_{oc}(V)$	$FF\%$	$PCE\%$	
22.92	1.184	83.67	22.72	This work
20.40	1.14	87	20.35	[46]
23.69	1.113	77.3	20.40	[47]
23.79	1.09	79.23	20.54	[48]

3.4.2 Effect of defects at ETL/Bulk interface

In this section, we will examine the impact of defects caused by instability or degradation factors. Figure 3.13 illustrates the influence of recombination centers (N_R), shallow donors (N_{DT}), and shallow acceptors (N_{AT}) on the J-V characteristic when these defects are introduced at the interface between the Electron Transport Layer (ETL) and the perovskite layer. The result is summarized in Table.3.4. The foremost notable feature is that NR exerts the most pronounced influence on V_{oc}, followed by N_{AT} and then N_{DT}. However, J_{sc} is affected only by N_{AT}. The explanation for the influence on Jsc is as follows: At the

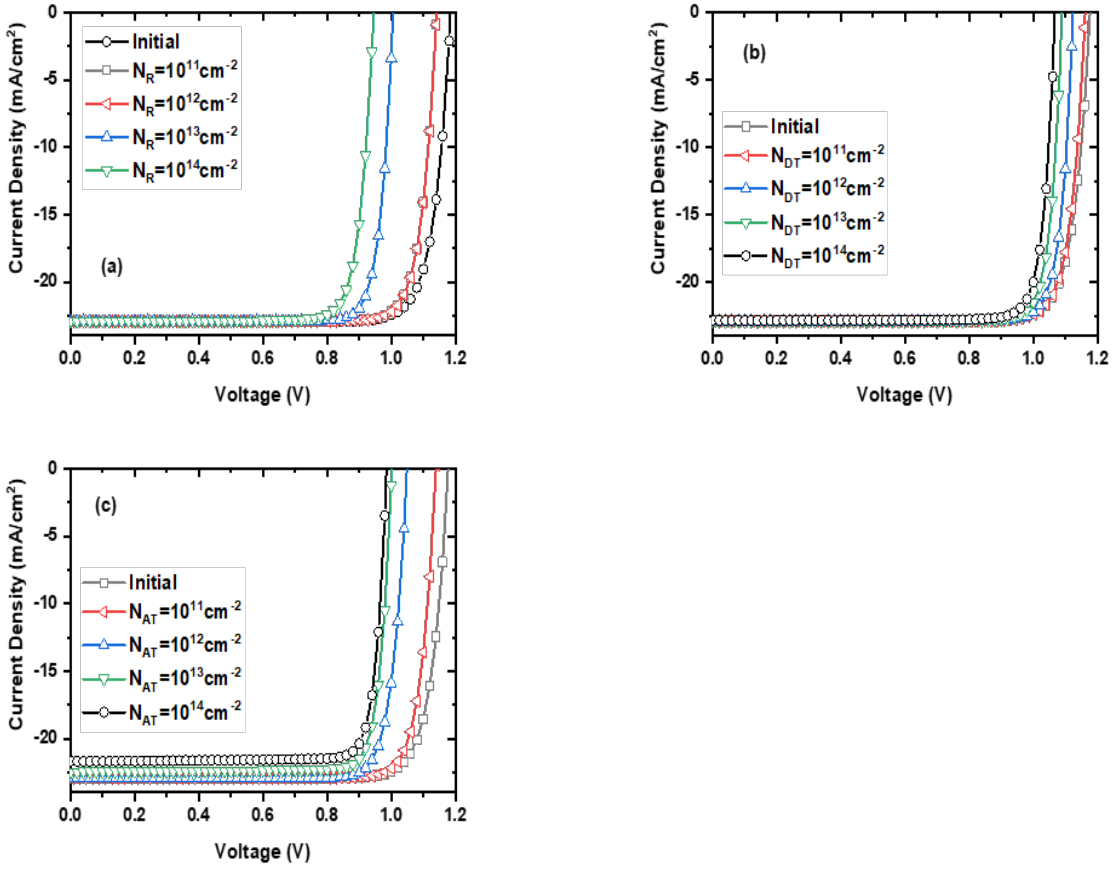

Figure 3.13: J-V characteristic calculated by SCAPS when defects are at the interface ETL/perovskite: (a) recombination center, (b) shallow donor and (c) shallow accepter.

ETL/Perovskite interface, the minority carriers consist of free holes, as deduced from the band gap energy diagram. It is a well-established fact that in n/p-based devices (including n-i-p), minority carrier movement predominantly commands the current. Moreover, the front side of the solar cell is the primary site for free carrier photo-generation. Consequently, this elucidates why N_{AT}, acting as shallow hole traps, solely induces a reduction in J_{sc}.

Besides, the V_{oc} variation with defects can be explained as follows: It is well established that V_{oc}, is the result of the collection of photo-generated carriers, primarily at the depletion region, onto both the n and p sides under light bias and open circuit conditions. Recombination centre has it energy level positioned at mid-bandgap. This enables it to capture and subsequently recombine both types of charge carriers—electrons and holes—thereby diminishing the overall number of carriers collected at the n and p sides. This clarifies why N_R has the most significant effect on V_{oc}. Subsequently, N_{AT}, which acts on minority carriers (holes), exerts the second most prominent reducing effect. Finally, N_{DT}; that affects majority carriers.

Consequently as shown in Table 3.4, the most affecting defect is N_R that reduces V_{oc} to 0.946 V and the cell PCE to 18.18% , at its high density. Then, N_{AT} that decreases J_{sc} to 21.69 mA/cm^2, V_{oc} to 0.985 V and PCE to 18.44%. Finally N_{DT} that reduces V_{oc} to 1.067

V and PCE to 21.06%. However, FF increases for the high densities of both N_{AT} and N_{DT} to 86.28% and 86.32%, respectively. This means that there is an improvement of the ratio $P_M/(V_{oc} \cdot J_{sc})$ even with the reduction of the PCE. It is noticed that $P_M = J_M \cdot V_M$ is the maximum power provided by the solar cell and J_M and V_M are the corresponding current density and voltage.

Table 3.4: Effect of interface ETL/perovskite defects on electrical output of the solar cell when defect density is 10^{14} cm^{-2} .

	$J_{sc}(mA/cm^2)$	$V_{oc}(V)$	$FF\%$	$PCE\%$
Initial	22.92	1.184	83.67	22.72
N_R	22.91	0.946	83.87	18.18
N_{DT}	22.85	1.067	86.32	21.06
N_{AT}	21.69	0.985	86.28	18.44

When the considered defects all are present together and have a high density of 10^{14} cm^2, the obtained outputs are as follow : J_{sc}=22.91 $mAcm^{-2}$; V_{oc}=0.897 V; FF=82.37% and PCE=16.61%. The significant decrease is in V_{oc} and in PCE. By comparing this decrease magnitude in PCE with illumination-induced degradation reported in [49] in which the stated PCE degraded from $\sim$ 23 to $\sim$ 14 %, it is possible to relate the ETL/perovskite defects to illumination degradation.

3.4.3 Effect of defects in bulk-Perovskite

Figures 3.14 illustrates the influence of recombination centers (N_R), deep and shallow donors (N_{DP}, N_{DT}), and shallow acceptors (N_{AT}) on the J-V characteristic when these defects are introduced in the bulk perovskite layer. The electrical outputs variations are summarized in Table 3.5.

Table 3.5: Effect of bulk defect on electrical output of the solar cell when defect density is 10^{16} cm^{-3} .

	$J_{sc}(mA/cm^2)$	$V_{oc}(V)$	$FF\%$	$PCE\%$
Initial	22.92	1.184	83.67	22.72
N_R	22.53	0.933	72.16	15.18
N_{DP}	7.47	0.899	64.66	4.34
N_{DT}	14.37	1.065	77.20	11.83
N_{AT}	22.81	1.124	87.89	22.53

According to the obtained results, it appears that N_{DP} with a density of 10^{16} cm^{-3} exerts the most pronounced degrading effect on the cell performance. The bulk of the cell is an intrinsic region that comprises the depletion region. It seems that in the intrinsic layer, the deep electron traps has the dominant effect. All the outputs degraded severely, mainly J_{sc} that reaches 7.47 mA/cm^2 and PCE that decreases to 4.34 %. Then, the

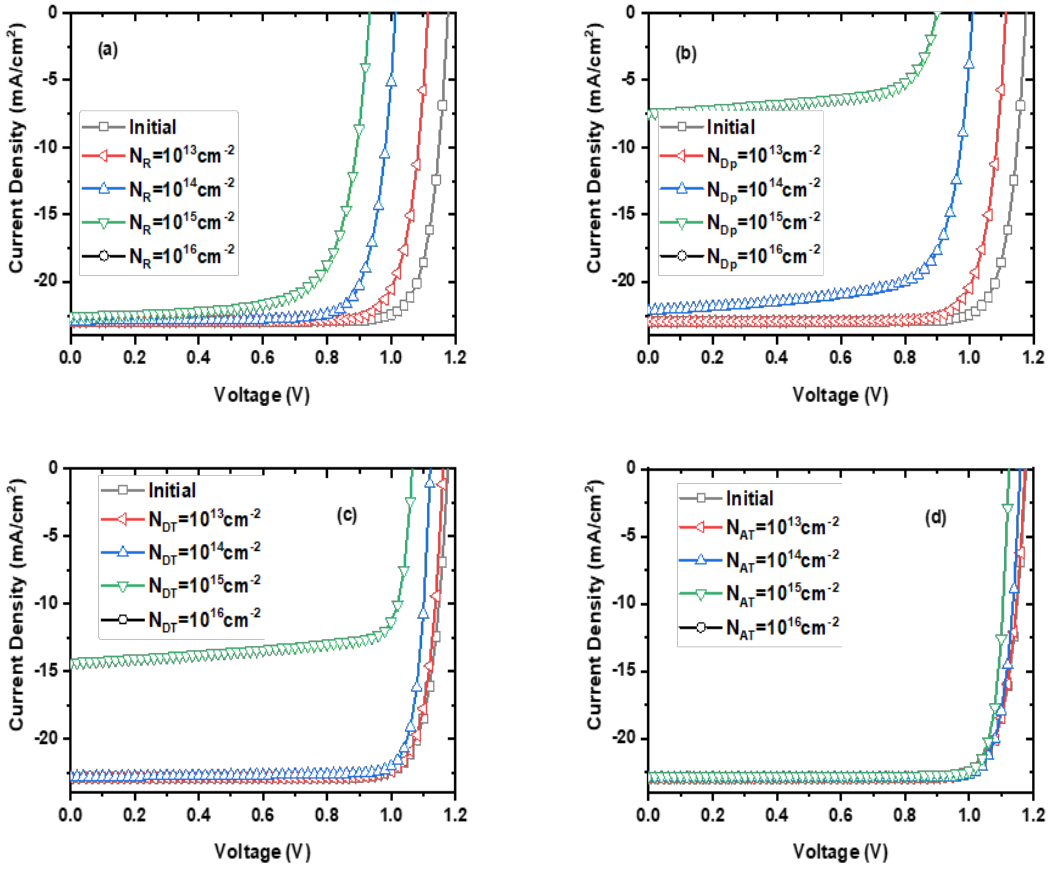

Figure 3.14: J-V characteristic calculated by SCAPS when defects are in the bulk of the perovskite: (a) recombination center, (b) deep donor, (c) shallow donor and (d) shallow accepter.

second important influence is that of the Shallow donor (N_{DT}). For instance, J_{sc} and PCE are reduced to 14.37 mA/cm^2 and 11.83 %, respectively. In the third position, comes N_R that has the most effect on V_{oc} that decreases significantly to 0.933 V, FF to 72.16% and PCE to 15.18%. Finally, the minor effect is that of N_{AT}. One possible interpretation of this observation is that in the intrinsic region, where photo-generation is favored, electrons exhibit higher mobility than holes. As a result, they predominantly dictate the electrical behavior. Consequently, electron traps, particularly the deeper ones, exert a more significant influence.

A question arises as to why N_R has a minor or negligible effect on J_{sc} compared to its impact on V_{oc} ? a possible answer is that at the short circuit condition, there is only a photo-generation that occurs continuously, and the recombination center is located deep at the mid-gap so its interaction with photo-generated carriers (given rise to J_{sc}) will be minor compared to less deep traps like N_{DP} or N_{DT}. However, the open circuit condition highlights the collection of carriers after their traversal across the intrinsic layer, making them more susceptible to the influence of recombination centers.

The electrical outputs obtained when all defects in the perovskite absorber layer (intrinsic layer) have a high density of 10^{16} cm^{-3} are: J_{sc}=4.56 mA/cm^2 ; V_{oc}=0.853 V ; FF=62.53 % and PCE=2.43%. This demonstrates the significant impact of high defect accumulation on the electrical outputs of the solar cell. All outputs decrease sharply compared to the initial state and the PCE in this case drops to 2.43% , which is close to 2.36% reported in [50]. Consequently, the bulk defects can be probably related to a perovskite material subjected to thermal degradation.

3.4.4 Effect of defects at Perovskite/HTL interface

Figures 3.15 depicts how the presence of recombination center N_R, shallow donors N_{DT}, and shallow acceptors N_{AT} affects the J-V characteristic when these defects are incorporated at the interface between the perovskite layer and the Hole Transport Layer (HTL). A summary of the resulting outputs can be found in Table 3.6.

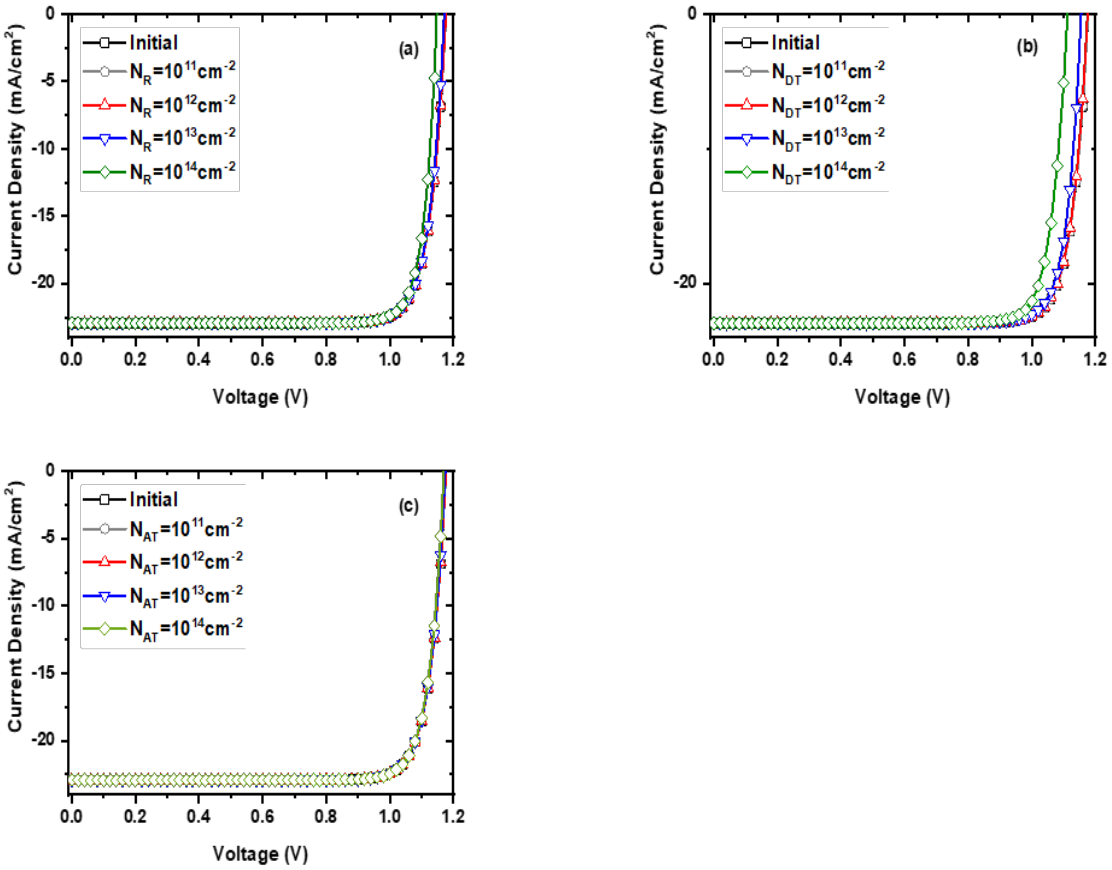

Figure 3.15: J-V characteristic calculated by SCAPS when defects are at the interface perovskite/HTL: (a) recombination center, (b) shallow donor and (c) shallow accepter.

On a global scale, the impact of perovskite/HTL defects on the electrical outputs of the cell remains minimal. At this interface, the minor carriers primarily consist of electrons. J_{sc} remains practically constant. However, there is a slight decrease in V_{oc},

Table 3.6: Effect of interface perovskite/HTL defects on electrical output of the solar cell when defect density is 10^{14} cm^{-2} .

	$J_{sc}(mA/cm^2)$	$V_{oc}(V)$	$FF\%$	$PCE\%$
Initial	22.92	1.184	83.67	22.72
N_R	22.92	1.148	85.50	22.50
N_{DT}	22.93	1.112	84.20	21.48
N_{AT}	22.91	1.174	84.41	22.64

notably dropping to 1.112 V in the case of N_{DT}. Conversely, FF experiences a slight increase, particularly when $NR = 10^{14}cm^{-2}$, where it reaches 85.50%. Notably, PCE exhibits a relatively significant decrease, dropping to 21.48% for $N_{DT} = 10^{14}cm^{-2}$.

Also when all defects are present at a density of $10^{14}cm^{-2}$, the electrical outputs are : J_{sc}=22.92 mA/cm^2 ; V_{oc}=1.091 V; FF=86.85% and PCE=21.73%. J_{sc} remains virtually unchanged, while V_{oc} experiences a slight decrease to 1.091 V. However, FF notably increases to 86.85%, leading to a slight decrease in the PCE to 21.73%. Interestingly, this PCE value is marginally better than the 21.48% obtained in the previous case of $N_{DT} = 10^{14}cm^{-2}$, likely due to the improved FF.

The hysteresis effect reported by S-A Kim et al [48] that reflects instability related to forward and reverse bias in ITO/TiO_2/perovskite/spiro-OMeTAD/Au is presented in Table 3.7. In addition, in the same table a comparison is achieved for deviation between reverse and forward outputs [48] with defects effects reported in this work. According to our simulation results, it can be suggested that hysteresis effect is related mainly to defects at perovskite/HTL interface.

Table 3.7: Possible defects responsible of Hysteresis effect.

	$J_{sc}(mA/cm^2)$	$V_{oc}(V)$	$FF\%$	$PCE\%$
Reverse [48].	23.79	1.09	79.23	20.54
Forward [48].	23.81	1.07	77.19	19.66
	$\Delta J_{sc}(mA/cm^2)$	$\Delta V_{oc}(V)$	$\Delta FF\%$	$\Delta PCE\%$
[48]	0.02	0.02	2.04	0.88
Our work (N_{DT})	0.01	0.072	0.53	1.24
Our work (All defects)	/	0.093	3.18	0.99

3.5 PbS buffer layer to reduce instability-induced defects effect

In this section and based on experimental study carried out by S-A Kim et al [48], we suggest the introduction of PbS buffer layer between $MAPbI_3$ (bulk) and spiro-OMeTAD (HTL). Indeed, in a remarkable good agreement with what has been reported in [48], there

is a significant improvement on the electrical outputs subject to defect's degradation as shown in Figure 3.16.

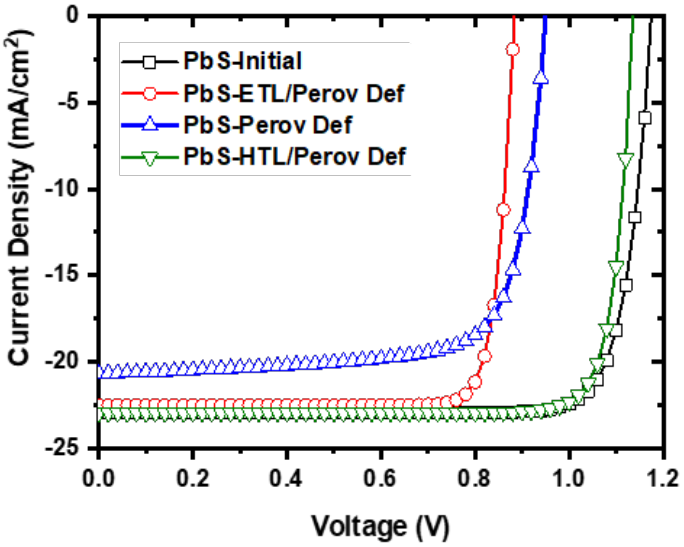

Figure 3.16: J-V characteristic calculated by introducing PbS buffer layer at HTL/bulk interface to reduce defects effect at the different locations considered in this study; interfaces and bulk.

Table 3.8: Effect of PbS buffer layer at perovskite/HTL interface on electrical output of the solar cell subject to degradation-induced defects.

	$J_{sc}(mA/cm^2)$	$V_{oc}(V)$	$FF\%$	$PCE\%$
Initial	22.94	1.175	83.88	22.61
ETL/Bulk defects	22.50	0.883	85.82	17.06
Bulk defects	20.67	0.950	75.22	14.78
Bulk/HTL defects	22.94	1.136	85.76	22.35

According to the summarized results in Table 3.8, despite in the initial state there is a slight decrease in the solar cell performance in comparison to the case without PbS layer, in the degraded state however there is a remarkable improvement. For instance for the ETL/bulk defects case, PCE increased from 16.61 to 17.06%. For bulk defects, a significant improvement occurred in PCE that increased from 2.43 to 14.78%. For HTL/bulk also a slight increase in PCE from 21.73 to 22.35% was achieved.

3.6 Conclusion

In this chapter, we have explored the instability issues associated with perovskite solar cells using SCAPS simulation. We investigated the impact of defects introduced at interfaces within the solar cell structure and the bulk perovskite layer. Across the investigated sections, the influence of defects on the electrical outputs of perovskite solar cells is examined comprehensively, shedding light on critical factors impacting device performance due to stability issues.

In the section addressing defects at the ETL/Perovskite interface, it is evident that recombination centers (N_R) have the most significant effect on V_{oc}, followed by shallow acceptors (N_{AT}) and shallow donors (N_{DT}), with each defect type affecting distinct electrical parameters. The significant reduction in V_{oc} (1.184 to 0.897 V) and PCE (22.72 to 16.61%), in the presence of all defects (recombination and shallow interface defects), highlights the critical role of interface ETL/ perovskite defects in limiting device performance. These defects were attributed to illumination-degradation since the interface is the first important place subject to light incidence.

Moving to defects within the bulk perovskite layer, deep donors (N_{DP}) emerge as the primary contributor to performance degradation, significantly impacting all electrical outputs. The intrinsic region's susceptibility to electron traps was ascribed to thermal degradation and induced a severe drop in PCE to 2.43%.

At the Perovskite/HTL interface, while defects exert a less impact, variations inV_{oc} and PCE are relatively notable, particularly with the presence of shallow donors (N_{DT}). PCE has been reduced to 21.48% . In this case, the interface defects were suggested to be responsible of hysteresis effect. On the other hand, the intricate interplay between defects and electrical parameters, such as the observed improvement in fill factor despite PCE reduction, underlines a complex optimization setting for the device.

The introduction of a PbS buffer layer at HTL/bulk interface has improved considerably the electrical outputs degradation, mainly that related to bulk defects. In summary, these findings emphasize the multifaceted nature of defect influence due stability issues on perovskite solar cell performance, mainly that induced by illumination, thermal effect and hysteresis. The work highlights the need for targeted defect mitigation strategies to unlock the full potential of these promising photovoltaic materials.

References of Chapter 3

[1] Deng, J., Yang, X., and Wang, P., 2015, "Study on the Second-Order Transfer Function Models for Dynamic Tests of Flat-Plate Solar Collectors Part I: A Proposed New Model and a Fitting Methodology," Solar Energy, 114.

[2] Yang, X., Liu, C., Walker, B. D., and Ren, P., 2020, "Accurate Description of Molecular Dipole Surface with Charge Flux Implemented for Molecular Mechanics," Journal of Chemical Physics, 153(6).

[3] Burgelman, M., Decock, K., Niemegeers, A., Verschraegen, J., and Degrave, S., 2019, "SCAPS Manual," University of Gent, (february).

[4] Duan, L., and Uddin, A., 2022, "Defects and Stability of Perovskite Solar Cells: A Critical Analysis," Mater Chem Front, 6(4), pp. 400–417.

[5] Prakash, J., Singh, A., Sathiyan, G., Ranjan, R., Singh, A., Garg, A., and Gupta, R. K., 2018, "Progress in Tailoring Perovskite Based Solar Cells through Compositional Engineering: Materials Properties, Photovoltaic Performance and Critical Issues," Mater Today Energy, 9.

[6] Lin, Y., Fang, Y., Zhao, J., Shao, Y., Stuard, S. J., Nahid, M. M., Ade, H., Wang, Q., Shield, J. E., Zhou, N., Moran, A. M., and Huang, J., 2019, "Unveiling the Operation Mechanism of Layered Perovskite Solar Cells," Nat Commun, 10(1).

[7] Shi, P., Ding, Y., Ren, Y., Shi, X., Arain, Z., Liu, C., Liu, X., Cai, M., Cao, G., Nazeeruddin, M. K., and Dai, S., 2019, "Template-Assisted Formation of High-Quality α-Phase HC(NH2)2PbI3 Perovskite Solar Cells," Advanced Science, 6(21).

[8] Haque, F., Wright, M., Mahmud, M. A., Yi, H., Wang, D., Duan, L., Xu, C., Upama, M. B., and Uddin, A., 2018, "Effects of Hydroiodic Acid Concentration on the Properties of CsPbI3 Perovskite Solar Cells," ACS Omega, 3(9).

[9] Wang, Y., Ibrahim Dar, M., Ono, L. K., Zhang, T., Kan, M., Li, Y., Zhang, L., Wang, X., Yang, Y., Gao, X., Qi, Y., Grätzel, M., and Zhao, Y., 2019, "Thermodynamically Stabilized B-CsPbI3–Based Perovskite Solar Cells with Efficiencies ¿18%," Science (1979), 365(6453).

[10] Saliba, M., Matsui, T., Domanski, K., Seo, J. Y., Ummadisingu, A., Zakeeruddin, S. M., Correa-Baena, J. P., Tress, W. R., Abate, A., Hagfeldt, A., and Grätzel, M., 2016, "Incorporation of Rubidium Cations into Perovskite Solar Cells Improves Photovoltaic Performance," Science (1979), 354(6309).

[11] Zhang, S., Wu, S., Chen, R., Chen, W., Huang, Y., Yang, Z., and Chen, W., 2020, "Formamidine-Assisted Fast Crystallization to Fabricate Formamidinium-Based Perovskite Films for High-Efficiency and Stable Solar Cells," J Mater Chem C Mater, 8(5).

[12] Wu, X., Li, H., Wang, K., Sun, X., and Wang, L., 2018, "CH3NH3Pb1-: XEuxI3 Mixed Halide Perovskite for Hybrid Solar Cells: The Impact of Divalent Europium Doping on Efficiency and Stability," RSC Adv, 8(20).

[13] Arafat Mahmud, M., Kumar Elumalai, N., Baishakhi Upama, M., Wang, D., Gonçales, V. R., Wright, M., Justin Gooding, J., Haque, F., Xu, C., and Uddin, A., 2018, "Cesium Compounds as Interface Modifiers for Stable and Efficient Perovskite Solar Cells," Solar Energy Materials and Solar Cells, 174.

[14] Yang, M., Zhang, T., Schulz, P., Li, Z., Li, G., Kim, D. H., Guo, N., Berry, J. J., Zhu, K., and Zhao, Y., 2016, "Facile Fabrication of Large-Grain CH3 NH3 PbI3-x Brx Films for High-Efficiency Solar Cells via CH3NH3 Br-Selective Ostwald Ripening," Nat Commun, 7.

[15] Jung, E. H., Jeon, N. J., Park, E. Y., Moon, C. S., Shin, T. J., Yang, T. Y., Noh, J. H., and Seo, J., 2019, "Efficient, Stable and Scalable Perovskite Solar Cells Using Poly(3-Hexylthiophene)," Nature, 567(7749).

[16] Kim, M., Kim, G. H., Lee, T. K., Choi, I. W., Choi, H. W., Jo, Y., Yoon, Y. J., Kim, J. W., Lee, J., Huh, D., Lee, H., Kwak, S. K., Kim, J. Y., and Kim, D. S., 2019, " Methylammonium Chloride Induces Intermediate Phase Stabilization for Efficient Perovskite Solar Cells," Joule, 3(9).

[17] Chen, L., Wu, J., Li, G., Wang, S., Wang, C., Zhu, S., Chen, X., Tan, L., Du, Y., Sun, W., and Lan, Z., 2021, "Efficient and Stable Perovskite Solar Cells Doped by Cesium Acetate," Solar Energy, 230.

[18] Zhao, Y., Xu, H., Wang, Y., Yang, X., Duan, J., and Tang, Q., 2019, "10.34%-Efficient Integrated CsPbBr3/Bulk-Heterojunction Solar Cells," J Power Sources, 440.

[19] Ye, Q., Zhao, Y., Mu, S., Ma, F., Gao, F., Chu, Z., Yin, Z., Gao, P., Zhang, X., and You, J., 2019, "Cesium Lead Inorganic Solar Cell with Efficiency beyond 18% via Reduced Charge Recombination," Advanced Materials, 31(49).

[20] Wang, Y., Liu, X., Zhang, T., Wang, X., Kan, M., Shi, J., and Zhao, Y., 2019, "The Role of Dimethylammonium Iodide in CsPbI3 Perovskite Fabrication: Additive or Dopant?," Angewandte Chemie - International Edition, 58(46).

[21] Wang, H., Song, Y., Kang, Y., Dang, S., Feng, J., and Dong, Q., 2020, "Reducing Photovoltage Loss at the Anode Contact of Methylammonium-Free Inverted Perovskite Solar Cells by Conjugated Polyelectrolyte Doping," J Mater Chem A Mater, 8(15).

[22] Cao, Q., Li, Y., Zhang, H., Yang, J., Han, J., Xu, T., Wang, S., Wang, Z., Gao, B., Zhao, J., Li, X., Ma, X., Zakeeruddin, S. M., Sha, W. E. I., Li, X., and Grätzel, M., 2021, "Efficient and Stable Inverted Perovskite Solar Cells with Very High Fill Factors via Incorporation of Star-Shaped Polymer," Sci Adv, 7(28).

[23] Liu, B., Cui, R., Huang, H., Guo, X., Dong, J., Yao, H., Li, Y., Zhao, D., Wang, J., Zhang, J., Chen, Y., and Sun, B., 2020, "Elucidating the Mechanisms Underlying PCBM Enhancement of CH3NH3PbI3 Perovskite Solar Cells Using GIXRD and XAFS," J Mater Chem A Mater, 8(6).

[24] Tai, Q., Guo, X., Tang, G., You, P., Ng, T. W., Shen, D., Cao, J., Liu, C. K., Wang, N., Zhu, Y., Lee, C. S., and Yan, F., 2019, "Antioxidant Grain Passivation for Air-Stable Tin-Based Perovskite Solar Cells," Angewandte Chemie - International Edition, 58(3).

[25] Wang, L., Zhou, H., Hu, J., Huang, B., Sun, M., Dong, B., Zheng, G., Huang, Y., Chen, Y., Li, L., Xu, Z., Li, N., Liu, Z., Chen, Q., Sun, L. D., and Yan, C. H., 2019, "A Eu 3+ -Eu 2+ Ion Redox Shuttle Imparts Operational Durability to Pb-I Perovskite Solar Cells," Science (1979), 363(6424).

[26] Lin, R., Xiao, K., Qin, Z., Han, Q., Zhang, C., Wei, M., Saidaminov, M. I., Gao, Y., Xu, J., Xiao, M., Li, A., Zhu, J., Sargent, E. H., and Tan, H., 2019, "Monolithic

All-Perovskite Tandem Solar Cells with 24.8% Efficiency Exploiting Comproportionation to Suppress Sn(Ii) Oxidation in Precursor Ink," Nat Energy, 4(10).

[27] Yin, Y., Fu, S., Zhou, S., Song, Y., Li, L., Zhang, M., Wang, J., Mariyappan, P., Alshehri, S. M., Ahamad, T., and Yamauchi, Y., 2020, "Efficient and Stable Ideal Bandgap Perovskite Solar Cell Achieved by a Small Amount of Tin Substituted Methylammonium Lead Iodide," Electronic Materials Letters, 16(3).

[28] Chen, C., Xu, Y., Wu, S., Zhang, S., Yang, Z., Zhang, W., Zhu, H., Xiong, Z., Chen, W., and Chen, W., 2018, "CaI2: A More Effective Passivator of Perovskite Films than PbI2 for High Efficiency and Long-Term Stability of Perovskite Solar Cells," J Mater Chem A Mater, 6(17).

[29] Zhang, H., Li, R., Zhang, M., and Guo, M., 2020, "Effect of Sr Substitution on the Air-Stability of Perovskite Solar Cells," Ceram Int, 46(9).

[30] Wu, W. Q., Rudd, P. N., Ni, Z., Van Brackle, C. H., Wei, H., Wang, Q., Ecker, B. R., Gao, Y., and Huang, J., 2020, "Reducing Surface Halide Deficiency for Efficient and Stable Iodide-Based Perovskite Solar Cells," J Am Chem Soc, 142(8).

[31] Ranjan, R., Ranjan, S., Monalisa, M., Nalwa, K. S., Singh, A., Garg, A., and Gupta, R. K., 2021, "Enhanced Thermal and Moisture Stability via Dual Additives Approach in Methylammonium Lead Iodide Based Planar Perovskite Solar Cells," Solar Energy, 225.

[32] Ranjan, R., Usmani, B., Pali, S., Ranjan, S., Singh, A., Garg, A., and Gupta, R. K., 2020, "Role of PC60BM in Defect Passivation and Improving Degradation Behaviour in Planar Perovskite Solar Cells," Solar Energy Materials and Solar Cells, 207.

[33] Ranjan, R., Usmani, B., Ranjan, S., Weerasinghe, H. C., Singh, A., Garg, A., and Gupta, R. K., 2019, "Enhanced Efficiency and Thermal Stability of Mesoscopic Perovskite Solar Cells by Adding PC70BM Acceptor," Solar Energy Materials and Solar Cells, 202.

[34] Agiorgousis, M. L., Sun, Y. Y., Zeng, H., and Zhang, S., 2014, "Strong Covalency-Induced Recombination Centers in Perovskite Solar Cell Material CH3NH3PbI3," J Am Chem Soc, 136(41).

[35] Buin, A., Comin, R., Xu, J., Ip, A. H., and Sargent, E. H., 2015, "Halide-Dependent Electronic Structure of Organolead Perovskite Materials," Chemistry of Materials, 27(12).

[36] Buin, A., Pietsch, P., Xu, J., Voznyy, O., Ip, A. H., Comin, R., and Sargent, E. H., 2014, "Materials Processing Routes to Trap-Free Halide Perovskites," Nano Lett, 14(11).

[37] Eames, C., Frost, J. M., Barnes, P. R. F., O'Regan, B. C., Walsh, A., and Islam, M. S., 2015, "Ionic Transport in Hybrid Lead Iodide Perovskite Solar Cells," Nat Commun, 6.

[38] Kim, J., Lee, S. H., Lee, J. H., and Hong, K. H., 2014, "The Role of Intrinsic Defects in Methylammonium Lead Iodide Perovskite," Journal of Physical Chemistry Letters, 5(8).

[39] Walsh, A., Scanlon, D. O., Chen, S., Gong, X. G., and Wei, S. H., 2015, "Self-Regulation Mechanism for Charged Point Defects in Hybrid Halide Perovskites," Angewandte Chemie - International Edition, 54(6).

[40] Xu, J., Buin, A., Ip, A. H., Li, W., Voznyy, O., Comin, R., Yuan, M., Jeon, S., Ning, Z., McDowell, J. J., Kanjanaboos, P., Sun, J. P., Lan, X., Quan, L. N., Kim, D. H., Hill, I. G., Maksymovych, P., and Sargent, E. H., 2015, "Perovskite-Fullerene Hybrid Materials Suppress Hysteresis in Planar Diodes," Nat Commun, 6.

[41] Yin, W. J., Shi, T., and Yan, Y., 2014, "Unusual Defect Physics in CH3NH3PbI3 Perovskite Solar Cell Absorber," Appl Phys Lett, 104(6). [42] Wang, D., Wright, M., Elumalai, N. K., and Uddin, A., 2016, "Stability of Perovskite Solar Cells," Solar Energy Materials and Solar Cells, 147.

[43] Aldakov, D., and Reiss, P., 2019, "Safer-by-Design Fluorescent Nanocrystals: Metal Halide Perovskites vs Semiconductor Quantum Dots," Journal of Physical Chemistry C, 123(20).

[44] Elumalai, N. K., Mahmud, M. A., Wang, D., and Uddin, A., 2016, "Perovskite Solar Cells: Progress and Advancements," Energies (Basel), 9(11).

[45] Azri, F., 2022, " Study of Hybrid Organic-Inorganic Solar Cells Based on Perovskite Materials ". PhD thesis, University of Biskra.

[46] Eslami, F., and Matloub, S., 2023, "Advancing Perovskite Solar Cell Performance: Enhanced Efficiency and Stability through Superimposed PbS QDs," Solar Energy, 265.

[47] Zhao, P., Kim, B. J., and Jung, H. S., 2018, "Passivation in Perovskite Solar Cells: A Review," Mater Today Energy, 7, pp. 267–286.

[48] Kim, S. A., Kim, H. S., Lee, W., Jeon, N. J., Lim, J., and Yang, T. Y., 2023, "Improvement of Stability of Perovskite Solar Cells with PbS Buffer Layer Formed by Solution Process," Appl Surf Sci, 626.

[49] Ni, Z., Jiao, H., Fei, C., Gu, H., Xu, S., Yu, Z., Yang, G., Deng, Y., Jiang, Q., Liu, Y., Yan, Y., and Huang, J., 2021, "Evolution of Defects during the Degradation of Metal Halide Perovskite Solar Cells under Reverse Bias and Illumination," Nature Energy 2021 7:1, 7(1), pp. 65–73.

[50] Sharma, R., Sharma, A., Agarwal, S., and Dhaka, M. S., 2022, "Stability and Efficiency Issues, Solutions and Advancements in Perovskite Solar Cells: A Review," Solar Energy, 244, pp. 516–535.

Conclusion

In conclusion, our study delved into the instability issues present in $TiO_2 - MAPbI_3 - Spiro - OMeTED$ (n-i-p type) perovskite solar cells, employing SCAPS-1D numerical simulation software. Through the computation of current-voltage density characteristics (J-V) and the determination of key photovoltaic output parameters such as short-circuit current density (J_{sc}), open-circuit voltage (V_{oc}), fill factor (FF), and power conversion efficiency (PCE), we explored the consequences of defects induced by various degradation factors including prolonged illumination, UV radiation, corrosion, oxidation, and humidity, etc.... These defects, identified as N_R (recombination center), N_{DP} (deep donor), N_{DT} (shallow donor), and N_{AT} (shallow acceptor), were found to primarily manifest at critical interfaces within the solar cell structure—specifically, between the electron transport layer (ETL) and perovskite, the hole transport layer (HTL) and perovskite, and within the bulk perovskite layer. Our findings revealed that while initial electrical parameters aligned closely with experimental values, the presence of high-density defects within the bulk layer (at 1016 cm-3) exerted the most substantial adverse impact, precipitating a drastic reduction in PCE to 2.43%. Moreover, defects at the ETL/perovskite interface, characterized by a surface density of $10^{14} cm^{-2}$, resulted in a notable decline in PCE to 16.61%, whereas defects at the perovskite/HTL interface induced a comparatively smaller reduction, leading to a PCE decrement down to 21.73%. These defects were associated, respectively, to thermal stress, illumination and hysteresis effects. The introduction of a PbS buffer layer at HTL/bulk interface has improved considerably the electrical outputs degradation, mainly that related to bulk defects. This comprehensive analysis underscores the critical importance of defect qualification strategies, particularly within the bulk perovskite layer, to enhance the stability and performance of perovskite solar cells. Future research events should aim to further elucidate the underlying mechanisms governing defect formation and migration, paving the way for the development of more resilient and efficient photovoltaic technologies.

ABSTRACT

Our study investigates instability issues in $TiO_2 - MAPbI_3 - Spiro - OMeTED$ (n-i-p type) perovskite solar cells using SCAPS-1D numerical simulation software. The current-voltage density characteristics (J-V) and key photovoltaic output parameters, including short-circuit current density (J_{sc}), open-circuit voltage (V_{oc}), fill factor (FF), and power conversion efficiency (PCE) are calculated. The work focuses on the impact of defects induced by degradation factors such as prolonged illumination, UV radiation, corrosion, oxidation, and humidity. These defects, namelyN_R (recombination center),N_{DP} (deep donor), N_{DT} (shallow donor), and N_{AT} (shallow acceptor), are identified based on previous research. The possible defect locations, are at the interfaces; between the electron transport layer (ETL) and perovskite or the hole transport layer (HTL) and perovskite, as well as within the bulk perovskite layer. Initial electrical parameters are in agreement with wide range of experimental values, with J_{sc}=22.92mA/cm^2, V_{oc}=1.184V, FF=83.67%, and PCE=22.72%. However, high-density defects in the bulk layer (all $10^{16}cm^{-3}$) have the most significant impact, reducing PCE to 2.43%. Defects at the ETL/perovskite interface, with a surface density of $10^{14}cm^{-2}$, lower PCE to 16.61%, while defects at the perovskite/HTL interface result in a smaller decrease of PCE down to 21.73%. These defects were associated, respectively, to thermal stress, illumination and hysteresis effects. The introduction of a PbS buffer layer at HTL/bulk interface has improved considerably the electrical outputs degradation, mainly that related to bulk defects

Keywords: instability issues, perovskite solar cells, SCAPS-1D, interfaces, defects, cell efficiency

ملخص:

تبحث دراستنا في مشكلات عدم الاستقرار في خلايا البيروفسكايت الشمسية TiO_2-$MAPbI_3$-Spiro-OMeTED (نوع n-i-p) باستخدام برنامج المحاكاة العددية SCAPS-1D. يتم حساب خصائص كثافة الجهد الحالي (J-V) ووسائط الخروج الكهروضوئية الرئيسية، بما في ذلك كثافة تيار الدارة القصيرة (J_{sc})، وجهد الدارة المفتوحة (V_{oc})، ومعامل التعبئة (FF)، ومردود تحويل الطاقة (PCE). يركز العمل على تأثير العيوب الناجمة عن عوامل التحلل مثل الإضاءة الطويلة والأشعة فوق البنفسجية والتآكل والأكسدة والرطوبة وما إلى ذلك. تم تحديد هذه العيوب، وهي N_R (مركز إعادة التركيب)، وN_{Dp} (المانح العميق)، وN_{DT} (المانح غير العميق)، وN_{AT} (الاخذ غير العميق)، بناءً على اعمال بحثية سابقة. مواقع العيوب المحتملة موجودة في الواجهات؛ بين طبقة نقل الإلكترون (ETL) والبيروفسكايت أو طبقة نقل الثقب (HTL) والبيروفسكايت، وكذلك داخل طبقة البيروفسكايت . تتوافق وسائط الخروج الكهربائية الأولية مع نطاق واسع مع القيم التجريبية، مع J_{sc}=22.92 mA/cm^2، V_{oc} =1.184 V، FF=83.67%، وPCE=22.72%. وجدنا ان العيوب عالية الكثافة في طبقة البيروفسكيت (جميعها بكثافة 10^{16} cm^{-3}) لها التأثير الأكثر أهمية، مما يقلل من مردود التحويل للخلية إلى 2.43٪. يلي ذلك العيوب في واجهة ETL/perovskite، بكثافة سطحية تبلغ 10^{14} cm^{-2}،تؤدي إلى انخفاض PCE إلى 16.61%، بينما تؤدي العيوب في واجهة perovskite/HTL إلى انخفاض أصغر في PCE إلى 21.73%. أرجعت العيوب لتأثير الإجهاد الحراري ، الإضاءة و الهستيريزيس الناجم عن الإستقطاب الكهربائي. خفض تأثيرها بطبقة PbS عند السطح الفاصل HTL/bulk.

الكلمات المفتاحية: مشاكل اللااستقرار، الخلايا الشمسية البيروفسكية، SCAPS-1D ،الواجهات , العيوب ,مردود الخلية.

REPUBLIQUE ALGERIENNE DEMOCRATIQUE ET POPULAIRE
MINISTERE DE L'ENSEIGNEMENT SUPERIEUR
ET DE LA RECHERCHE SCIENTIFIQUE
UNIVERSITE MOHAMED KHIDER - BISKRA
Faculté des SE&SNV

الجمهورية الجزائرية الديمقراطية الشعبية
وزارة التعليم العالي والبحث العلمي
جامعة محمد خيضر بسكرة
كلية العلوم الدقيقة وعلوم الطبيعة والحياة

Département des Sciences de la matière

قسم :علوم المادة

Filière: Physique

شعبة :الفيزياء

تصريـح شرفـــي

خاص بالالتزام بقواعد النزاهة العلمية لإنجاز بحث

(ملحق القرار 1082 المؤرخ في 2021/12/27)

أنا الممضي أسفله،

السيد(ة): عنصر سليسل .....

الصفة: طالب سنة ثانية ماستر فيزياء تخصص: فيزياء طاقوية وطاقات متجددة

الحامل(ة) لبطاقة التعريف الوطنية رقم: 200434.073 الصادرة بتاريخ: 31/07/2023

المسجل بكلية: علوم المادة وعلوم الطبيعة والحياة قسم: علوم المادة .....

والمكلف بانجاز أعمال بحث : مذكرة ماستر في الفيزياء

عنوانها: study of instability issue in perovskite solar cell .....

أصرح بشرفي أني ألتزم بمراعاة المعايير العلمية والمنهجية ومعايير الأخلاقيات المهنية والنزاهة الأكاديمية المطلوبة في انجاز البحث المذكور أعلاه وفق ما ينص عليه القرار رقم 1082 المؤرخ في 2021/12/27 المحدد للقواعد المتعلقة بالوقاية من السرقة العلمية ومكافحتها.

التاريخ: 2024/02/22 .....

إمضاء المعني بالأمر